Metabolic Flux Analysis and Population Heterogeneity In Mammalian Cell Culture

By

BRIAN D. FOLLSTAD

Bachelor of Chemical Engineering, 1994

University of Minnesota

Submitted to the Department of Chemical Engineering in

Partial Fulfillment of the Requirements for the Degree of

DOCTOR OF PHILOSOPHY IN CHEMICAL ENGINEERING

at the

MASSACHUSETTS INSTITUTE OF TECHNOLOGY

February, 2000

Author: _____

Department of Chemical Engineering
December 20, 1999

Certified by: _____

Daniel I. C. Wang
Institute Professor
Thesis Supervisor

Accepted by: _____

Robert E. Cohen
St. Laurent Professor of Chemical Engineering
Chairman, Committee for Graduate Students

Metabolic Flux Analysis and Population Heterogeneity In Mammalian Cell Culture

By
Brian D. Follstad

Submitted to the Department of Chemical Engineering on December 20, 1999
In Partial Fulfillment of the Requirements for the Degree of
Doctor of Philosophy in Chemical Engineering

ABSTRACT

Metabolic flux and population heterogeneity analysis were used to develop relations between mammalian cell physiology and specific culture environments and to formulate strategies for increasing cell culture performance. Mitochondrial characteristics associated with respiration, membrane potential, and apoptosis along with physiological state multiplicity involving both metabolism and apoptotic death played a key role in this research.

Research involving the accurate calculation of metabolic flux and the analysis of cellular behavior occurring in continuous cultures set the stage for subsequent research on physiological state multiplicity. This phenomena was observed in continuous cultures when at the same dilution rate, two physiologically different cultures were obtained which exhibited similar growth rates and viabilities but drastically different cell concentrations. Metabolic flux analysis conducted using metabolite and gas exchange rate measurements revealed a more efficient culture for the steady state with the higher cell concentration, as measured by the fraction of pyruvate carbon flux shuttled into the tri-carboxylic (TCA) cycle for energy generation. This metabolic adaptation was unlikely due to favorable genetic mutations and was implemented in subsequent research aimed at improving cell culture performance.

A hypothesis stating that mitochondrial physiology and cellular physiology are correlated was tested and confirmed. A mammalian cell population was separated using FACS into subpopulations based on their mean mitochondrial membrane potential (MMP) as measured using the common mitochondrial stain, Rhodamine 123. The MMP sorted subpopulations were subjected to apoptosis inducers, and the apoptotic death was characterized both morphologically through the determination of apoptosis related chromatin condensation and also biochemically through the measurement of caspase-3 enzymatic activity. The results showed dramatic differences in apoptotic death kinetics with the higher MMP subpopulations demonstrating a higher resistance to apoptotic death.

These results were applied in the development of novel fed-batch feeding and operating strategies. The first strategy showed that overfeeding cells later in culture leads to an increase in culture viable cell concentration, viability, and productivity. The second strategy showed that cell populations with a higher mean MMP are able to resist apoptosis during fed-batch culture. These results indicate that mammalian cell populations have considerable flexibility in their ability to redistribute metabolic flux in central carbon metabolism. Furthermore, these cell populations contain subpopulations that vary in their resistance to apoptotic death. The analysis of mitochondrial physiology and metabolic flux led to these discoveries, and these areas will play a key role in future mammalian cell culture research.

Thesis Supervisor: Daniel I. C. Wang
Title: Institute Professor

ACKNOWLEDGEMENTS

At the risk of overlooking someone, I would like to thank a number of people who have contributed to this thesis in ways too numerous to list. Although acknowledgement sections can reach epic proportions (Phys. Rev. Lett. *74*: 2626-2631), I will try to make this as brief and as complete as possible.

First and foremost, I thank Professor Wei-Shou Hu at the University of Minnesota for convincing me that graduate school is a worthwhile endeavor. Not only do I remember your first words to me as a UROP ("Who's funding you?") and your last ("Beware of MIT!") but also all of your helpful advice and encouragement during those four years. Also at the U of M, Dr. Madhusudan Peshwa deserves credit for teaching me the tools of the trade in biochemical engineering, and Sridhar Rao deserves a tremendous amount of thanks for helping me get through the undergraduate ChemE program.

I would also like to express my gratitude to my thesis advisor, Prof. Daniel I.C. Wang, and my thesis committee members, Prof. Gregory Stephanopoulos, Prof. Anthony Sinskey, and Prof. Douglas Lauffenburger. Thank you for soliciting insightful comments and suggestions which were greatly appreciated (sometimes long after the fact). I think that you all uniquely personify the phrase coined by Neil Peart: "Genius is the fire that lights itself."

I would like to express my appreciation to the administrative staff: Janet Fisher and Elaine Aufiero at the Chemical Engineering graduate student office and Lorraine Cable, Audrey Childs, Daniel Darling, Sonia Foster, John Galvin, Joya Gargano, John Langrill, Lynne Lenker, James Leung, Sara Puffer, and Darlene Ray at the BPEC office. These people deserve credit for doing all of the administrative work that graduate students too often take for granted.

The National Science Foundation, the National Institute for Health, and the Biotechnology Process Engineering Center all deserve thanks for generously funding my research.

A majority of my education and entertainment came from my coworkers; they are what make the difference between either enjoying or enduring graduate school. As both an REU and a graduate student, I valued your company: Dawn and Mark Applegate, David Chang, John Chung, Aleks Engel, Javier Femenia, Joydeep Goswami, Sherry Gu, Jean-Francois Hamel, Bryan Harmon, Klaudyne Hong, Mario Jolicoeur, Daniel Kamei, Brian Kelly, Maria Klapa, Bettina Knorr, Mattheos Koffas, John Konz, Stelios Kouvroukoglou, Dan Lasko, Kyong Lee, Steve Meier, Fredrik Möllburn, Gautam Nayay, Chandra Papudesu, Sung Park, Mark Powers, Jakob Rasmussen, Martin Reinecke, Cliff Rutt, Anna Sanfeliu, Eric Scharin, Marc Shelikoff, Troy Simpson, Rahul Singhvi, Araba Lamousé-Smith, Dan Stafford, Dave Stevenson, Gaspar Taroncher, Pat Walton, Stefan Wildt, Bruce Woodson, Kurt Yanagimachi, Inn Yuk, Liangzhi Xie, Jifeng Zhang, and Craig Zupke.

Some extra special "thank you's" for the people who helped with my lab work. The members of the chemostat project team, Robert Balcarcel (a.k.a. Brian and/or Gregg) and Gregg Nyberg (a.k.a. Robert and/or Brian), helped me (a.k.a. Robert and/or Gregg) with a tremendous amount of the continuous culture work described in this thesis. Dr. Mike Cardone also deserves credit for helping me get up to speed on apoptosis research. I would also like to thank Glenn Paradis and Mike Connolly at the Cancer Research Center for their help in the FACS research.

I was able to work with a number of UROPs and REUs who provided help and entertainment in the lab: Gus Blomquist, Anya Freedman, Brad Gray, Muneera Kapadia, Ha Ly, and Suketu Shah.

Outside of the lab, I would like to thank the "E.E. gang," especially Constantine Papageorgiou and Eric Reed, and everyone who has lived at 1 Fifth Street: Jerry Bieszczad, Craig Boyce, Brian Goodlin, Aaron Moment, Seth Rodgers, Jeff Vanness, Rajesh Venkataramani, and Mike Wong. In addition, I would like to thank the Cambridge Community Center for the opportunity to be a tutor.

Finally, I would like to thank my family. I know you still wonder what I do all day, and hopefully this thesis will give you at least some idea. Mom and Dad, thanks for doing all the things that helped me get to this point (I could never possibly list them all), and Linda, thanks for your support and for tolerating my presence (and absence!) over the years.

TABLE OF CONTENTS

LIST OF FIGURES

LIST OF TABLES

1. INTRODUCTION

1.1 Historical Review

Jacob Bronowski cites the biological revolution as "the change from which civilization took off."

> It is usually called the 'agricultural revolution'. But I think of it as something much wider, the biological revolution. There was intertwined in it the cultivation of plants and the domestication of animals in a kind of leap-frog. And under this ran the crucial realization that man dominates his environment in its most important aspect, not physically but at the level of living things - plants and animals (Bronowski, 1976).

This realization of mans' dominance over living things led to thousands of years of conscious manipulation of biological systems though the domestication and selection of animals and crops. However, man also unknowingly used unseen biological systems for his benefit as well as demonstrated in the use of microorganisms in fermentation processes producing beer, wine, and other products. Leeuwenhoek's observation of microscopic "animalcules" in 1676 and Pasteur's discovery that "wine is a sea of organisms" in 1857 led the way for the scientific analysis of these unseen biological systems through modern biology (Prescott et al., 1993).

Although fermentation is an ancient industry, when restricted to the production of chemically defined biological substances, modern biotechnology is considered to be about 100 years old. Biotechnology's early efforts to produce organic chemicals such as acetone and citric acid before and during the First World War led the way for antibiotic and secondary metabolite production during and after the Second World War. The microorganisms used in these production processes were obtained through "what G. Pontecorvo described as a 'prehistoric'

technique: mutation and screening (selection) from the available gene pool" (Prescott et al., 1993). Although these techniques are still used today, they are oftentimes complemented with recombinant DNA technology. Developed in the 1970s, this technology gave scientists the techniques to cut, join, and replicate DNA and reverse transcribe RNA giving them the unprecedented ability to deliver and express foreign DNA in a host cell. In 1980, the first recombinant DNA company, Genentech, announced an initial public offering on Wall Street that resulted in a multimillion dollar market valuation. Soon after, the first recombinant therapeutic protein, insulin, was marketed in 1982, and this opened the way for the modern biotechnology industry.

Many therapeutic proteins are now produced in mammalian cell culture due to the ability of these cells to properly perform post-translational modifications, such as glycosylation, on the protein products. Interferon, tissue plasminogen activator, erythropoietin, and factor VIII are just a few of the products that have helped propel mammalian cell culture derived therapeutic production into becoming a multi-billion dollar industry.

1.2 Motivation

> Biological systems in general, and their interaction with their environment, abound with an overwhelming complexity of detail through which general concepts and relationships cannot readily be perceived. Because of this complexity, many biologists are concerned with details, and have tended to neglect problems associated with integrated systems. On the other hand, engineers who have not yet encountered such complexity in manufacturing facilities are concerned with integrated systems which are just beginning to approach the complexity of biological systems (Tsuchiya et al., 1966).

These comments are still relevant to biochemical engineering today as shown through the differences in how scientific research is conducted in biology and engineering. Molecular biology is still criticized for being too qualitative, detail oriented, and in need of a more quantitative framework for analyzing biological systems (Bailey, 1999; Maddox, 1992). Conversely, engineering is oftentimes not detailed enough for a proper analysis of the complexity involved in biological systems. The current problems in biochemical engineering concerning the minimization of cell death and the maximization of culture cell concentration and productivity illustrate the need for quantitative methodologies designed for the analysis of complex biological systems such as cellular metabolic pathways and regulatory networks and their relations with cellular behavior.

These methodologies have been developed to describe a variety of biological phenomena such as cell cycle control, cell migration, and receptor trafficking (Lauffenburger and Linderman, 1993). In addition, metabolic flux analysis provides another such framework, and cell culture performance can be further improved by analyzing carbon flux in central carbon metabolism to determine key nutrient requirements, potential rate controlling biochemical reactions, and mechanisms that regulate the control of metabolic flux flowing through metabolic reaction networks. This thesis applies metabolic flux analysis to elucidate the physiological state of mammalian cells at different continuous culture environmental conditions with the ultimate goals of identifying environments and operating conditions that result in optimal culture performance and factors that contribute to the regulation of metabolic flux distribution.

One significant source of complexity in biological systems is the tremendous amount of physiological multiplicity and population heterogeneity that occurs even under constant environmental conditions. In biochemical engineering, the observed variance in survival ability

and metabolic adaptation in culture demonstrates the need to provide a methodology to analyze this population heterogeneity. In this thesis, the technique of directed evolution through FACS separation was utilized in order to characterize subpopulations that demonstrate variances in their survival ability, and these findings were then applied in the creation of novel cell culture processes.

1.3 Thesis Objectives

This research was conducted in an effort to quantitate and understand cultured mammalian cell behavior with respect to metabolic flux distribution, population survival heterogeneity, and cell death. In addition to studying the experimental data needed to calculate accurate metabolic fluxes, the physiology and metabolic adaptation of cultured mammalian cells at various growth rates was investigated. Of particular interest was the observed steady state multiplicity, whereby drastically different cell concentrations were observed at the same growth rate and viability. The observed variations in the efficiency of pyruvate utilization in the tri-carboxylic (TCA) cycle for the multiple steady states led to the hypothesis that TCA cycle efficiency variations could be used as a basis for developing strategies for feeding fed-batch cultures and for selecting high mitochondrial activity (high TCA cycle activity) subpopulations for culture inoculums. The presence of steady state multiplicity led to an investigation of culture population heterogeneity, mitochondria, and apoptotic cell death, and subsequent experimental work involved the use of FACS analysis of mitochondrial parameters as a basis for determining the influence of mitochondrial properties on cell death. Since apoptosis accounts for a significant amount of death in mammalian cell cultures, the link between mitochondrial parameters and apoptosis was investigated under both short term conditions involving specific

apoptosis inducing conditions and under the more general long-term apoptosis inducing conditions found in fed-batch cultures.

Specifically, this thesis addresses these objectives:

- What experimental techniques and data are required for accurate metabolic flux calculations?
- How does cellular metabolic flux distribution vary at different cellular growth rates?
- Can variance in metabolic flux distribution result in culture cell concentration and viability variance?
- Does culture population heterogeneity exist with respect to apoptotic death?
- Are mitochondrial properties related to cellular physiology and susceptibility to apoptotic death?
- Can metabolic adaptation and mitochondrial heterogeneity be used in the design of novel fed-batch operational strategies?

1.4 Thesis Organization

This thesis consists of nine chapters. The first three chapters cover a brief discussion of the motivation and objectives for this research, a detailed review of the literature (metabolism, metabolic flux analysis, population heterogeneity, apoptosis, and mitochondria), and a description of the materials and methods used in the research. The next five chapters describe and discuss the experimental results. Specifically, the fourth chapter describes in detail the methodology used in metabolic flux calculations including the formulation of the biomass equation and the methods required for accurate flux calculations. In addition, the methodology required to obtain accurate pentose phosphate pathway metabolic flux data is included in order to demonstrate the additional effort required for accurate metabolic flux analysis tracer

experiments. The fifth and sixth chapters cover the continuous culture experiments performed using the Chinese hamster ovary and hybridoma cell lines. In particular, the fifth chapter emphasizes the metabolic flux distribution around the pyruvate branchpoint at varying growth and death rates, and the sixth chapter describes variances in flux distribution around the pyruvate branchpoint and their relation to steady state multiplicity. The seventh chapter describes the research conducted on the mitochondrial membrane potential sorted cell subpopulations that were characterized for both their morphological and biochemical responses to apoptosis inducers. The eighth chapter applies the results from the previous chapters in the design of novel strategies for fed-batch culture operation. The ninth chapter reviews the main conclusions of this research and gives recommendations for future work. The remaining two sections list the nomenclature and references used in this thesis.

2. LITERATURE REVIEW

2.1 Mammalian Cell Culture

Mammalian cells have been used extensively in the production of therapeutic protein products due to their ability to produce properly folded and glycosylated versions of these proteins which have been correlated with specific activity and circulatory half life (Goochee et al., 1991; Kaufman, 1989; Kaufman et al., 1988). Although yeast, insect, plant, and mammalian cells are capable of glycosylating proteins, only mammalian cells produce glycoforms similar to those required for human therapeutics (Goochee et al., 1991; Kaufman, 1989; Kaufman et al., 1988). Therefore, mammalian cells will undoubtedly serve as the preferred cell type for complex therapeutic protein production.

However, mammalian cell cultures exhibit several complex problems not found in microbial fermentations such as difficulty in achieving high cell concentrations and viabilities and therefore high protein product concentrations. Some of these problems stem from the sensitivity of fragile mammalian cells to their environment resulting in slow growth, poor productivity, low cell concentrations, and necrotic cell death. Cell damage due to hydrodynamic effects in the bioreactor has been shown to contribute to cell death (Hu and Peshwa, 1991). In addition, sparging for bioreactor oxygenation has proven to be another problem resulting in cell death (Jöbses et al., 1991; Meier et al., 1999). Osmolarity, pH, and temperature can also significantly affect the performance of a culture process (Borys et al., 1993; Miller et al., 1988; Ozturk and Palsson, 1991; Xie, 1997). A variety of methods have been proposed to address these problems such as altering the reactor system and reactor operating conditions (Avgerinos et al., 1990; Batt et al., 1990; Hu and Peshwa, 1991).

In addition, the cellular nutrient environment is critical in mammalian cell culture. Mammalian cells need a complex mixture of glucose, amino acids, vitamins, trace metals, and salts (Butler and Jenkins, 1989). In addition, they oftentimes require growth factors and other serum components which activate cell proliferation and provide protection from apoptotic death (Barnes and Sato, 1980; Chung et al., 1997; Glassy et al., 1988). These requirements are rather specific and deviations can cause cell death. In addition, the metabolism of cultured mammalian cells is atypical and can have high rates of aerobic glycolysis, glutaminolysis, and byproduct production (Glacken et al., 1986; Lanks and Li, 1988; Xie, 1997). High glucose and glutamine concentrations result in the production of high levels of waste metabolites such as lactate, ammonia, and alanine illustrating the inefficient utilization of these substrates (Glacken et al., 1986; Hansen and Emborg, 1994; Hassell et al., 1991; Xie, 1997). These factors all contribute to the need to develop novel feeding strategies in order to improve culture viable cell concentrations and to maintain cell viability.

Several hypotheses on the proper way to design and feed medium have been proposed to satisfy mammalian cell culture requirements. Several researchers have suggested that cultures should be controlled at low glutamine and glucose concentrations in order to reduce toxic lactate and ammonium build-up. This strategy resulted in a lower lactate and ammonium production and a subsequent increase in cell concentration (Glacken et al., 1986; Ljunggren and Häggström, 1994). Another strategy involved fortifying the medium with a balanced amount of nutrients in order to achieve high cell concentrations in batch culture. This strategy resulted in an increase in cell density to $1.0*10^7$ viable cells/ml and a five- to eight-fold increase in product concentration even though the lactate and ammonia concentrations were higher than those found in typical cultures (Jo et al., 1990). Medium concentrates and on-line nutrient feeding have also been

utilized in fed-batch processes to improve cell culture performance (Bibila et al., 1994; Zhou et al., 1995). Xie and Wang formulated a strategy that employed a stoichiometric approach toward medium design. Characteristics of the cell line composition were used to formulate a medium in a fed-batch culture. This culture was also controlled at low glucose and glutamine concentrations to reduce byproduct production, and the nutrient feeding was based on the cell growth in the culture. This strategy resulted in viable cell concentrations of up to $1.7*10^7$ viable cells/ml, a twenty-fold increase in product concentration, and a substantial decrease in byproduct concentrations (Xie and Wang, 1994c). These approaches all resulted in higher viable cell concentrations. On the other hand, substantial cell death still occurred at the end of the cultures indicating that these strategies have not completely solved the problem of cell death. In addition, these complex feed medium and feeding strategies as well as the reduction in specific growth rate contribute to the increased culture development and operation time.

The genetic background of the cell line has proven to be another critical parameter for mammalian cell culture, and research has demonstrated the utility of enhancing the cellular genetic controls of the cell cycle and apoptosis (programmed cell death). The expression of recombinant cyclin E in CHO cells stimulated cell progression through the cell cycle and resulted in enhanced proliferation that required no exogenous growth factors (Renner et al., 1995). Furthermore, the addition of a cell cycle arresting agent, rapamycin, to a hybridoma cell line with a deregulated cell cycle resulted in an increase in culture cell concentration, viability, and productivity (Balcarcel, 1999). This strategy was similar to one proposed by Mosser and Massie (Mosser and Massie, 1994) in which the proto-oncogene, *c-myc*, was downregulated to prevent unregulated cell cycle entry. In addition, the overexpression of anti-apoptotic proteins such as Bcl-2 in mammalian cell lines has also increased the culture viability by protecting cells

from apoptotic death triggered by nutrient and growth factor limitations as well as other proapoptotic signals (Adams and Cory, 1998; Chung et al., 1998; Garland and Halestrap, 1997; Goswami et al., 1999; Mosser and Massie, 1994; Simpson et al., 1999; Simpson et al., 1998).

2.2 Modeling Metabolism in Mammalian Cell Culture

2.2.1 Mammalian Cell Culture Modeling

Numerous efforts have been made to increase the efficiency of cell culture processes through model-based culture design and control. The most common strategy involves utilizing unstructured and structured models to optimize bioreactor operations. The unstructured or empirical models have been used most often due to their simplicity, but they can only be used for a limited range of operating conditions. Structured models are based on a detailed description of cellular metabolism and can be employed for a wider range of process conditions. However, these models are oftentimes both complicated and incomplete, and they do not describe the complex and oftentimes unknown regulatory mechanisms that govern growth behavior (Pörtner and Schäfer, 1996; Tsuchiya et al., 1966). A few models, such as E-CELL, have attempted to describe entire cells by including not only metabolic reactions but protein-DNA interactions and gene expression, but these models are still too simplified to fully account for the regulation of significant cellular processes (Tomita et al., 1999).

An example of unstructured cell culture model development was presented by Glacken et al. (Glacken et al., 1988; Glacken et al., 1989a; Glacken et al., 1989b). This model was formulated and optimized by combining an unstructured initial growth rate model with transient data obtained through additional experiments. Fractional factorial experiments were used to reduce the number of significant culture variables in the model. The chosen independent variables: glucose, glutamine, serum, ammonium, lactate, and basal DMEM concentration, were

reduced to two major factors: serum and ammonium. The initial growth rate was then expressed as a function of these two major factors along with the glutamine concentration due to the contribution of glutamine to ammonium levels through degradation. Ammonium was determined to be a strong, noncompetitive inhibitor whereas lactate was observed to be a weak inhibitor of the initial growth rate (Glacken et al., 1988). The model was then expanded to include serum degradation which was attributed to thiol chemistry and the culture redox state (Glacken et al., 1989a). Finally, this model was applied in the simulation of fed-batch reactor runs. For these simulations, the unstructured model was modified with additional equations to account for the time lag associated with medium composition changes. This model successfully described the transient behavior of a fed-batch process, but was unable to predict productivity (Glacken et al., 1989b).

Numerous other unstructured models have been formulated to describe cell culture processes. Monod-type equations form the basis of these models with glucose and glutamine serving as limiting substrates and lactate and ammonium serving as inhibiting compounds. However, these models are generally criticized for their significant error and unpredictable nature attributed to a lack of understanding about fundamental aspects of cellular metabolism (Pörtner and Schäfer, 1996). In fact, this variability is most likely due to the unpredictability associated with the general lack of understanding of metabolic regulation and its relations with cellular physiology. Furthermore, this variability can be associated with physiological state multiplicity, and this point is discussed in more detail in chapters six, seven, and eight.

Several structured models have been proposed in order to incorporate a more detailed description of cellular metabolism. Batt and Kompala (Batt and Kompala, 1989) presented one excellent example of such models. Their compartment-type structured model was based on

cellular metabolic reactions and lumped intracellular constituents into metabolic pools expressed as fractions of the biomass. This enabled them to calculate the instantaneous specific growth rate. The pools consisted of cellular amino acids, nucleotides, proteins, and lipids, secreted lactate, ammonium, and product, and substrate glucose, glutamine, and medium amino acids. The system of dynamic equations was used to simulate mammalian cell culture growth dynamics. Under both steady state and transient conditions, the researchers obtained good agreement with experimental data although the accuracy could clearly be improved by adding more metabolic regulatory information (Batt and Kompala, 1989).

Another structured modeling technique involves modeling cell growth as an optimum process. This model assumes that organisms are optimal strategists that choose substrates that will maximize their growth. The metabolic regulatory control is deduced as being the "optimal solution to a problem of resource allocation for achieving maximal growth" (Bailey and Ollis, 1986). This "cybernetic model" has been applied successfully in describing and matching experimental data for diauxic and triauxic microbial growth (Kompala et al., 1986).

The structured and unstructured models typically used to describe and rationalize culture data and cell growth are oftentimes not clear due to the large number of parameters and are not informative since they rely on assumptions concerning cellular behavior (Pörtner and Schäfer, 1996; Zeng et al., 1998). In fact, the unpredictable nature of mammalian cell culture is extremely difficult to model through current methodologies due to the lack of understanding of actual *in-vivo* metabolism and metabolic regulation (Pörtner and Schäfer, 1996). In addition, these models oftentimes make no attempts to incorporate or even recognize features of metabolic regulation (Bailey and Ollis, 1986). Furthermore, cell death and its relations with metabolism are still not addressed, particularly in the case of programmed cell death or apoptosis. Much of

this understanding of actual *in-vivo* metabolism and metabolic regulation under culture conditions can be obtained through a methodology that integrates metabolite exchange rates and shows their relations to cellular physiology and behavior. The information obtained though this framework could then be incorporated into more accurate metabolic models that would allow for more realistic models designed for bioreactor operation optimization.

2.2.2 Metabolic Flux Analysis

Metabolic flux analysis provides such a framework, and cell culture performance can be further improved by analyzing carbon flux in central carbon metabolism to determine key nutrient requirements and potential rate controlling biochemical reactions. Prior metabolic research has elucidated metabolic reactions in the framework of biochemical networks. Metabolic flux analysis provides the methodology for analyzing these metabolic networks and has been applied in the quantitation of physiological states and the interpretation of experimental data in addition to metabolic engineering, optimal medium development, process design, and process optimization (Varma and Palsson, 1994). In short, flux analysis provides researchers with a useful tool to extract additional information from cell culture data that can be utilized in cell culture modeling and design.

However, metabolic flux control is still poorly understood due to the complexity of biological systems and the limited availability of *in-vivo* flux data. Previous research has demonstrated that large variations in metabolic flux and flux distribution can result even when *in-vitro* measured enzyme activities exhibit little change (Vriezen and van Dijken, 1998). This shows a strong dependence of metabolic flux on the *in-vivo* regulation of enzyme activity and not the *in-vitro* assayed activity. Dynamic models of *in-vivo* metabolism have been attempted, but they require extensive enzyme kinetic and regulatory data (Joshi and Palsson, 1989a; Joshi

and Palsson, 1989b; Joshi and Palsson, 1990a; Joshi and Palsson, 1990b). Furthermore, the application of *in-vitro* enzyme kinetics to *in-vivo* kinetics ignores numerous *in-vivo* aspects of enzyme regulation. Enzymatic specific activity can be regulated through allosteric effects, activators, inhibitors, and covalent modification. The enzyme concentration can be controlled through transcription and translation regulatory mechanisms. Finally, cellular microenvironments involving multi-enzyme complexes and membrane associated enzymes and enzyme complexes all contribute to the *in-vivo* regulation of metabolic flux (Liao and Delgado, 1993). Modeling and simulation environments for biochemical and genetic processes have been developed, but these models describe only simplified, hypothetical cells (Tomita et al., 1999). These observations caste doubt on the usefulness of strictly analytical approaches toward the analysis of real biological systems.

Numerous attempts have been made to model *in-vivo* metabolic reaction dynamics through empirical measurements to determine metabolic flux control. Recently, emphasis has been placed not on the flux control exercised by individual enzymes but rather on metabolic pathway flux control, and this systems approach has been termed metabolic control analysis (Heinrich and Rapoport, 1974; Kacser and Burns, 1973). This method states that the key to understanding metabolic network regulation is through the quantitation of a network's response to a parameter perturbation (Liao and Delgado, 1993). Elasticity, response, and control coefficients are all used to quantify these responses. Furthermore, these coefficients are related to one another through various theorems. This methodology has been applied to obtain metabolic network control data through genetic perturbations (gene dosage and expression level) and environmental perturbations (chemical control of enzyme levels and inhibition titration). These techniques were applied in the analysis of microorganism metabolism and mitochondria

respiration (Liao and Delgado, 1993). This framework was extended through a top-down approach in which groups of reactions are analyzed for their control on metabolic reaction networks (Stephanopoulos and Simpson, 1997). These techniques provide a useful framework to analyze metabolic regulation in real biological systems. However, a complete analysis requires a considerable amount of experimental work to obtain network perturbations, and obtaining this data has proven to be rather difficult (Liao and Delgado, 1993; Varma and Palsson, 1994). Furthermore, these results are valid for a narrow range of operating conditions. Finally, large flux control coefficient values do not imply that the specific enzyme controls regulation through feedback control loops (Stephanopoulos and Vallino, 1991).

Metabolic flux analysis involving mass balances or metabolite balancing is particularly useful in the investigation of regulated cellular metabolism under varying environmental conditions when specific enzyme regulation is not known and one does not have the resources for network perturbations to conduct metabolic control analysis. This framework involves the steady state or pseudo steady state analysis of metabolic pathways where mass balances are applied to a stoichiometric network model of major metabolic reactions. Measured extracellular production and consumption rates are combined with this reaction network, a least squares analysis is performed, and then the metabolic fluxes are calculated (Stephanopoulos et al., 1998). This technique can yield a significant amount of information on metabolic fluxes, and enables one to conduct principle node and flux distribution analysis. This technique has been applied in a number of situations, and nutrient, waste metabolite, dissolved oxygen, and peptide hydrolysate concentrations have all been shown to cause metabolic responses that can be quantitated using flux analysis resulting in information concerning potential feeding strategies, medium

formulations, and genetic manipulations necessary to improve cell culture performance (Bonarius et al., 1996; Bonarius et al., 1998a; Nyberg et al., 1999a; Zupke et al., 1995b).

One significant problem encountered in metabolite balancing techniques involves the analysis of cyclic metabolic pathways which result in linearly dependent or singular networks (Bonarius et al., 1996; Bonarius et al., 1998b; Vallino, 1991). One method that solves this problem is to measure co-metabolites produced in cyclic pathways. The pentose phosphate pathway and the TCA cycle still pose a problem due to the fact that they both produce CO_2, and this requires the addition of constraints such as assuming a pentose phosphate pathway activity or maximizing ATP or NAD(P)H production in the solution (Bonarius et al., 1998b).

One of the principle applications of metabolic flux analysis has been to not just obtain metabolic fluxes but also to analyze branchpoint flux control through the calculation of flux split ratios (Stephanopoulos and Vallino, 1991). A comparison of metabolic flux distribution for various environments enables one to classify key network junctions as being either flexible, weakly rigid, or rigid nodes (Stephanopoulos et al., 1998). Furthermore, alternative pathways and maximum theoretical yields can be determined through flux analysis (Stephanopoulos et al., 1998).

Metabolite balancing combined with isotopic tracers has also been devised for the analysis of intracellular flux *in-vivo* (Mancuso et al., 1998; Mancuso et al., 1994; Portais et al., 1993; Sharfstein et al., 1994; Wiechert and de Graaf, 1996; Zupke and Stephanopoulos, 1995a). Isotopic tracers detectable either through radioactivity measurements or NMR are incorporated into metabolites depending upon the fluxes of the corresponding biochemical reactions. Therefore, the latter can be, in principle, determined from measurements of isotope enrichment of selected metabolites.

Isotope enrichment has been applied in the analysis of a number of metabolic networks. For example, ^{13}C enrichment of extracellular lactate was used to validate flux estimates obtained through metabolite balancing (Zupke and Stephanopoulos, 1995a). Another set of experiments utilized [1-^{13}C]glucose to quantitate the effect of the medium glutamine concentration. This work indicated that glutamine levels have a significant effect on energy metabolism only when abruptly changed; the fact that no changes in energy metabolism occurred for gradual glutamine level perturbations led to the hypothesis that futile cycles exist in metabolic networks (Mancuso et al., 1998). In another series of experiments, researchers directly determined that lactate carbon comes predominantly from glucose and that the pentose phosphate pathway flux is much lower than the glycolytic flux when cells are cultured under low growth rate conditions. Additional findings were that the malate shunt flux is high and that pyruvate carbon flows through the pyruvate dehydrogenase complex and not through pyruvate carboxylase. Other isotope experiments yielded data on glycolysis, biosynthesis, and metabolite exchange with TCA cycle intermediates (Mancuso et al., 1994; Sharfstein et al., 1994).

The data from ^{13}C enrichment can be further analyzed for NMR spectrum fine structure to determine isotopomer levels. This method can be extremely powerful due to the additional information obtained by determining the actual position of a tracer molecule within a metabolite (Christensen and Nielsen, 1999; Klapa et al., 1999; Park et al., 1999; Wiechert and de Graaf, 1996; Wittmann and Heinzle, 1999). These isotopomers can be distinguished from one another through NMR spectrum fine structure analysis. A metabolite with n carbons can result in 2^n isotopomers resulting in a significant amount of data. Although more isotopomer fractions can be analyzed through NMR, mass spectroscopy has become increasingly popular in the analysis of these isotopomers (Christensen and Nielsen, 1999; Wittmann and Heinzle, 1999).

Figure 2-1 summarizes the various experimental methods one can use to obtain metabolic flux data through the use of a simple example metabolic network described in Wiechert and de Graaf (Wiechert and de Graaf, 1996). In the first illustration, the production and consumption rates of the metabolites A, F, G, H, and I can be used to obtain the network metabolic fluxes through metabolite balancing techniques. The second illustration shows the fate of each carbon in the reaction network as well as the fate of a substrate isotope tracer (A) when placed in the network. The shading of the carbon atom represents the relative carbon enrichment and shows how the various distribution of isotope enrichment can be used to determine metabolic flux. Finally, the third illustration shows the various isotopomers that result from the addition of an isotope tracer. These isotopomers can yield more detailed data due to the ability to determine the exact fate of each isotope tracer carbon atom in the metabolic reaction network.

Although techniques that utilize isotope tracers are powerful in determining metabolic flux, the low sensitivity of NMR as well as the difficulties posed by the analysis of radioactive isotope incorporation into metabolites inhibit the general use of these methods for cell culture flux analysis. High cell densities are required for isotope label analysis resulting in the need to use hollow-fiber bioreactor systems (Mancuso et al., 1998; Mancuso et al., 1994; Sharfstein et al., 1994). Additionally, the cellular growth rate in these reactors is extremely low which may present metabolic flux information that is not relevant for cells growing under normal culture conditions. Furthermore, reaction reversibility has been shown to complicate flux determination in certain pathways due to label redistribution although this reversibility could be used to obtain useful information concerning metabolic phenomena such as futile cycles (Follstad and Stephanopoulos, 1998; Wiechert and de Graaf, 1997a; Wiechert et al., 1997b). This indicates

I. Metabolite Balancing

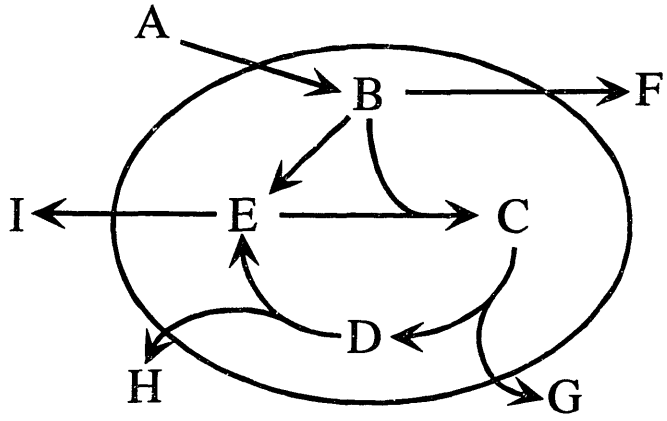

II. Carbon Isotope Enrichment

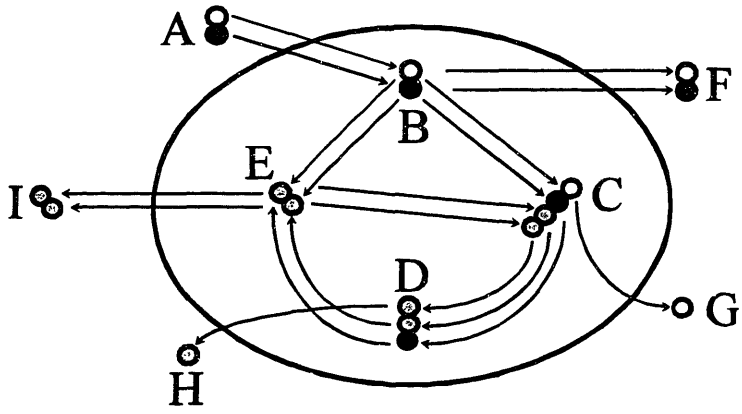

III. Isotopomer Analysis

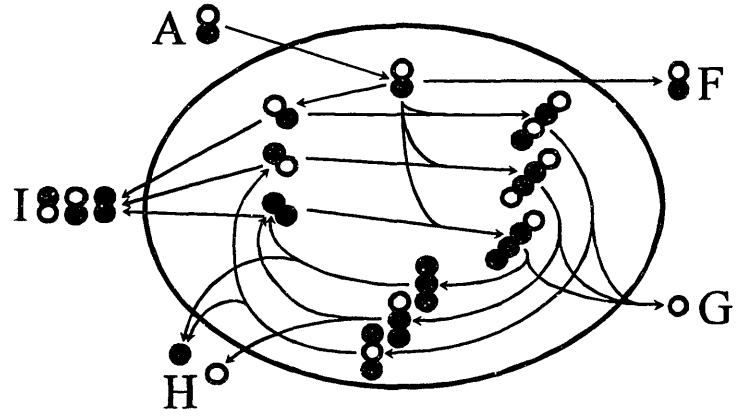

Figure 2-1. Techniques for metabolic flux analysis. A simple example metabolic network described in Weichert and de Graaf (1996) illustrates the three main techniques used for metabolic network analysis: metabolite balancing, carbon isotope labeling, and isotopomer analysis.

that a complete and thorough analysis must be conducted whenever one uses isotope labeled substrates in order to obtain valid data.

In general, for established metabolic networks, metabolite material balancing has proven to be a quick and effective way to determine metabolic fluxes and flux distribution patterns while requiring no kinetic or regulatory information. The use of redundant measurements enhances the usefulness of metabolite balancing by enabling one to determine the consistency of a data set and locate the source of gross inconsistencies among measurements or network bioreactions. This technique verifies and improves the accuracy of metabolite balancing through the use of extra constraints or measurements for a metabolic network. Statistical tests are utilized to not only detect errors but also to diagnose the source of these errors (Nyberg et al., 1999a; van der Heijden et al., 1994a; van der Heijden et al., 1994b; Wang and Stephanopoulos, 1983; Zupke and Stephanopoulos, 1995a).

2.3 Mammalian Cell Continuous Culture

Although flux analysis can be carried out using data obtained during transients (Zupke et al., 1995b; Zupke and Stephanopoulos, 1995a), continuous culture systems are preferable as they allow one to study cultured cells in controlled, well-defined environments where they can reach a metabolic steady state (Stephanopoulos et al., 1998; Wiechert and de Graaf, 1996). This contrasts sharply with batch and fed-batch culture where the conditions are constantly changing resulting in confusing data sets that can lead to incorrect conclusions concerning relations between cellular physiology, metabolism, and other culture parameters. In continuous culture, the various reactor residence times approximate the different environments that cells encounter both in the early and late portions of batch and fed-batch culture runs which allow a more precise determination of environmental influences on cellular physiology. Previous continuous culture

work involving mammalian cells has covered a wide variety of conditions including nutrient concentrations, dissolved oxygen levels, pH, dilution rate, and other variable reactor parameters (Hayter et al., 1992a; Hayter et al., 1993; Hayter et al., 1992b; Jan et al., 1997; Martens et al., 1993; Meijer and van Dijken, 1995; Miller et al., 1988). In addition, continuous culture has been utilized in the formulation and testing of Monod unstructured models in order to obtain empirical data describing cultured cell kinetic behavior (Frame and Hu, 1991a). Such work has yielded considerable information on metabolite production and consumption rates, cellular growth, and productivity at various reactor residence times and environmental conditions.

Perturbations involving the analysis of transients in continuous cultures were also conducted in an effort to determine the regulatory architecture of cultured cell metabolism. In theory, metabolic control analysis can be used with this transient data to determine this metabolic regulation (Delgado and Liao, 1992b; Delgado and Liao, 1992a). Oftentimes, no metabolic control analysis or flux analysis is performed in continuous culture research, but the effects of transients in input glucose, glutamine, amino acids, and vitamins concentrations have all been analyzed for mammalian cell continuous cultures (Hiller et al., 1994; Miller et al., 1989a; Miller et al., 1989b). Metabolic flux analysis has been performed on some mammalian cell continuous culture data that involved the analysis of peptide hydrolysates as well as the influence of ammonia levels on cellular metabolism (Bonarius et al., 1996; Bonarius et al., 1998a; Nyberg et al., 1999a).

Continuous culture reactor systems have also been utilized to examine cellular productivity for various environments and residence times. Although several researchers have indicated that specific productivity increases or remains constant with the specific growth, most researchers have data that support the hypothesis that an increase in specific productivity results

from a decrease in growth rate (Linardos et al., 1991; Miller et al., 1988). In addition, specific productivity has been observed to decline over the course of a continuous culture, and this decline was attributed to the formation of a nonproducing subpopulation of cells (Frame and Hu, 1991a; Frame and Hu, 1991b; Frame and Hu, 1990). Although the formation of nonproducing cell lines is oftentimes attributed to chromosome deletions, other experimental data have supported the hypothesis that mRNA translation is the source of the problem (Köhler et al., 1976).

2.4 Physiological Multiplicity and Population Heterogeneity in Biological Systems

The loss of antibody productivity due to the rise of a subpopulation of non-producing cells in continuous culture illustrates how selection dynamics can occur in a continuous culture resulting in a potentially evolving biological system. Modeling the behavior of cells in continuous culture has been performed since the 1960's, but only recently have studies presented thorough theories that demonstrate the potential for sustained oscillations and multiple steady states (Xiu et al., 1998). These modifications to the older theories involved the realization that models based on Monod kinetics are not acceptable for all situations and that metabolic pathway regulation must be taken into account. One recent theoretical analysis of continuous culture demonstrated how multiplicity can exist in a continuous culture system where product inhibition along with enhanced productivity under high substrate levels cause multiple steady states. In addition, product formation and inhibition can lead to oscillatory behavior (Xiu et al., 1998). This oscillatory behavior was also predicted using stability analysis performed on models that contain more structure than the Monod models (Bailey and Ollis, 1986).

Competition for a limiting substrate, changes in clumping characteristics, and production of an inhibitor are just a few of the ways subpopulations may compete with one another in

continuous cultures. "Specific selection" refers to a known mutation in a cell line, whereas "non-specific selection" or "periodic selection" refers to a situation in which the genes responsible for the selection are unknown and its occurrence is partly unpredictable (Dykhuizen and Hartl, 1983). Mutational changes in *Escherichia coli* and *Saccharomyces cerevisiae* are reproducible in several cases in which the selected mutants obtained from replicate glucose substrate continuous culture experiments have predictable changes with a defined genetic and physiological basis (Appenzeller, 1999; Dykhuizen and Hartl, 1983). Furthermore, other researchers discovered high temperature adaptation is reproducible even at the DNA sequence level. However, other evolutionary forces such as maltose substrate feeding and bacteriophage infection led to unpredictable phenotypes and genotypes suggesting that numerous complexities are involved in this issue (Appenzeller, 1999; Dykhuizen and Hartl, 1983).

These observations point to one of the most important questions in research on evolution: how much of the results of evolution are the consequence of either chance or adaptation? In other words: is evolution reproducible? Oftentimes, at the level of adaptive performance and phenotype, evolution appears to be reproducible with similar cellular physiologies resulting from similar environmental stresses (Dykhuizen and Hartl, 1983). However, on the genetic scale, evolution is less reproducible as demonstrated when the adapted subpopulations are exposed to a new environment that results in variability in the survival for each subpopulation. However, in some cases genetic changes that are a result of evolution and selection are predictable, even at the DNA sequence level (Appenzeller, 1999).

Population heterogeneity can result from a number of mechanisms. Development or differentiation can play a role in heterogeneity in which sister cells are not identical in morphological and / or biochemical characteristics. This phenomenon, termed "asymmetric cell

division," has been studied in a wide number of cell types such as *Bacillus subtillis*, *Saccharomyces cerevisiae*, *Caenorhabditis elegans*, and *Caulobacter crescentus*. The mechanism behind this developmental heterogeneity can involve intrinsic properties such as the partitioning of molecules (membrane proteins or RNA) in specific cellular regions before cellular division causing the sister cells to have different physiologies. In addition, asymmetry in the cell division plane involving the orientation of the mitotic spindle can contribute to asymmetric cell division as well. Cell signaling can also play a role in which cells differentiate after they have divided (Horvitz and Herskowitz, 1992). However, determining the exact mechanism of asymmetric cell division can be extremely difficult due to the complexity involved in keeping track of individual cells (Jan and Jan, 1998).

Population heterogeneity can also result through non-developmental mechanisms. Recessive mutants can form and survive although they are not as robust as the wild-type cell line. Single nucleotide substitutions, DNA frameshifts, genetic "hotspots", and jumping genes can all contribute to the formation of new mutant subpopulations (Crow, 1983). Subpopulation selection can occur within the context of sexual reproduction according to the Hardy-Weinberg rules of heredity with the resulting heterogeneous population forming as a result of the equilibrium between the forces of selection and mutation (Crow, 1983). Additionally, a number of biological phenomena have been attributed to threshold mechanisms in which a sensitive biological switch converts a cell from one physiological state to another (Chung and Stephanopoulos, 1996). Although theoretical deterministic models can explain population heterogeneity, the non-uniqueness of the model solutions suggests that chance plays a role in the appearance of heterogeneity in which slight changes in the levels of certain factors results in

macroscopic physiological changes (Chung and Stephanopoulos, 1996; Spudich and Koshland, 1976).

Cell populations that are genetically homogeneous and contained in a homogeneous environment still exhibit population heterogeneity which is not a function of variances in the extracellular environment or cell cycle (Spudich and Koshland, 1976). Non-genetic population heterogeneity is believed to be caused by differences in transcriptional state controlled by threshold mechanisms resulting in the induction or repression of genes (Dykhuizen and Hartl, 1983). This hypothesis is supported by the recent finding that many genetic regulatory compounds operate at low concentrations, and this results in large fluctuations in genetic regulation and translation (McAdams and Arkin, 1999; McAdams and Arkin, 1998). Also, cells characterized by specific morphological features still vary in functionality. For example, pancreatic β-cells demonstrate heterogeneity in glucose responsiveness *in-vitro* (Pipeleers, 1992). All of these observations indicate that the assumption that a cell culture contains a homogeneous population lacks both experimental (Horvitz and Herskowitz, 1992; Jan and Jan, 1998; Pipeleers, 1992; Spudich and Koshland, 1976) and theoretical (Chung and Stephanopoulos, 1996) support.

2.5 Mitochondria and Oxidative Phosphorylation

Virtually all eukaryotic cells contain mitochondria which are organelles that contain a number of critical cellular components such as the respiratory chain and other enzymes required for the TCA cycle and fatty acid oxidation. An endosymbiotic partnership involving the combination of an oxygen-respiring ancestor of modern purple bacteria with mastigotes resulted in the creation of a protoeukaryotic cell with the endosymbiotic bacteria eventually evolving into mitochondria (Margulis, 1996; Margulis, 1998). These semi-autonomous organelles are

responsible for a large number of important cellular functions such as the regulation of metabolism and energetics as well as the regulation of apoptosis (programmed cell death). The mitochondrial matrix contains the enzymes involved in the citric acid or tricarboxylic (TCA) cycle, and mitochondria are responsible for the generation of the majority of cellular ATP through oxidative phosphorylation carried out in the respiratory assemblies situated in the inner mitochondrial membrane (Mitchell, 1979; Stryer, 1988).

Mitochondria contain both an inner and outer membrane. Inside the inner membrane is the mitochondrial matrix which contains the enzymes required for pyruvate and fatty acid oxidation. The inner membrane is folded into numerous ridges called cristae which allow for a significant increase in membrane surface area which in turn allows for a high respiratory chain activity. In fact, the total cellular inner mitochondrial membrane surface area can be over seventeen times larger than the total plasma membrane area (Lodish et al., 1995). The outer membrane is permeable to small molecules and ions whereas the inner membrane is virtually impermeable to all ions and other polar molecules. Molecules and proteins can be transported across the inner membrane through specific protein carriers (Stryer, 1988).

Mitochondria electron transport (oxidative phosphorylation) involves three main complexes and is illustrated in figure 2-2. The first complex, NADH-Q reductase, accepts electrons from NADH and transfers them to a second complex, cytochrome reductase, through ubiquinone. Ubiquinone also accepts electrons from $FADH_2$. Cytochrome reductase transfers the electrons to cytochrome *c* which then transfers them to cytochrome oxidase. There, the electrons are transferred four at a time to molecular oxygen resulting in the production of two water molecules. The electrons are transferred though each complex and carried through iron-sulfur and heme complexes. Electron transfer can be inhibited at each of the complexes through

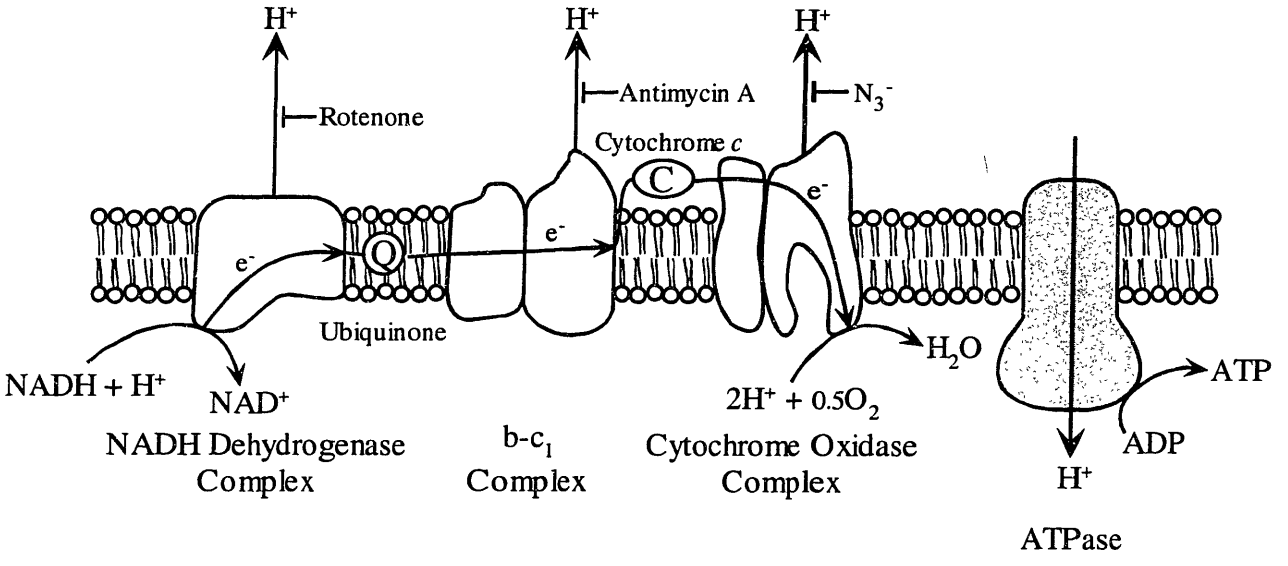

Figure 2-2. Mitochondria electron transport. In the inner mitochondrial membrane, electrons are transferred through a series of protein complexes resulting in the pumping of protons out of the matrix. ATPase uses the proton gradient to generate ATP. Various compounds can specifically inhibit each protein complex.

the use of the specific compounds shown in figure 2-2. The electron transfer occurring through each complex causes the pumping of protons out of the mitochondrial matrix. These protons flow back into the mitochondrial matrix through ATPase resulting in ATP generation (Mitchell, 1979; Stryer, 1988). Protons may also leak across the inner mitochondrial membrane resulting in a lower effective ATP production efficiency (Brand et al., 1994).

Mitochondrial membrane potential (MMP) can not be measured using microelectrodes due to their small size, but it can be measured using membrane permeable lipophilic cationic dyes such as Rhodamine 123 (Rh123), 3,3'-dihexyloxacarbocyanine iodide ($DiOC_6$), 5,5',6,6'-tetrachloro-1,1',3,3'-tetraethylbenzimidazolylcarbocyanine iodide (JC-1), (Benel et al., 1989; Juan et al., 1994; Salvioli et al., 1997). These dyes incorporate according to the Nernst equation (equation 2.1).

$$\Delta p = \Delta\Psi_m + \frac{RT}{nF}\Delta pH \qquad (2.1)$$

The proton motive force (Δp) consists of both an electric ($\Delta\Psi_m$) and chemical activity (ΔpH) potential. The values for each potential are approximately 160 - 180 mV for the mitochondrial membrane potential ($\Delta\Psi_m$) and 60 mV for the pH gradient component (Kamo et al., 1979; Lodish et al., 1995; Mitchell, 1979). Researchers have experimentally verified a direct correlation between to the electric potential component of the proton motive force (mitochondrial membrane potential) and Rh123 cellular uptake (Chen, 1988; Emaus et al., 1986). Electron transport inhibitors, such as azide, antimycin A, or rotenone acting as shown in figure 2-2, drastically reduce Rh123 uptake. In addition, azide and oligomycin together completely eliminate Rh123 uptake unlike other mitochondrial membrane potential stains which can still incorporate to some small degree into mitochondrial membranes without the presence of a membrane potential (Chen, 1988). Rh123 is frequently used in experiments due to its low

toxicity, and it has been utilized to develop relations between mitochondrial membrane potential and cell growth, cell differentiation, cell motility, and concentrations of agents that influence membrane potential (Chen, 1988; Ferlini et al., 1995).

Most eukaryotic cells have a mitochondrial volume of 15 - 25% (Bereiter-Hahn and Vöth, 1994; Lodish et al., 1995; Stryer, 1988). Mitochondria have been observed to associate with energy consuming cellular structures such as the nucleus, rough endoplasmic reticulum, and plasma membrane. This heterogeneity in cellular location indicates that adenine nucleotide diffusion may be limiting resulting in cytoplasmic ATP gradients. This hypothesis is supported by the fact that cells contain intracellular pH and O_2 gradients and that mitochondrial activity can vary for those mitochondria situated centrally in a cell versus those located peripherally. These gradients may be beneficial in situations such as local hypoxia around the nucleus in order to reduce the number of free radicals that can attack nucleic acids (Bereiter-Hahn and Vöth, 1994). In addition, this heterogeneity can vary as a function of cell-cell contact and intracellular acidic vesicle location (Diaz et al., 1999). Mitochondria have also been observed to change shape and location and can move at a speed of 2 - 30 μm/min (maximum speed of 100 μm/min). Mitochondria can respond to local changes in ATP levels induced through microinjection, and this response varies depending on the cellular metabolic state (Bereiter-Hahn and Vöth, 1994). These observations illustrate the dynamic behavior mitochondria have which enables them to respond to cellular needs.

Over the course of the cell cycle, mitochondrial mass and volume doubles. Mitochondrial biogenesis occurs mostly in the G1 phase of the cell cycle but can occur in the late S phase. Imbalances between mitochondrial proliferation and cell growth have been observed indicating that the mitochondrial growth rate differs from the cellular growth rate. This

mitochondrial growth rate can also vary with the cell cycle and cellular metabolic state (James and Bohman, 1981).

As mentioned previously, functional heterogeneity for mitochondria within a single cell has been observed. This means that experimental data collected using one mitochondrial subpopulation isolated from cells may not represent the actual intracellular distribution of the mitochondrial properties being studied. For example, within the same mitochondrial population, various subpopulations of mitochondria that were isolated through density gradient centrifugation had different mitochondrial membrane potentials (MMP) and other morphological and biochemical features that varied as a function of the metabolic state of the cell (Cossarizza et al., 1996). At the single organelle level under membrane depolarization conditions, a small class of mitochondria that still maintain a high membrane potential have been observed (Diaz et al., 1999). Also, the physiological environment contributes to the appearance of various classes of mitochondria that differ in membrane potential even when size and density changes are taken into account (Cossarizza et al., 1996; Petit et al., 1990).

2.6 Apoptosis

Recently, cell death has received significant attention due to the discovery that apoptosis or programmed cell death is accomplished through specialized and highly regulated cellular mechanisms. This complex series of events involves the active participation of cell surface receptors, proteases, organelles, and other cellular components. This active process contrasts with the conventional view of cell death, termed necrosis, in which violent environmental conditions cause plasma membrane rupture and disintegration. A typical pattern of necrosis, coagulation necrosis, involves the denaturation and coagulation of cellular protein as a result of ischemia, hypoxia, chemical toxins, infection, and trauma, whereas a different type of necrosis,

colliquative necrosis, occurs when tissue becomes rapidly liquefied due to violent damage (Buja et al., 1993). Apoptosis, on the other hand, causes distinct morphological changes in which chromosomal DNA condenses and fragments, the cell membrane blebs, and finally apoptotic vesicles begin to form causing the cell to fragment into numerous apoptotic bodies. Cellular DNA is also cleaved at linker regions producing 180 base pair fragments which show up as a DNA ladder on gels of extracts taken from apoptotic cells (Hale et al., 1996). Apoptosis can also be characterized by additional, less obvious cellular changes. The mitochondrial membrane potential drops early on in the apoptotic death pathway. In addition, the plasma membrane asymmetry breaks down, causing phosphatidylserine to translocate to the outer cell surface. Caspases, or intracellular proteases, are also activated which cleave specific sites on specific proteins which cause apoptosis related morphological changes. Cytochrome *c*, apoptosis inducing factor (AIF), and other proteins that are either activated in the cytosol or released from mitochondria also contribute to the activation of caspases (Bedner et al., 1999).

Apoptosis can be triggered through a variety of cellular genetic or chemical perturbations that affect the cell surface, cytosol, cytoskeleton, nucleus, and intracellular signaling pathways (Wertz and Hanley, 1996). Tumor necrosis factor, reactive oxygen species, cytotoxic agents, mitogenic oncogenes, and insulin and IGF-1 withdrawal are just a few of the vast number of apoptosis inducing stimuli (Alnemri, 1999; Ashkenazi and Dixit, 1998; Wertz and Hanley, 1996; Yang et al., 1996). In mammalian cell culture, nutrient deprivation as well as growth factor deprivation contribute to apoptosis (Chung et al., 1998; Simpson et al., 1998). Mitochondrial electron transport chain inhibitors also induce apoptosis (Wolvetang et al., 1994). The diversity of apoptosis inducing stimuli and the prevalence of apoptosis occurring in a variety of cell types have caused a dramatic rise in the study of this mode of cell death. Furthermore, research is

conducted not only on the prevention of apoptosis occurring in mammalian cell culture but also in the induction of apoptosis in cancerous cell lines.

Several genes have been implicated in the mediation and modulation of apoptosis. The initial research in this area that was aimed at determining the genetic players of apoptosis was performed on the nematode *Caenorhabditis elegans*. The *C. elegans* genes, *ced-3* and *ced-4*, promote apoptosis and *ced-9* prevents apoptosis, and a number of mammalian genes homologues have been discovered (Hale et al., 1996; Steller, 1995). One of the first oncogenes that was discovered to have proapoptotic activity was *c-myc*. Deregulated *c-myc* is associated with cancer, cellular proliferation, and the loss of cell cycle control (Evan and Littlewood, 1998; Williams and Smith, 1993). Experimental evidence indicates that cell renewal and cell death are linked demonstrating that cell proliferative and apoptotic pathways are coupled. The *p53* tumor suppressor gene encodes for a DNA transcription factor that is inactive in numerous cancers indicating that this gene is oftentimes required to prevent the proliferation of somatic cells. *p53* activation causes one of two responses: growth arrest and apoptosis. This response depends upon the cell type, cellular environment, and other factors (Evan and Littlewood, 1998). The *bcl-2* gene family is homologous to *ced-9* in *C. elegans* and is linked to apoptosis. This gene family contains both pro and antiapoptotic genes, and *bcl-2* has been used extensively to enhance cell resistance to apoptosis (Adams and Cory, 1998; Chung et al., 1998; Garland and Halestrap, 1997; Goswami et al., 1999; Hockenbery, 1995; Mosser and Massie, 1994; Simpson et al., 1999; Simpson et al., 1998; Steller, 1995; Vaux et al., 1988; Williams, 1991).

The general mechanism of apoptosis is presented in figure 2-3. This figure illustrates the basic outline of two apoptotic pathways that have been elucidated in the literature. The first pathway involves death receptors, such as Fas, TNFR1, or DR3, in which a ligand binds to the

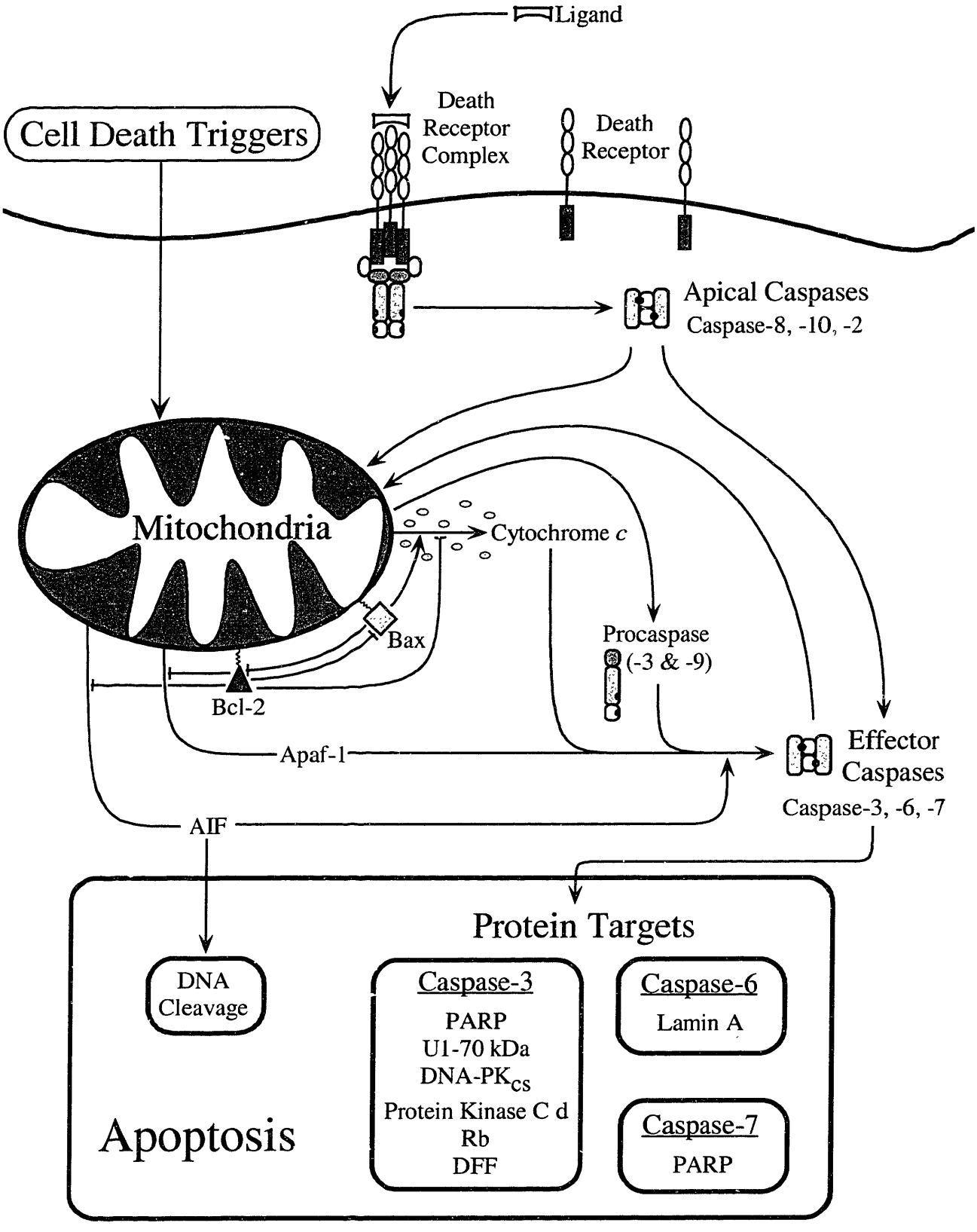

Figure 2-3. General mechanism of apoptosis. Death receptor complexes and other cell death triggers activate the caspase cascade. The effector caspases carry out the apoptotic death signal by cleaving specific cellular protein targets resulting in the morphological and biochemical changes associated with apoptosis.

receptor causing receptor oligomerization and activation of apical caspases (caspase-2, -8, or -10). These caspases then activate the effector caspases (caspase-3, -6, or -7) whose activity results in the morphological features associated with apoptotic cells (Alnemri, 1999; Ashkenazi and Dixit, 1998). The second apoptotic pathway involves the changes that occur in mitochondria (Green and Reed, 1998; Kroemer et al., 1995; Petit et al., 1996; Petit et al., 1997; Susin et al., 1998; Zamzami et al., 1996). A variety of cell death triggers result in the release of apoptosis inducing proteins such as cytochrome *c*, Apaf-1, apoptosis inducing factor (AIF), and procaspases from mitochondria which result in the activation of effector caspases (Alnemri, 1999). These two pathways are not independent, but rather they are interrelated through receptor activated caspases that induce apoptotic changes in mitochondria (Bossy-Wetzel and Green, 1999).

The main component of the apoptosis pathway consists of a proteolytic cascade of proteins termed caspases. This family of cysteine proteases cleaves specific proteins, activating or deactivating them, resulting in the morphological and biochemical changes associated with apoptosis (Cohen, 1997; Salvesen and Dixit, 1997; Thornberry and Lazebnik, 1998). Caspases are originally expressed in inactive forms (procaspases) that are activated by apoptosis inducing signals. The procaspase contains three domains: an $-NH_2$ terminal region, a large subunit (approximately 20 kD), and a small subunit (approximately 10 kD). The $-NH_2$ is highly variable among the various caspases and is involved in the regulation of caspase activation (Cohen, 1997; Thornberry and Lazebnik, 1998). Caspases are activated through the proteolytic cleavage of the three domains followed by the association of the large and small subunits resulting in an active heterodimeric enzyme (Thornberry and Lazebnik, 1998). The crystal structures of a couple of caspases have also shown that these heterodimers associate to form a tetramer. The active

caspase has a primary recognition pocket that specifically accepts the aspartic acid side chain (S_1). Additional amino acids surrounding the pocket are specific for a variety of other amino acid residues (S_2 – S_4), and this specificity for a specific tetrapeptide sequence helps to differentiate the various caspase enzymes from one another. The specificity of these caspases enables them to cleave specific proteins resulting in apoptosis inhibitor deactivation, cell structure cleavage, and specific protein deregulation (Cohen, 1997; Salvesen and Dixit, 1997). Caspase cleavage is extremely efficient with a k_{cat}/K_m constant value greater than 10^6 $M^{-1}s^{-1}$ (Thornberry and Lazebnik, 1998).

The apoptotic proteolytic caspase cascade can be divided into two main groups, one consisting of initiator or apical caspases and one consisting of executioner or effector caspases. Caspase-8, -9, -10, and -2 are in the apical caspase group and serve as regulators of the caspase cascade. These caspases are activated through the binding of a specific cofactor such as the FADD and DED domains of a death receptor complex as in the case of caspase-8 or through the binding of Apaf-1, cytochrome *c*, and dATP as in the case of caspase-9 (Li et al., 1997; Thornberry and Lazebnik, 1998). These activated apical caspases activate the effector caspases through proteolytic cleavage. Caspase-3, -6, and -7 are in the effector caspase group, and they carry out the execution of cell death through cell disassembly. This cascade model of effector caspase activation is supported by a significant amount of experimental evidence obtained from a variety of cell types which suggests that this mechanism exists in most cell types that undergo apoptosis (Muzio et al., 1998; Salvesen and Dixit, 1997; Thornberry and Lazebnik, 1998).

The effector caspase, caspase-3, has been identified as one of the key caspases involved in apoptosis. This particular caspase has been linked to the proteolytic cleavage of a number of protein substrates including PARP (DNA repair), Acinus (chromatin condensation), DNA-PK_{CS}

(DNA double-strand break repair), lamins (nuclear structure), U1-70 kDa (RNA splicing), Fodrin (cytosol structure), Protein kinase C, SREBP (sterol-regulatory element-binding protein), and Gelsolin (actin modulating protein) in addition to the activation of CAD (DNase) and DNA fragmentation factor (Cohen, 1997; Enari et al., 1998; Kothakota et al., 1997; Liu et al., 1997; Sahara et al., 1999). Caspase-3 is specific for a DXXD-like substrate (Cohen, 1997). In addition, procaspase-3 has been identified as having a cytosolic and mitochondrial distribution in nonapoptotic cells and can be activated through either the receptor mediated apoptotic pathway through caspase-8 or through the mitochondria mediated pathway involving the apoptosome (procaspase-9, Apaf-1, and cytochrome *c*) or AIF (Li et al., 1997; Mancini et al., 1998; Stennicke et al., 1998; Zou et al., 1997).

A number of inhibitors of caspases have been characterized. Several viral inhibitors, including CrmA, p35, and a family of IAPs (inhibitors of apoptosis proteins), have been discovered (Cohen, 1997; Deveraux et al., 1998). In addition, the peptide z-VAD-fmk (benzyloxcarbonyl-Val-Ala-Asp[OMe] fluormethyl ketone) irreversibly binds to the caspase active site causing permanent loss of caspase activity (Cohen, 1997; Thornberry and Lazebnik, 1998). Researchers have applied inhibitors in an effort to prevent apoptosis in cultured cells with varying degrees of success (Cohen, 1997; Goswami et al., 1999).

As mentioned previously, the caspase proteolytic cascade can be initiated through two different mechanisms, and the first mechanism involves death receptor activation. Two well characterized death receptors are CD95 (Fas or Apo1) and TNFR1 (p55 or CD120a) with their corresponding ligands termed CD95L and TNF respectively. Other death receptors are DR3 (Apo3 or TRAMP), DR4 (TWEAK) and DR5 (Apo2, TRAIL-R2, or KILLER). All of these death receptors belong to the tumor necrosis factor (TNF) receptor superfamily (Ashkenazi and

Dixit, 1998). These receptors contain an intracellular region termed the "death domain" through which the receptor activates the cellular apoptotic pathway. This death domain (DD) has been identified in both the TNFR1 and CD95 death receptors as a region of approximately 70 to 80 amino acids that is critical for the initiation of the apoptotic death signal (Tartaglia et al., 1993). The ligand binding results in receptor-receptor coupling which results in a receptor trimer complex. The death domains (DD) cluster and bind which in turn causes a series of additional proteins to bind to the complex such as FADD, TRADD, and RIP (Fraser and Evan, 1996; Wallach, 1997). This binding then activates the apical caspase, caspase-8, which in turn activates the effector caspases that cause apoptotic morphology changes (Ashkenazi and Dixit, 1998).

Receptor activation has been linked to the loss of mitochondrial function. The mitochondrial function of cells undergoing Fas-mediated apoptosis was examined through measurement of the oxygen consumption of mitochondria isolated from the apoptotic cells. These mitochondria were subjected to a series of substrates and inhibitors specific for various parts of the electron transport chain. The results indicated that cytochrome *c* becomes either inhibited or inactivated during apoptosis resulting a loss of electron transport chain function. In addition, the caspase inhibitor, z-VAD-fmk, was shown to inhibit this cytochrome *c* inactivation, indicating that a caspase proteolytic event must occur in order to explain this loss of cytochrome *c* activity (Krippner et al., 1996). In addition, oxidative phosphorylation uncouplers were found to enhance Fas receptor death signaling, and the maintenance of mitochondrial membrane integrity was found to prevent TNF induced apoptosis (Linsinger et al., 1999; Pastorino et al., 1996). The caspase proteolytic link to mitochondrial events was investigated in other work. Caspase-8 was observed to induce the rapid release of cytochrome *c* from mitochondria although

this reaction required the presence of unknown cytosolic factors indicating the indirect nature of the caspase-8 interaction. Caspase-8 and -3 were observed to cleave Bid, a proapoptotic member of the Bcl-2 family, which induced cytochrome *c* release. In addition, caspase-6 and -7 also induced cytochrome *c* release through the action of an unknown, bid-independent mechanism (Bossy-Wetzel and Green, 1999).

The events associated with apoptosis all tend to focus on one key cellular organelle, mitochondria, and a significant amount of experimental evidence supports the key role this organelle plays in apoptosis (Earnshaw, 1999; Green and Reed, 1998; Kroemer et al., 1995; Petit et al., 1996; Petit et al., 1997; Susin et al., 1998; Zamzami et al., 1996). For several decades, scientists hypothesized that endonuclease and caspase activation were the key players in the apoptotic death pathway. The idea that mitochondria were not involved in apoptosis stemmed from the observation that no significant morphological changes occur in mitochondria during apoptosis and that cells with no mitochondrial DNA (ρ^o cells) can still undergo apoptosis. However, this view has changed dramatically in the last several years as a consequence of a significant amount of reproducible experimental observations that point to mitochondria as one of the key players in apoptosis. These observations include events that occur during apoptosis such as changes in mitochondria membrane potential ($\Delta\Psi_m$) and electron transport function and the release of apoptosis stimulating compounds from mitochondria as well as the fact that compounds that stabilize mitochondrial membranes inhibit apoptosis (Bedner et al., 1999; Petit et al., 1997; Susin et al., 1998). Furthermore, the mitochondrial release of caspase activating factors such as cytochrome *c*, AIF, and procaspases all support the central role mitochondria play in apoptosis (Bossy-Wetzel et al., 1998; Earnshaw, 1999; Susin et al., 1999b; Susin et al., 1999a). Additionally, the Bcl-2 family of proteins is predominantly located in mitochondria

(Kluck et al., 1997; Mancini et al., 1998; Susin et al., 1999a; Susin et al., 1998; Wolter et al., 1997; Yang et al., 1997). Finally, death signals from death receptors and caspases act on mitochondria which indicates that apoptotic death pathways appear to all converge on the mitochondria (Bossy-Wetzel and Green, 1999; Green and Reed, 1998).

Mitochondria are ideally situated for life and death signaling pathways due to the importance of mitochondria in cellular energetics and their sensitivity to the cellular physiological state. Mitochondria can trigger cell death through a variety of mechanisms. Numerous kinetic studies have demonstrated that mitochondria lose their membrane integrity early on in the apoptotic death pathway. Lipophilic cationic dyes that accumulate in the mitochondrial matrix such as $DiOC_6$, Rhodamine 123, and JC-1 have been utilized to determine the mitochondrial membrane potential ($\Delta\Psi_m$) of cells undergoing apoptosis. In a majority of cases, a decrease in the $\Delta\Psi_m$ precedes any biochemical and morphological changes associated with apoptosis (Bedner et al., 1999; Susin et al., 1998). The disruption of the electron transport chain and the generation of reactive oxygen species (ROS) and superoxide radicals accompany this loss of ($\Delta\Psi_m$) during the later stages of apoptosis. The formation of ROS has been linked to necrosis type death morphology although a number of researchers have implicated ROS as a signaling molecule for apoptosis (Goossens et al., 1996; Mignotte and Vayssière, 1998). Antioxidant enzyme expression has been linked to the maintenance of mitochondrial membrane integrity suggesting a link between ROS and apoptosis (Kowaltowski et al., 1998). The loss of cytochrome *c* function has been observed to occur early on in apoptotic cell death resulting in the loss of mitochondrial function (Heiskanen et al., 1999; Krippner et al., 1996). This evidence all supports the hypothesis that mitochondrial membranes and electron transport function are compromised during apoptosis (Susin et al., 1998).

Cell-free systems also support the key role mitochondria play in apoptosis. The induction of nuclear apoptosis characterized by DNA fragmentation and chromatin condensation requires the presence of mitochondria or mitochondria products (Juin et al., 1998; Susin et al., 1998). In addition, cytosolic extracts from cells dying from apoptosis can induce mitochondria extracted from healthy cells to release proapoptotic factors such as cytochrome *c*. Furthermore, the addition of mitochondria to apoptotic cytosol increases caspase-3-like activity (Juin et al., 1998).

Mitochondria release a variety of proteins that are linked to caspase activation and the caspase cascade. Cytochrome *c* is released from mitochondria and forms part of the apoptosome consisting of cytochrome *c*, Apaf-1, and procapase-9 (Li et al., 1997). This results in the activation of capsase-9 which in turn activates caspase-3 and the caspase cascade. In addition, mitochondria have been observed to release procaspases suggesting the presence of an inner-mitochondrial pool of procaspases that are released upon receiving an apoptotic death signal (Green and Reed, 1998; Mancini et al., 1998; Susin et al., 1999b). Furthermore, the release of an apoptosis inducing factor (AIF) from mitochondria has been identified and linked to chromatin condensation, DNA fragmentation, and cytochrome *c* release (Susin et al., 1999a).

The mitochondrial megachannel has also been linked to apoptotic events. The permeability transition (PT) is associated with the opening of the mitochondrial megachannel (PT pore) that is situated at the contact site between the inner and outer mitochondrial membranes. The exact structure of the mitochondrial membrane megachannel is unknown but it contains the inner membrane protein, adenine nucleotide translocator (ANT), and outer membrane proteins such as porin (voltage dependent anion channel; VDAC). These proteins work together and create a channel large enough for molecules less than 1.5 kD to pass through. This PT pore helps to regulate mitochondrial matrix Ca^{++}, pH, $\Delta\Psi_m$, and volume. Inhibitors of

the PT pore, such as bongkrekic acid and cyclosporins, prevent the loss of $\Delta\Psi_m$ and other indicators of apoptosis (Fulda et al., 1998; Green and Reed, 1998; Pastorino et al., 1996; Susin et al., 1998). Conversely, stimuli that disrupt the PT pore cause $\Delta\Psi_m$ loss and the release of cytochrome *c* and other proapoptotic factors (Green and Reed, 1998; Susin et al., 1998).

An additional link between mitochondria and apoptosis is formed through the relations between the Bcl-2 family of proteins and mitochondria. The Bcl-2 family consists of three subfamilies: a prosurvival Bcl-2 subfamily (Bcl-2, Bcl-X_L, Bcl-w, *etc.*), a proapoptosis Bax subfamily (Bax, Bak, and Bok), and another proapoptosis BH3 subfamily (Bid, Bad, *etc.*). The Bcl-2 homology consists of four domains (BH1 to BH4), and all Bcl-2 family proteins contain at least part of one of these domains. The prosurvival Bcl-2 proteins contain several of the domains whereas the proapoptosis Bcl-2 proteins contain only part of the BH3 domain. The fact that pro and antiapoptosis family members can heterodimerize indicates that their relative concentrations may play a role in the regulation of apoptosis (Adams and Cory, 1998). Bcl-2, Bcl-X_L, and Bax all form channels in lipid bilayers *in-vitro* and are believed to be involved with pore formation in mitochondria (Reed, 1997). Several Bcl-2 proteins contain membrane anchor regions that enable them to be anchored in the outer mitochondrial membrane with the protein oriented toward the cytosol (Green and Reed, 1998). Bcl-2 and its homologs have been linked to a number of mitochondrial events associated with apoptosis, and can prevent the release of cytochrome *c* into the cytosol and therefore inhibit caspase activation (Green and Reed, 1998; Kluck et al., 1997; Reed, 1997; Yang et al., 1997). Bcl-2 was also found to inhibit Bax-induced apoptosis even after cytochrome *c* was released revealing additional complexity concerning the role of Bcl-2 in the inhibition of apoptosis (Rossé et al., 1998). Bcl-X_L binds with caspase-9 and Apaf-1 resulting in the inhibition of apoptosis (Pan et al., 1998). Bcl-X_L was also shown to regulate the

mitochondrial membrane potential and volume homeostasis as well as prevent mitochondrial loss of cytochrome *c* during apoptosis (Kim et al., 1997; Vander Heiden et al., 1997). The proapoptosis Bcl-2 protein, Bax, moves from the cytosol to mitochondria during apoptosis resulting in an acceleration of death which can be inhibited by Bcl-X_L and Bcl-2 (Antonsson et al., 1997; Finucane et al., 1999; Wolter et al., 1997). Bcl-2 can also be converted into a Bax-like death factor through caspase-3 cleavage under *in-vitro* conditions which can result in the promotion of cytochrome *c* release from mitochondria (Cheng et al., 1997; Kirsch et al., 1999). These observations all support the hypothesis concerning the key role mitochondria related proteins play in apoptosis.

The overall apoptosis death pathway can be divided into three main phases. The first phase is the premitochondrial phase during which signal transduction pathways are initiated. For this phase, the PT pore is hypothesized to serve as the central site which allows mitochondria to integrate a variety of proapoptosis signals. The second phase is termed the mitochondrial phase that involves the apoptosis signal amplification process through the release of cytochrome *c* and other factors. In addition, mitochondrial membrane integrity and function are lost during this phase. The final phase is called the postmitochondrial phase during which caspases are activated. This model summarizes the basic mechanism of apoptosis and emphasizes the central role mitochondria play in programmed cell death (Susin et al., 1998).

2.7 Summary

Biochemical engineering has focused on developing techniques for increasing and maintaining high viable cell concentrations in culture in order to produce higher concentrations of therapeutic protein products. A number of beneficial bioreactor operation strategies have been developed along with additional techniques for enhancing the robustness of cultured cell lines.

However, cell death has proven to still be a significant problem for mammalian cell culture, and the primary goal of this thesis was to development methods for reducing death in mammalian cell culture.

The modeling techniques used to develop operating strategies for cell culture have not addressed the extensive amount of regulation governing the flow and distribution of metabolic flux in central carbon metabolism. Metabolic flux analysis coupled with continuous culture experiments can provide a more rigorous platform not only for the analysis of cultured cells subjected to various culture environments but also as a means of determining the true flexibility and adaptability of cellular behavior in culture. Although these results would not necessarily be directly relevant to industry, they could be utilized in the formulation of novel hypotheses that could then be applied in the optimization of industrial culture operations.

Population heterogeneity has proven to be a significant but largely neglected section of biochemical engineering. Cell selection dynamics, development, differentiation, and stability are all involved in population heterogeneity. Furthermore, heterogeneous events occur not only at the cellular level but also at the intracellular organelle and genetic regulation levels, resulting in variability in intracellular microenvironments and genetic expression. One goal of this thesis was to address population heterogeneity within the context of biochemical engineering in order to develop analysis methods and applications for the formulation of novel bioreactor operating strategies.

Additionally, mitochondria play a fundamental role in this thesis. The TCA cycle, respiration, and apoptosis are topics that all revolve around mitochondria. The research presented in this thesis demonstrating physiological multiplicity involved the analysis of mitochondrial respiration and TCA cycle activity. Furthermore, mitochondrial properties were

used as the basis for analyzing population heterogeneity in mammalian cell culture with the ultimate goal of utilizing these mitochondrial parameters for the optimization of cell cultures.

3. MATERIALS AND METHODS

3.1 Cell Culture

3.1.1 Cell Lines and Media

The initial continuous culture experiments were performed using a Chinese hamster ovary (CHO) cell line that produced recombinant human gamma-interferon (Devos et al., 1982; Scahill et al., 1983). This γ-CHO cell line was originally anchorage dependent and grown in serum containing medium. For the continuous culture experiments, the cells were grown in a serum-free medium that contained an animal tissue hydrolysate (Primatone RL; Quest International, Norwich, NY). The final serum-free medium contained RPMI-1640 (Sigma Chemical Co.) supplemented with 2.5 g/L Primatone RL, 0.4 g/L 2-hydroxypropyl-β-cyclodextrin (Sigma), 1 g/L (0.1%) Pluronic F-68, 5 mg/L insulin (USB), 5 mg/L transferrin (USB), 1 mM sodium pyruvate, 1 μM putrescine, 11 mg/L choline chloride, 100 μM ethanolamine, 1.5 μM linoleic acid, 0.25 μM methotrexate, 10,000 units/L penicillin - 10 mg/L streptomycin (Sigma), 6.3 mg/L EDTA, and trace minerals (10 nM sodium selenite, 1 nM manganese sulfate, 10 nM molybdic acid, 10 nM ammonium metavanadate, 10 nM cupric sulfate, 3 μM zinc sulfate, and 5 μM ferric citrate).

The subsequent continuous culture, mitochondrial membrane potential FACS sorted cell subpopulation, and fed-batch experiments were conducted using a murine hybridoma cell line (ATCC CRL-1606) producing IgG against human fibronectin (Schoen et al., 1982). The hybridoma cell line was grown in glutamine-free IMDM medium (Specialty Media, Inc., Lavallette, NJ) supplemented with 4.0 mM L-glutamine (Sigma Chemical Co.), 1 U/ml penicillin - 1 μg/ml streptomycin (Sigma), 5 mg/L transferrin (USB), 10 mg/L insulin (USB), 2.44 μL/L 2-

aminoethanol, 3.5 μL/L 2-mercaptoethanol, and 7.5 mg/L protease free bovine serum albumin (Sigma).

3.1.2 Culture Maintenance

The cell lines were obtained from frozen stocks stored in a liquid nitrogen cell bank. The frozen cell stocks were prepared by centrifuging cells obtained from cultures that had a viability greater than 95% at 200*g* for 8 minutes and resuspending them to a concentration of $7.0*10^6$ cells/ml in freezing medium (7.5% DMSO, 46.25% fresh medium, 46.25% conditioned medium). Cryogenic vials (Corning Inc., Corning, NY) containing 1ml of the cell suspension were placed in a cryogenic freezing container (Cole-Parmer, Niles, IL) and then placed in a -70^0C freezer. The freezing container limited the freezing rate to -1^0C/min. For a culture inoculation, the frozen cell stocks were thawed rapidly and slowly resuspended dropwise into 19 ml of fresh medium. The cells were subcultured every 2-4 days (γ-CHO) or 2-3 days (CRL-1606 hybridoma) at $2.0*10^5$ cells/ml in a 37^0C humidified incubator (95% relative humidity) with either a 5% (γ-CHO) or a 10% (CRL-1606 hybridoma) CO_2 atmosphere. The experiments were performed when the viability was greater than 95%.

3.2 Analytical Methods

3.2.1 Cell Enumeration

The cell concentration and viability were determined using a hemacytometer and the trypan blue dye exclusion method. In addition, the extent of apoptotic death was determined using an acridine orange / ethidium bromide stain as described in Mercille and Massie (Mercille and Massie, 1994). At least 200 cells were counted in each determination of the culture viability and cell concentration.

3.2.2 Metabolite Assays

The steady state samples taken from the reactor were centrifuged at 200*g* for 8 minutes, and the supernatent was removed and stored at -20^{0}C for future analysis. To deproteinate the thawed samples, 100 μl of 20% m/v trichloroacetic acid was added to 340 μl of sample. After microcentrifugation at 7,000*g* for 10 minutes, 200 μl of the deproteinated sample was neutralized with 50 μl of 25% m/v potassium bicarbonate. The deproteinated samples were used in performing the lactate (826-UV Sigma assay protocol, Sigma) and glucose (16-UV Sigma assay protocol, Sigma) assays.

Amino acid analysis was conducted for samples that were deproteinated using Ultrafree-MC 5,000 MW cutoff ultrafilters microcentrifuged at 4^{0}C for 70 minutes at 4,000*g* (Millipore, Bedford, MA). The samples were diluted to ensure that the maximum expected amino acid concentration was less than 1 mM (the upper calibration limit). The amino acids were analyzed using the AminoQuant protocol on an HP 1090 HPLC (Hewlett Packard, Palo Alto, CA) as described in Nyberg et al. (Nyberg et al., 1999a).

3.2.3 Protein Product Measurement

Antibody concentrations were determined using a standard ELISA procedure. First, 100 μl of a solution containing a capture antibody (Sigma M8770) diluted to 5 μg/ml in a capture antibody solution (Sigma C3041) containing 0.1% (w/v) sodium azide was added to a 96 well plate and incubated at 37^{0}C for 30 minutes. Then, 200 μl of a blocking solution (SuperBlock^{TM}, Pierce 37515) was added and removed three times. After that, 100 μl of either samples or standards (Sigma M9269), diluted in a solution of 1 part blocking solution to 9 parts washing solution (PBS with 0.05% w/v Tween 20), was added and incubated for 1 hour at room temperature. Then, 100 μl of a detection antibody solution (sample and standard diluent solution

with detection antibody Sigma A2304) was added and incubated for 1 hour at room temperature. After each of the previous steps, the plate was washed three times in washing solution. Finally, 200 μl of a substrate solution (SigmaFAST^{TM} OPD, Sigma P9187) was added and incubated for 30 minutes in the dark. The reaction was stopped with 3 M HCl and the absorbance was read at 492 nm on a microplate reader (Molecular Devices, Palo Alto, CA).

3.2.4 FACS Analysis and Mitochondria Staining

A fluorescence activated cell sorter (FACS, Becton Dickinson, FACSCAN) was used to analyze cells stained for mitochondria potential using Rhodamine 123 (Rh123; Molecular Probes, Eugene, OR). Cells were diluted with the appropriate medium to a concentration of 5-6*10^5 cells/ml and stained with a final concentration of 2 μg/ml Rh123 and incubated for ten minutes in a 37^{0}C incubator. The cells were microcentrifuged at 200*g* for 6 minutes, resuspended in PBS, and stored on ice in the dark. The stained cells were analyzed on the FACS within 15-30 minutes. The Rh123 fluorescence values were determined to be stable for up to an hour after this staining procedure.

3.2.5 Cell Cycle Analysis

Cell cycle analysis was performed by fixing the cells in ethanol, staining them with propidium iodide (PI), and then analyzing them on the FACS. Cell were collected in the exponential phase at approximately 1.0*10^6 cell/ml, microcentrifuged at 200*g* for 6 minutes, and then resuspended in 0.3 ml of PBS. Then, 0.7 ml of cold ethanol was added dropwise to the tube while vortexing. After leaving the tube on ice for 15-30 minutes, the cells were microcentrifuged at 2,000 rpm at 4^{0}C for 6 minutes. The supernatent was removed, and the cell pellet was resuspended in 0.5 ml PBS with 50 μl of 0.5 mg/ml RNase. After letting the mixture stand at room temperature for more than 30 minutes, 0.5 ml of PI solution (20 mg/L in PBS) was

added. The cells were then run through a fluorescence activated cell sorter (FACS, Becton Dickinson, FACSCAN) and the raw data was analyzed using the Modfit Lt v.2 analysis software (Verify Software House, Topsham, ME).

3.2.6 Caspase Enzymatic Activity

Caspase-3 (DEVDase) activity was measured using an assay that measured the amount of p-nitroaniline (pNA) chromophore cleaved from the colorimetric substrate (Ac-DEVD-pNA). The caspase activity was also inhibited using the peptide z-VAD-fmk. The sample where apoptosis was not induced was referred to as the positive control whereas the apoptosis induced sample (via. staurosporin or other compounds) inhibited by z-VAD-fmk was referred to as the negative control. The difference between the apoptosis induced sample and the negative control was the amount of caspase activity present in the sample.

The CaspACE assay kit (Promega, Madison, WI) was used to measure the caspase-3 activity. To prepare the sample extract, cells were grown under normal conditions until reaching mid-exponential phase. Then, the cell concentration was adjusted to $1.0*10^6$ cells/ml and then the apoptosis inducer was added. After incubating the cells for the proper time required to induce apoptosis, the cells were centrifuged at 200*g* for 10 minutes at 4^0C. The cells were then washed once with ice cold PBS and kept constantly on ice. After the washing step, the cells were resuspended in a cell lysis buffer (Promega, CaspACE assay system – colorimetric) at a concentration of $1.0*10^8$ cells/ml. The cells were lysed by freezing (-20^0C) and thawing them once. The cell lysate was incubated on ice for 15 minutes and then centrifuged at 15,000*g* (13,000 rpm on 24 tube microfuge, Heraeus Biofuge 15) for 20 minutes at 4^0C. The supernatent was collected and stored at -80^0C.

The caspase-3 assay was performed using a 96 well plate (flat bottom, clear polystyrene). The protein concentration of the extracts was determined using a Bradford protein assay (Bio-Rad Protein Assay 500-0002, Bio-Rad, Hercules, CA) with a BSA reference standard. 50 μg of extract protein was added to each well. The wells were prepared as described in Table 3-1.

Table 3-1. 100 μl reaction preparation for the caspase-3 enzymatic activity assay (CaspACE assay system, Promega, WI).

	Blank	Negative Control	Induced Apoptosis	Inhibited Apoptosis
Caspase assay buffer	32 μl	32 μl	32 μl	32 μl
DMSO	2 μl	2 μl	2 μl	2 μl
100 mM DTT	10 μl	10 μl	10 μl	10 μl
Untreated cell extract	-	x μl	-	-
Induced apoptosis cell extract	-	-	x μl	-
Inhibited apoptosis cell extract	-	-	-	x μl
Add DI water to final volume	98 μl	98 μl	98 μl	98 μl

The cell extract protein concentration was identical for all reactions. The Caspase assay buffer consisted of 315 mM HEPES (pH 7.5), 31.25% sucrose, and 0.3125% CHAPS. After the wells were prepared, 2 μl of the DEVD-pNA substrate was added to all of the wells which were then incubated at 37^0C for 3 hours. The absorbance for each well was measured at 405 nm using a microplate reader (Molecular Devices). The pNA calibration curve was obtained using a pNA standard that was diluted using DMSO. The pNA absorbance readings at 405 nm were linear up to a concentration of 1 mM pNA.

The *in-vitro* induction of caspase-3 activity using cytochrome *c* was performed by preincubating the samples with 10 μM cytochrome *c* (from rat heart; Sigma C7892) and 1 mM

dATP (USB 14245) for 30 minutes at 32^0C. The caspase-3 enzymatic activity was then determined according to the procedure described previously.

3.3 Continuous Culture

3.3.1 Culture Medium Conditions

The continuous culture reactor was operated under glutamine limited conditions (0.8 mM L-glutamine) and inoculated at $2.0*10^5$ cells/ml.

3.3.2 Bioreactor Operation

The continuous cultures were performed in a 2.0 liter Applikon (Foster City, CA) reactor with a 1.2 liter working volume and a heated water jacket. The temperature was maintained at 37^0C and the agitation was set at 200 rpm. An ML-4100 multi-loop process controller (New Brunswick Scientific, Edison, NJ) was used to control the pH and dissolved oxygen in the reactor using the AFS software from New Brunswick Scientific (Edison, NJ). The pH was controlled at 7.20 ± 0.05 using the addition of either 320 mM HCl or a basic solution consisting of 6.2 g/L NaOH and 0.4 g/L KOH (160 mM). Oxygen was supplied to the reactor through surface aeration by adjusting an air mixture consisting of nitrogen and oxygen, and the dissolved oxygen concentration was maintained at 50% of air saturation. The gas flow rate was controlled using a mass flow controller set at 35 mol/day. The ML-4100 controller was also used to log process data: time, temperature, dissolved oxygen concentration, pH, acid and base addition, and headspace gas composition. After waiting 5 residence times at a particular dilution rate, the reactor was assumed to be at steady state if the total cell density, viable cell density, glucose and lactate concentrations, and oxygen uptake rate were steady within a 10% range for 48 hours.

3.3.3 Gas Exchange Rate Measurement

Oxygen uptake rate (OUR) was calculated through a mass balance for reactor liquid phase oxygen

$$OUR = k_L a(C^* - C_R) + D(C_F - C_R) \tag{3.1}$$

The first term accounts for the headspace aeration across the gas-liquid interface, and the second term accounts for the net inflow of oxygen due to the liquid streams. The liquid phase oxygen concentrations were measured using a blood gas analyzer (Ciba Corning Diagnostics, Medfield, MA). The gas phase oxygen concentration was measured using a paramagnetic oxygen sensor (Columbus Instruments, Columbus, OH), and the equilibrium oxygen concentration (C^*) was calculated based on the gas phase oxygen concentration at the reactor exit. The partial pressure of oxygen was converted to a liquid concentration using Henry's Law.

$$C_{O_2} = \frac{P_{O_2}}{H_{O_2}} \tag{3.2}$$

The Henry's constant was determined using correlations for determining gas solubilities in medium (Schumpe et al., 1982).

The CO_2 evolution rate (CER) was determined through a similar method involving a mass balance for reactor carbon dioxide

$$CER = \frac{n_g}{V_R}(z^R_{CO_2} - z^F_{CO_2}) + D(C^R_L - C^F_L) \tag{3.3}$$

The first term accounts for the net inflow of CO_2 through the gas streams, and the second term accounts for CO_2 in the liquid streams. The mole fraction of CO_2 was measured with a gas analyzer with an IR CO_2 sensor (Columbus Instruments, Columbus, OH). The CO_2 levels in the liquid streams were measured using a blood gas analyzer (Ciba Corning Diagnostics, Medfield,

MA). Both the CO_2 and bicarbonate were determined using equilibrium relations (Nyberg et al., 1999a).

3.4 Rhodamine123 Sorted Subpopulations

The hybridoma cells were sorted into subpopulations based on their mitochondrial membrane potential as measured using Rhodamine 123. A fluorescence activated cell sorter (FACS, Becton Dickinson, FACSCAN) was used to sort the cells into high (H; top 15%) and low (L; bottom 15%) fractions. The fractions were grown in 6 well plates and then subsequently scaled up into T-flasks under normal growth conditions as described in the culture maintenance section. The cells were frozen down when enough cells were grown for making five or more stock vials (>$35.0*10^6$ cells).

3.5 Fed-Batch Cultures

The fed-batch cultures were performed in spinner flasks (250 ml total volume; 75 ml working volume) using the stoichiometric feeding method developed by Xie and Wang (Xie and Wang, 1994c; Xie and Wang, 1994b; Xie and Wang, 1994a)(1994). The spinners were agitated at 70 rpm in a 37^0C incubator (95% relative humidity) in a 10% CO_2 atmosphere. The cells were inoculated at $2.0*10^5$ cells/ml in either low glucose and glutamine IMDM medium as described in the cell lines and media section or in the same medium with MOPS to enhance the buffering capacity as indicated in the results section for these experiments. The medium osmolarity was adjusted to 270 mOsm/kg using NaCl. The supplemental medium was designed as specified by the software written by Möllborn (Möllborn, 1996). Samples and cell counts were taken approximately every 12 hours, and then the cultures were fed according the stoichiometric feeding protocol specified by the software developed by Xie (Xie, 1997) and Möllborn (Möllborn, 1996).

4. PATHWAY AND FLUX ANALYSIS OF CENTRAL CARBON METABOLISM

4.1 Central Carbon Metabolism Reaction Network

Cellular metabolism consists of a vast number of anabolic and catabolic enzymatic reactions that produce cellular energy, reducing power, and biosynthetic precursors for cellular growth and function. The metabolic reaction network for central carbon metabolism in mammalian cells is shown in Figure 4-1. The main metabolic reactions are included such as glycolysis, the tri-carboxylic acid (TCA) cycle, and glutaminolysis, and serial reactions were lumped into single reactions. A more complete description of these reactions can be found in Stryer (Stryer, 1988) and Zupke (Zupke, 1993). In addition, metabolite requirements for biomass and product synthesis were considered as described in Zupke and Stephanopoulos (Zupke and Stephanopoulos, 1995a) using the cell composition described in Xie and Wang (Xie and Wang, 1994c) and Zupke and Stephanopoulos (Zupke and Stephanopoulos, 1995a). This procedure is described in more detail in section 4.4. The pentose phosphate pathway was analyzed by considering only the biosynthetic demand for ribose carbon skeletons. Although obtaining pentose phosphate pathway metabolic fluxes could be useful, labeled substrates must be used in order to obtain accurate flux data for this pathway. The methodology needed to obtain this more accurate flux data is described later in this chapter, but due to the complexity involved in these labeled substrate analysis techniques, this method was not utilized in the continuous culture flux analysis experiments. In addition, the production of NADPH could not be used to determine the pentose phosphate pathway recycle flux due to the uncertainty of transhydrogenase activity in this cell line as well as the fact that the malic enzyme may use either NAD^+ or $NADP^+$ (Eigenbrodt et al., 1985). Therefore, reducing power was lumped into an NAD(P)H pool. This

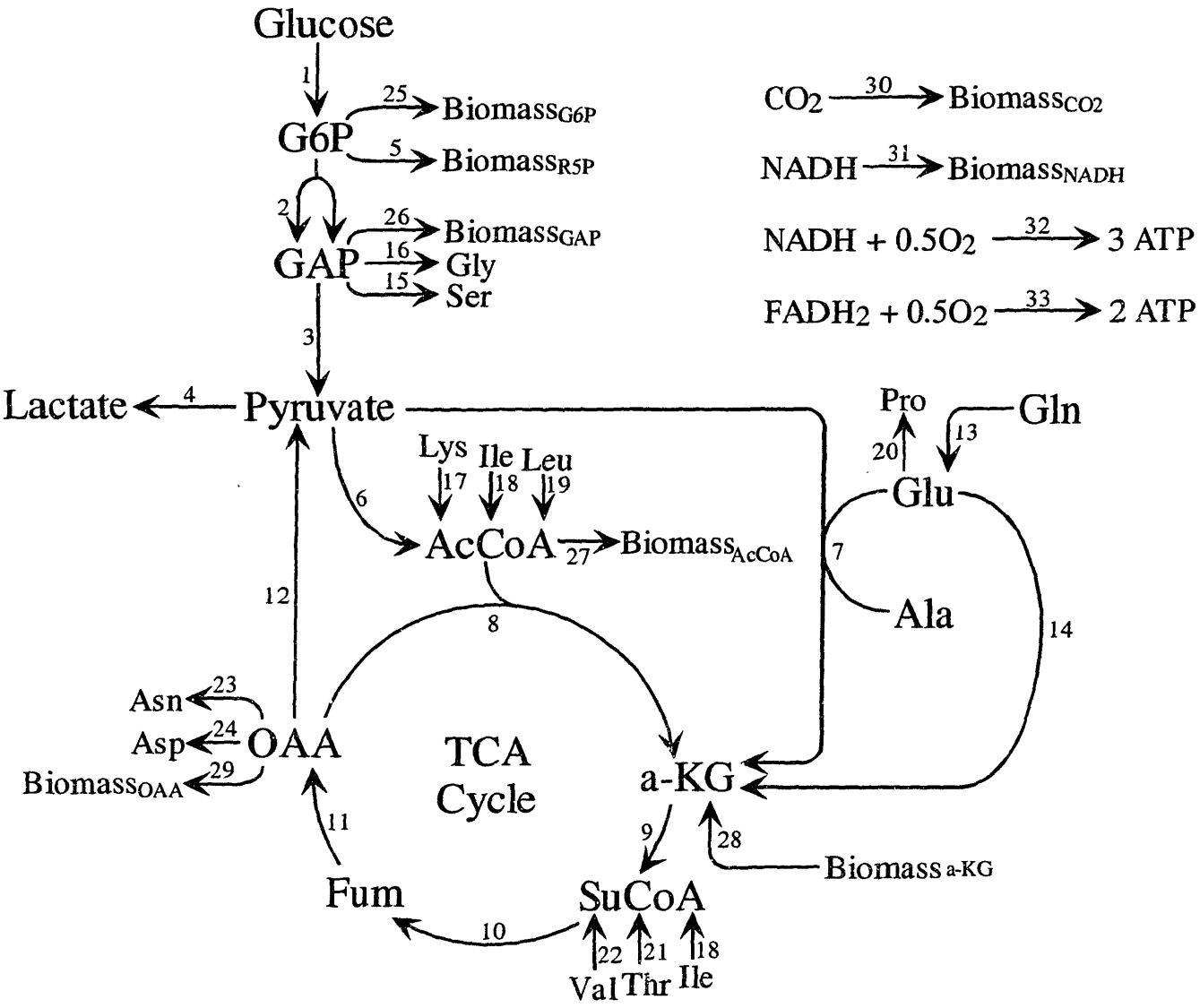

Figure 4-1. The central carbon metabolism reaction network. Serial reactions are lumped into single reactions. In addition, biosynthetic requirements for metabolic intermediates have been included.

may introduce some error in distinguishing CO_2 released from the pentose phosphate pathway and the TCA cycle.

4.2 Metabolic Pathway Analysis

Cellular metabolism contains an extensive number of enzymatic reactions that are involved in numerous cellular activities, and organizing these metabolic networks into independent pathways and key junction points is oftentimes difficult and conducted using arbitrary methods. Metabolism contains several key junction points termed metabolic branchpoints or nodes, and characterizing these nodes is critical for determining their influence on the regulation of metabolic flux. These key link metabolites can be determined through the analysis of the junctions between various independent pathways through a given reaction network. These independent pathways can be determined by formulating a steady state internal metabolite matrix (**N**) consisting of the reaction stoichiometry and then calculating the kernel matrix (**K**) using equation 4.1.

$$\mathbf{N} \bullet \mathbf{K} = \mathbf{0} \tag{4.1}$$

Link metabolites are identified as the metabolite that is located at the point of separation between independent pathways (Stephanopoulos and Simpson, 1997). Although several link metabolites exist for central carbon metabolism, only pyruvate is the one common metabolite for all independent pathways (Simpson et al., 1999). Pyruvate serves as the major link between glycolysis, the TCA cycle, and the production of lactate and several amino acids, and enzymatic regulation partitions the metabolic flux around this branchpoint to satisfy the catabolic and biosynthetic needs of a cell. The flexibility of this branchpoint will ultimately determine the extent of control this branchpoint has over metabolic flux distributions in central carbon metabolism (Stephanopoulos and Vallino, 1991). Therefore, the flux distribution around

pyruvate for various physiological states serves as an indicator of the flexibility of this node. Furthermore, if this node is somewhat flexible, one could exploit this flexibility in order to increase the culture cell concentration and viability by diverting carbon away from waste metabolite production pathways into biomass and energy production pathways.

4.3 Metabolic Flux Analysis

The metabolic fluxes were calculated for mammalian cells growing under continuous culture conditions. Therefore, specific growth and death rates were determined from the total and viable cell balances around the bioreactor:

$$\frac{dN_T}{dt} = \mu N_V - DN_T \tag{4.2}$$

$$\frac{dN_V}{dt} = \mu N_V - k_d N_V - DN_V \tag{4.3}$$

yielding at steady state:

$$\mu = D\frac{N_T}{N_V} \tag{4.4}$$

$$k_d = \mu - D \tag{4.5}$$

Similarly, specific rates of metabolite production or uptake were determined from the balance:

$$\frac{dC}{dt} = DC_{in} - DC_{out} - q_c N_V \tag{4.6}$$

yielding at steady state:

$$q_c = \frac{D(C_{in} - C_{out})}{N_V} \tag{4.7}$$

For the central carbon metabolic reaction network, the flux of each reaction i can be represented as v_i (mmole/ viable cell hr). The stoichiometric coefficient, $\alpha_{i,j}$, represents the coefficient of metabolite j for reaction i. The specific consumption or production rate of

metabolite j can be represented as q_j. The resulting system of linear equations can be presented as

$$q_j = \sum_i \alpha_{i,j} v_i \tag{4.8}$$

In matrix form, this equation can be written as

$$\mathbf{Av} = \mathbf{r} \tag{4.9}$$

where the matrix of stoichiometric coefficients (**A**) times the vector of metabolic fluxes (**v**) equals the vector of metabolite production and consumption rates (**r**). The stoichiometric coefficient matrix is of dimension m x n, where n is the number of reactions and m is the number of metabolites. Since the stoichiometry of the network is known along with the metabolite production and consumption rates, one needs to invert equation 4.9 to solve for the metabolic fluxes. Also, because the stoichiometry matrix is rarely square, a linear least squares estimate must be calculated

$$\mathbf{v} = (\mathbf{A}^T\mathbf{A})^{-1}\mathbf{A}^T\mathbf{r} \tag{4.10}$$

Finally, a variance-covariance matrix (Ψ) can be added to weight the solution (Stephanopoulos et al., 1998; Zupke and Stephanopoulos, 1995a; Zupke, 1993).

$$\mathbf{v} = (\mathbf{A}^T\Psi^{-1}\mathbf{A})^{-1}\,\mathbf{A}^T\Psi^{-1}\mathbf{r} \tag{4.11}$$

The sensitivity of the metabolic reaction network to changes in the metabolite production and consumption measurements was also determined by calculating the condition number, c(A), of the stoichiometry matrix

$$c(\mathbf{A}) = \|\mathbf{A}\| \bullet \left\|\mathbf{A}^{-1}\right\| \tag{4.12}$$

with $\| \|$ indicating the matrix norm. This condition number is used in order to determine the upper bound of the potential magnification of error when solving equation 4.9. A reaction

network is considered well posed if the value of the condition number falls below 100 whereas a condition number that is above 1,000 indicates that the network can yield significant sensitivity problems. For the metabolic reaction network shown in figure 4-1, the condition number was calculated to be 69.

Redundant metabolite production and consumption measurements are necessary in order to test the validity of the metabolic reaction network and of the measured data set. Several methods have been proposed to elucidate whether a given data set is consistent (van der Heijden et al., 1994a; van der Heijden et al., 1994b; Wang and Stephanopoulos, 1983) and consistency analysis has been applied in a number of situations involving flux analysis (Nyberg et al., 1999a; Vallino, 1991; Zupke and Stephanopoulos, 1995a). For the procedure described in Wang and Stephanopoulos (Wang and Stephanopoulos, 1983), the redundant equations are written as

$$\mathbf{Er} = \mathbf{0} \tag{4.13}$$

in which the redundant equations matrix (**E**) times the vector of measurements equals the null matrix. Since experimental data always contains some amount of error, equation 4.13 will rarely be satisfied. Therefore, a statistical hypothesis testing method is utilized in order to determine if the error is within the bounds expected for random error or if the error is in fact a gross error due to inconsistent data. This hypothesis test involves the calculation of a consistency index, h, defined as

$$h = \varepsilon^T \varphi^{-1} \varepsilon \tag{4.14}$$

where

$$\varepsilon = -\mathbf{Er} \tag{4.15}$$

$$\varphi = \mathbf{E}^T \Psi \mathbf{E} \tag{4.16}$$

The consistency index, h, follows a χ^2 distribution where the number of redundant equations determines the degrees of freedom. Therefore, h can be used to determine when the residuals of equation 4.13 deviate from the expected distribution for a selected confidence level. When h is greater than the χ^2 value, there is a certain confidence level percentage chance that the data set contains either gross measurement errors or errors in the assumed metabolic reaction network stoichiometry. The elimination of each measurement can be used as a method to determine which measurement is incorrect (Wang and Stephanopoulos, 1983) although other techniques have been developed for gross error diagnosis (van der Heijden et al., 1994a; van der Heijden et al., 1994b).

4.4 Biomass Equation

The biomass equation involves the estimation of the amount of specific metabolites required to produce biomass and protein product. Central carbon metabolism provides a number of key metabolites that are used as biosynthetic precursors for the production of polysaccharides, lipids, proteins, and nucleotides. The biomass macromolecular composition (DNA, lipids, protein, and carbohydrate) is required in order to calculate the biomass equation. In addition, an estimate of the amino acid composition of the cellular and product protein is required. Once these compositions are determined, the overall amount of metabolites required to produce one mole of biomass (carbon basis) is calculated. For metabolic flux calculations, the amino acids required for protein production are subtracted from the metabolite production and consumption rates. The resulting rates are only those that affect the central carbon metabolism metabolic network. Then the biosynthetic precursor demands are factored into the flux calculations as shown in Figure 4-1. The exact procedure used is described in more detail in Zupke (Zupke, 1993).

4.5 Pentose Phosphate Pathway Analysis

4.5.1 Introduction

An important parameter in metabolic pathway analysis is the flux of carbon through the pathway. Accurate determination of metabolic fluxes *in-vivo* is a critical step in elucidating flux control in metabolic networks. Sensitive experimental techniques and rigorous modeling methods are both required for the calculation of accurate flux values. Currently, the methods used to calculate metabolic fluxes involve metabolite balancing and isotope labeled substrate analysis techniques (Bonarius et al., 1996; Bonarius et al., 1998a; Bonarius et al., 1998b; Mancuso et al., 1998; Mancuso et al., 1994; Marx et al., 1996; Park et al., 1999; Park et al., 1997; Sharfstein et al., 1994; Vallino and Stephanopoulos, 1994b; Vallino and Stephanopoulos, 1994a; Vallino and Stephanopoulos, 1993; Wiechert and de Graaf, 1997a; Wiechert and de Graaf, 1996; Wiechert et al., 1997b; Zupke et al., 1995b; Zupke and Stephanopoulos, 1995a). Isotope labeling techniques are particularly useful due to the additional information contained in the metabolite carbon label fractional enrichment values resulting from the scrambling of the input substrate label. However, the models used to analyze these isotope distributions frequently make assumptions about the reversibility of the reactions, and these assumptions can result in errors concerning the estimated metabolic fluxes and isotope label scrambling. This section concentrates on the development of a methodology that allows reaction reversibility to be included in more accurate calculations of metabolic fluxes in metabolic networks by explicitly accounting for the effect of reaction reversibility on metabolite labeling upon administration of labeled substrates. In addition, it addresses a fundamental problem of flux analysis concerning the uniqueness of flux estimates and the experimental measurements needed to obtain accurate solutions. Although this analysis was not utilized in the flux calculations for the continuous

cultures due to its complexity, it was performed in an effort to determine the data that are needed for accurate flux calculation using isotope tracers and also the potential errors that can arise when isotope tracer scrambling is not correctly analyzed.

Pentose phosphate pathway. The pentose phosphate pathway plays several key roles in metabolism. It contributes to the redox potential in a cell through the maintenance of the $NADPH/NADP^+$ ratio and is also source of biosynthetic carbon skeletons (Stryer, 1988). Recent research has demonstrated that the pentose phosphate pathway can carry a significant flux under certain physiological conditions and in various cell types (Bonarius et al., 1996; Landau and Wood, 1983). Finally, the pathway can redistribute metabolite carbon atoms leading to difficulties in determining fluxes in other pathways using labeled substrates (Berthon et al., 1993; Flanigan et al., 1993; Park et al., 1997). Therefore, the pentose phosphate pathway can have a significant impact not only in the maintenance of cellular function but in the analysis of isotope labeled substrate experiments as well.

The pentose phosphate pathway, commonly referred to as the classical pathway, was elucidated in the late 1950's using data from labeled substrate experiments, in particular labeled $^{14}CO_2$ evolution rates and metabolite conversion rates in tissue extracts (Katz and Wood, 1963; Katz and Wood, 1960; Williams, 1980). This classical pathway is divided into two different groups of reactions, the oxidative and nonoxidative branches. The oxidative branch begins with the dehydrogenation of glucose 6-phosphate by glucose 6-phosphate dehydrogenase to form 6-phosphogluconate and NADPH. An additional reaction produces another molecule of NADPH along with ribulose 5-phosphate, which can then be isomerized to ribose 5-phosphate and used for DNA and RNA nucleotide sugar biosynthesis. These reactions are all summarized in Figure 4-2 with v_1 representing the oxidative pathway and v_4, v_5, and v_6 referring to the nonoxidative

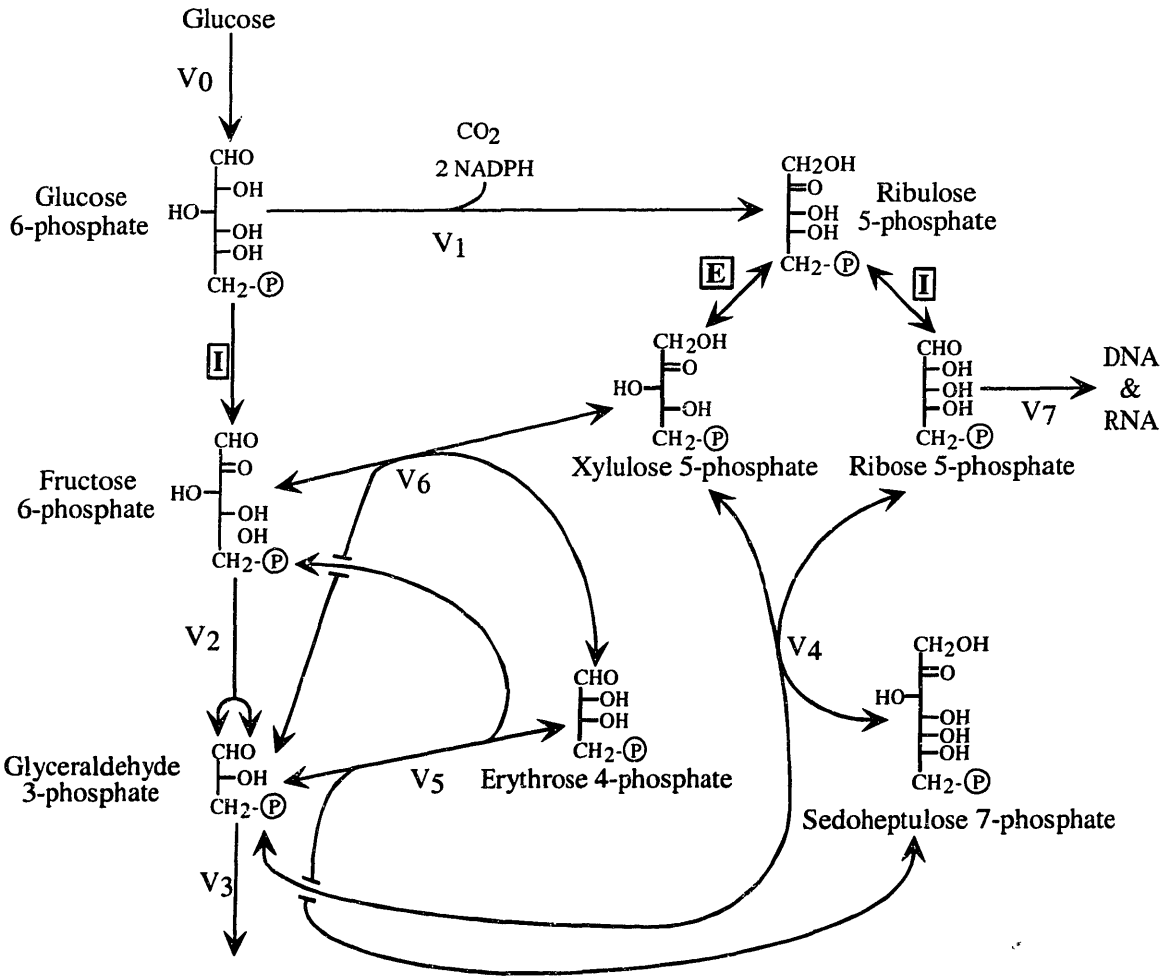

Figure 4-2. The classical pentose phosphate pathway reaction network. The oxidative reactions are referred to as v_1, and the nonoxidative reactions are denoted v_4, v_5, and v_6. The reactions that are part of the glycolytic pathway are v_0, v_2, and v_3. The isomerase and epimerase reactions (shown as E and I) between the hexose and pentose metabolites are considered to be fast and in equilibrium.

reactions. The isomerase and epimerase reactions between the hexose and pentose metabolites (E and I in Figure 4-2) are fast and in equilibrium (Katz and Rognstad, 1967; Landau and Wood, 1983; Wood, 1985). Therefore, glucose and fructose 6-phosphate are treated as one hexose pool (Hex6P), and the three pentose metabolites are treated as one pentose pool (Pen5P). Finally, the reactions v_0, v_2, and v_3 refer to the glycolysis reactions that are part of this network, and v_7 refers to the DNA and RNA biosynthetic pathway reactions (Stryer, 1988).

The reversible transketolase and transaldolase reactions in the nonoxidative pathway redistribute metabolite carbon atoms in an organized manner through the enzyme transfer of two and three carbon units to intermediate metabolites. The transfer scheme of the various metabolite carbon atoms in these reactions is illustrated in Figure 4-3 with the circles representing the various numbered metabolite carbon atoms. Since these reactions are all reversible, they are split into a forward reaction (v_i^+) and a reverse reaction (v_i^-). This reversibility can lead to further redistribution due to exchange with glycolytic intermediates, and this redistribution must be analyzed in order to interpret pentose phosphate pathway experimental data correctly.

Flux calculation - background. Isotopic labeling experiments have been performed and analyzed since the late 1950's and early 1960's with the aim of verifying the biochemistry of the classical pentose phosphate pathway (Katz and Wood, 1963; Katz and Wood, 1960). These experiments have all been analyzed using a simplified general model which assumes recycling of fructose 6-phosphate to glucose 6-phosphate through the isomerase reaction and also assumes isotopic steady state. Furthermore, the model assumes no reversibility of the transketolase and transaldolase reactions and thus no recycling of triose 3-phosphate and no label redistribution. The overall reaction for this simplified view of the pentose phosphate pathway is given as:

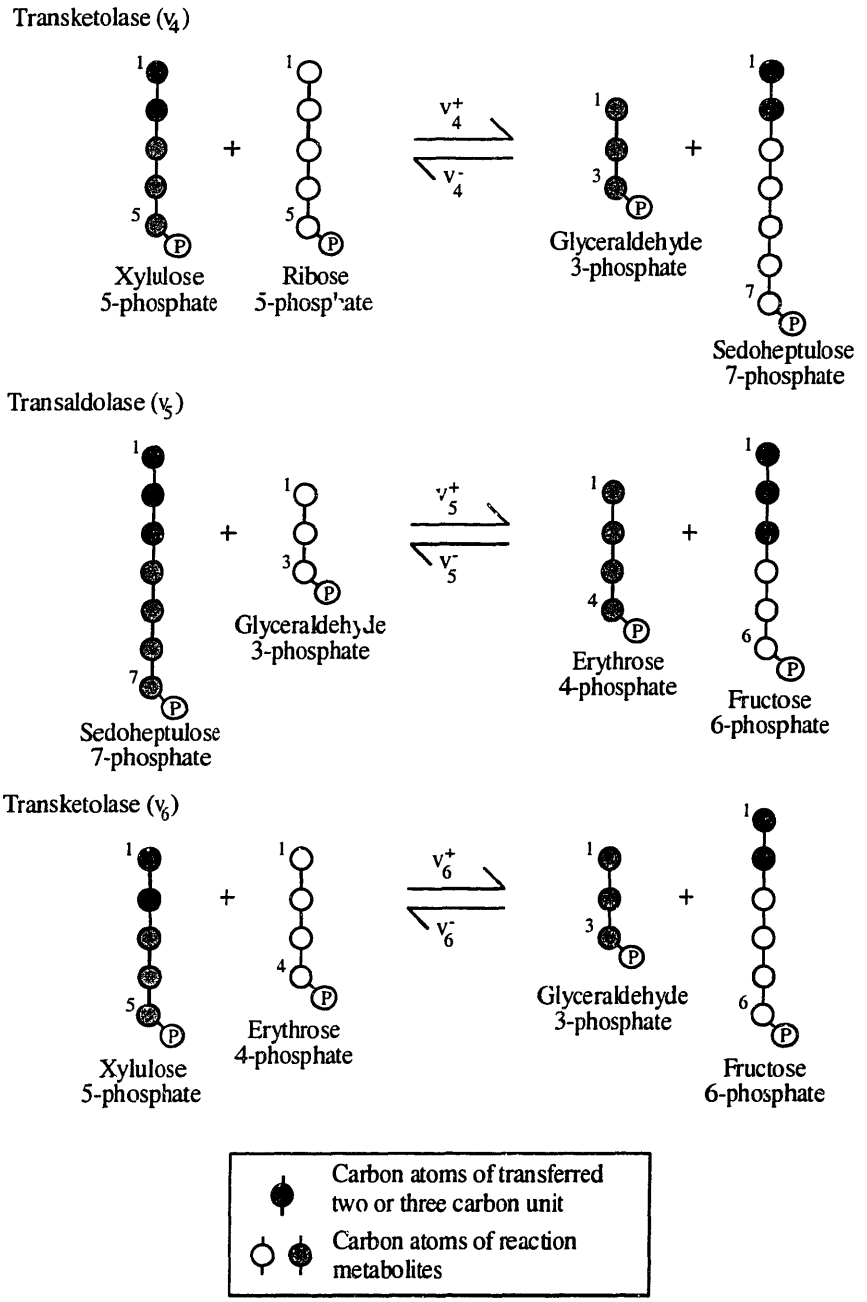

Figure 4-3. The nonoxidative pathway carbon atom redistribution scheme. The numbered circles refer to the metabolite carbon atoms. The black carbon atoms denote either the two or three carbon atom units that are transferred to the other metabolites in the reactions.

$$3\ \text{Hexose} \xrightarrow{3CO_2\uparrow} 3\ \text{Pentose} \longrightarrow 2\ \text{Hexose} + 1\ \text{Triose} \qquad (4.17)$$

To test this model, researchers used [1-^{14}C]glucose and [6-^{14}C]glucose labeled substrates which allowed them to differentiate between those glucose molecules metabolized through the pentose phosphate pathway versus those that pass exclusively through glycolysis. This strategy was also used in order to determine label loss and scrambling due to the tricarboxylic acid cycle. [1-^{14}C]glucose and [6-^{14}C]glucose both become [3-^{14}C]glyceraldehyde 3-phosphate after the aldolase glycolytic reaction, and the [3-^{14}C]glyceraldehyde 3-phosphate labeled carbon is subsequently scrambled and lost as $^{14}CO_2$ identically after this reaction. Therefore, any difference between radioactive carbon activities of the hexose monophosphate pool upon using [1-^{13}C]glucose and [6-^{13}C]glucose was assumed to be due to the pentose phosphate pathway. Observed differences between activities of the Hex6P pool for the two cases was used to determine the fraction of input hexose that flows through the nonoxidative branch of the pentose phosphate pathway (P) (defined as v_4/v_0):

$$\frac{\alpha_1}{\alpha_6} = \frac{1}{(1+2P)} \qquad (4.18)$$

α_i denotes the specific activity of the hexose 6-phosphate pool when [i-^{14}C] labeled glucose was used. The derivation of equation 4.18 (Follstad and Stephanopoulos, 1998) accounts for the outflow of labeled carbon via the pentose phosphate pathway versus other pathways (tricarboxylic acid cycle, *etc.*). This model can also be used to formulate equations to compare triose carbon label enrichment or the amount of labeled $^{14}CO_2$ released for cells fed with [1-^{14}C], [2-^{13}C], and [6-^{14}C]glucose (Katz and Wood, 1963; Katz and Wood, 1960; Landau and Katz, 1964).

Other models have been used to determine the pentose phosphate pathway flux. One model used a black-box approach to determine a lower limit to the pathway flux by measuring

labeled CO_2 release (Larrabee, 1989). Another model employed [3-^{13}C]lactate labeling resulting from [1-^{13}C] and [6-^{13}C]glucose to determine the pathway flux (Kingsley-Hickman et al., 1990; Willis et al., 1986). However, when these models were applied to experimental data of specific carbon activities of metabolites such as glucose 6-phosphate, glycogen, or lactate in various tissues, they could not fully account for the observed label distributions.

Disagreement between predictions of these simplified models and experimental data led researchers to propose alternative explanations for the observed labeling patterns. Inconsistencies in gluconeogenic rat liver data led to the hypothesis of an alternative L-type pentose phosphate pathway that contains several new intermediates resulting in a different carbon redistribution scheme (Williams, 1980; Williams and Blackmore, 1983; Williams et al., 1978). This hypothesis is still refuted in the literature by several researchers (Landau and Wood, 1983; Rognstad, 1995). Yet another hypothesis included fructose futile cycles to allow for carbon label scrambling. Finally, although researchers have included nonoxidative reaction reversibility in their models to account for label redistribution (Katz and Rognstad, 1967), the calculation of the individual extents of reaction reversibility using a general model is still not adequate. In summary, despite numerous hypotheses proposed to reconcile observed inconsistencies between models and experimental data in the pentose phosphate pathway, a method for the systematic quantitation and tracking of isotope labels has yet to be presented.

4.5.2 Theory

A general model utilizing mass balance equations can be formulated for any reaction network and then be used to analyze carbon label redistribution and extents of reaction reversibility. Other flux analysis models presented in the literature utilize similar basic concepts of mass balances for flux determination (Wiechert and de Graaf, 1997a; Wiechert et al., 1997b).

The model of this paper is based on the work of Park (Park, 1996) and Katz and Rognstad (Katz and Rognstad, 1967) and is applied to the pentose phosphate pathway reaction network illustrated in Figure 4-2. The metabolite pools are assumed to be well-mixed. Also, since the isomerase and epimerase pentose phosphate pathway reactions (E and I in Figure 4-2) are considered fast, they are assumed to be at equilibrium, hence the three pentose metabolites are treated as one pentose pool (Pen5P). Similarly, glucose and fructose 6-phosphate are treated as one hexose pool (Hex6P) due to the isomerase reaction. The nonoxidative reactions are assumed to follow the carbon redistribution scheme shown in Figure 4-3. Finally, the reaction velocity for DNA and RNA biosynthesis reactions (v_7) is assumed to be small and is neglected in this analysis. If this assumption proves to be incorrect in some systems, the addition of this reaction to the model equations will result in the need to calculate one additional parameter.

Mass balances. The model utilizes two types of mass balances, one of reaction network metabolite pools, and a second of metabolite carbon atoms. The first, (equation 4.19), describes the overall balance of network metabolite pools:

$$\frac{dx_j}{dt} = \sum_i \beta_{j,i} v_i \tag{4.19}$$

In the above equation, x_j refers to the concentration of metabolite j (mole/cell), $\beta_{j,i}$ is the stoichiometric coefficient for reaction i for metabolite j, and v_i refers to the velocity of reaction i (mole/hr/cell). For the pentose phosphate pathway depicted in Figure 4-2, the metabolite balance equations are listed in the appendix along with the steady state solutions. The value P represents the ratio of the nonoxidative reaction flux to the glucose uptake rate (v_4/v_0) as defined in Katz and Rognstad (Katz and Rognstad, 1967). For example, when P equals one, the oxidative flux is $3v_0$ and v_2 equals zero resulting in one glucose molecule being converted into three CO_2 molecules and one glyceraldehyde 3-phosphate molecule. Note that rates of reactions appearing

in the metabolite balances of equation 4.19 refer to the *overall* (or *net*) flux through the pentose phosphate pathway; no measure of reversibility can be calculated from these rates. The calculated flux values show that, at steady state, the net fluxes through the nonoxidative pathway reactions are equal.

Reaction reversibility can be accounted for by recognizing a forward (v_i^+) and reverse (v_i^-) reaction, with the extent of reaction reversibility represented by a_i which is scaled by the glucose uptake rate v_0:

$$v_i = v_i^+ - v_i^- \tag{4.20}$$

$$v_i^+ = v_i + a_i v_0 \tag{4.21}$$

$$v_i^- = a_i v_0 \tag{4.22}$$

The extents of reaction reversibility may all vary but still result in a constant steady state net flux. For example, Figure 4-4 shows two different cases for a metabolite pool (M). Here, the length of the arrows refers to the relative value of the flux (a large arrow depicting a large flux). In both cases, the net flux through the metabolite pool ($v_1=v_2$) is the same; however, reaction extents of reversibility may be different. Case 1 illustrates the pool at steady state with the same extents of reversibility for the two fluxes. Case 2 illustrates the same net flux, but the extents of reversibility for the two reactions are different. In this case, the values for v_2^+ and v_2^- are much greater than the values for v_1^+ and v_1^- although the difference between the two is the same. Differences in extents of reversibility affect the label redistribution of the intermediate metabolites. Therefore, assuming equal extents of reversibility for the transketolase and transaldolase reactions of the pentose phosphate pathway could lead to errors in the data analysis.

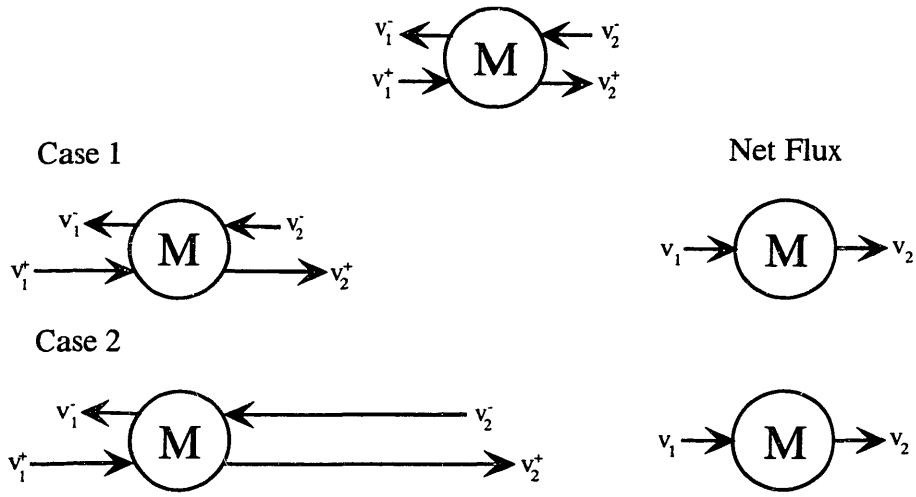

Figure 4-4. The extent of reaction reversibility can vary without altering the net flux. Here, the metabolite pool (M) has equal net input and output fluxes v_1 and v_2 with the length of the arrow referring to the relative value of the flux. Each net flux can be divided into a forward and reverse flux (ex. v_1^+ and v_1^-) with the extent of reversibility denoting the relative sizes of these two fluxes. In case 1, the extents of reversibility are equal, but the extents for case 2 are significantly different with reaction 2 having a larger reversibility that reaction 1.

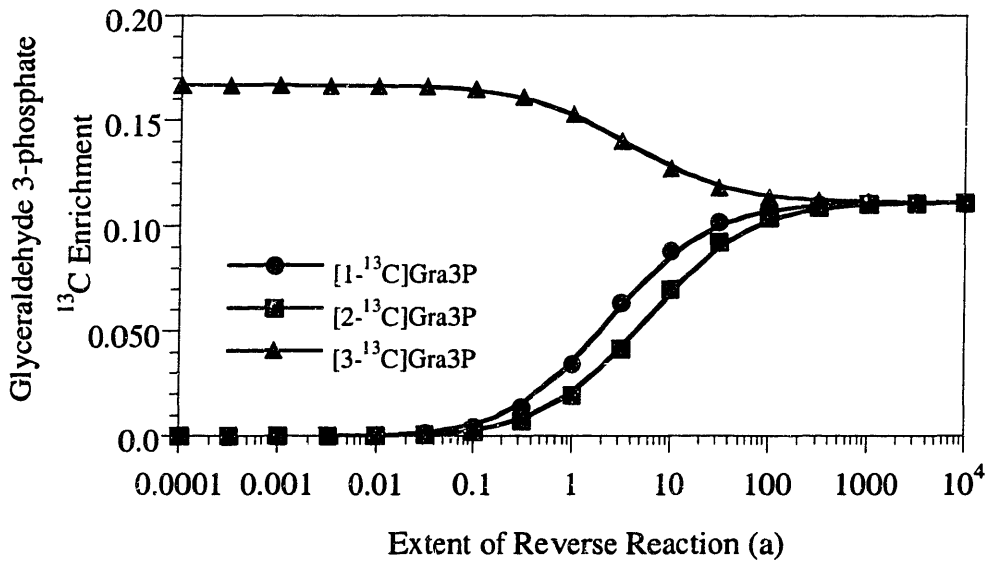

Figure 4-5. [1-^{13}C], [2-^{13}C], and [3-^{13}C]glyceraldehyde 3-phosphate fractional enrichments plotted as a function of a (a_4=a_5=a_6) resulting from [1-^{13}C]glucose input. The fractional enrichments vary with reaction reversibility and approach various asymptotic values as the reversibility becomes either small (<0.1) or large (>10).

The introduction of reversibility is accompanied by an increase in the number of unknown fluxes that must be determined for the complete description of the pathway. These additional unknowns can be determined from measurements of metabolite label distributions upon administration of labeled carbon substrates in conjunction with a second set of mass balance equations. These equations reflect overall balances on each carbon atom in the reaction network:

$$\frac{d\left(x_j y_j(m)\right)}{dt} = \sum_i \sum_l \beta_{l,i} v_i y_l(n) - y_j(m) \sum_i \beta_{j,i} v_i \qquad (4.23)$$

Here $y_j(m)$ denotes the fractional enrichment (^{13}C) or specific activity (^{14}C) of the m^{th} carbon atom of metabolite j. In addition, n denotes the carbon atom of metabolite l mapped to carbon atom m of metabolite j in reaction i (Follstad and Stephanopoulos, 1998). The above equation applied to the carbon atoms of the pentose phosphate pathway metabolites yields the equations given in Follstad and Stephanopoulos (Follstad and Stephanopoulos, 1998). At steady state, unknown metabolic fluxes (v_i) and nonmeasured fractional enrichments ($y_i(m)$) can be calculated from a sufficient number of extracellular metabolite fluxes and label fractional enrichments using a mathematical software program such as Mathematica or Matlab.

Algorithm for solving the balance equations. The mass balance equations (4.19 and 4.23) can be cast in the following matrix form (equation 4.24):

$$\begin{bmatrix} A_{1,1}(P,a_4,a_5,a_6) & \cdots & A_{1,j}(P,a_4,a_5,a_6) \\ \vdots & & \vdots \\ A_{i,1}(P,a_4,a_5,a_6) & \cdots & A_{i,j}(P,a_4,a_5,a_6) \end{bmatrix} \bullet \begin{bmatrix} y_1 \\ \vdots \\ y_j \end{bmatrix} = \begin{bmatrix} b_1 \\ \vdots \\ b_j \end{bmatrix} \qquad (4.24)$$

The matrix elements A_{ij} represent coefficients in the metabolite carbon balance equations, y_j stands for the nonmeasured carbon atom label fractional enrichments or activities, and the b_j values refer to the fractional enrichments of the labeled input substrate. If the fraction of input

hexose flowing through the nonoxidative pathway (P) and the three nonoxidative pathway extents of reversibility (a_4, a_5, and a_6) are known, the linear system of equations can be solved easily for the fractional enrichment values. This method was used to perform the variational studies presented in the results section. However, the determination of these variables from experimental fractional enrichment measurements is in general a non-trivial issue, for it entails the solution of nonlinear carbon atom balance equations. For the case of a small number of unknown reaction reversibilities, the following iterative procedure can be used: a) formulate the matrix $\mathbf{A} = \mathbf{A}(P, a_4, a_5, a_6)$ of equation 4.24; b) guess a set of initial values for a_4, a_5, and a_6; c) determine P from the overall metabolite balance and ensure that matrix **A** is invertible ($\det\mathbf{A} \neq 0$) for the guessed values of a_4, a_5, and a_6; d) determine y by solving $\mathbf{A}y = b$; e) adjust the values of a_4, a_5, and a_6 by applying typical gradient methods with the ultimate goal of matching the experimental data ($y_{i,meas.}$) with the calculated values $y_{i,calc.}$ (i.e. iterate the algorithm and adjust the values until $y_{i,calc.}$ equals $y_{i,meas.}$).

In this paper, this iterative procedure was employed to calculate the extents of reaction reversibility for sets of experimental data obtained from the literature. Other solution methods can also be used to solve this nonlinear system of equations, such as the Newton-Raphson method or nonlinear regression methods.

4.5.3 Results

The above method was applied to the classical pentose phosphate pathway reaction network to study the effect of varying extents of reaction reversibility on label distribution and achieve the reconciliation of published data sets.

Effect of reaction reversibility. Label enrichments of intermediate metabolites were calculated first as a function of two parameters: the fraction of the input glucose utilized through

the nonoxidative pathway (P), and the extent of reversibility in the transaldolase and transketolase reactions (a). Figure 4-5 shows the labeling of [1-^{13}C], [2-^{13}C], and [3-^{13}C]glyceraldehyde 3-phosphate resulting from [1-^{13}C]glucose input for varying values of the extent of reversibility a, initially assumed to be the same for all reactions. These figures show that the enrichment approaches different asymptotic values for very small reversibilities (<0.1) but converges to the same value as the reversibility becomes large (>10). Figure 4-6 shows the label enrichment of [3-^{13}C]glyceraldehyde 3-phosphate resulting from [1-^{13}C]glucose, as a function of both P and a. As P increases, the fractional enrichment decreases and becomes less sensitive to the extent of reaction reversibility. The use of [2-^{13}C] and [3-^{13}C]glucose input yields more complicated enrichment patterns due to more extensive label scrambling (data not shown), while [4-^{13}C], [5-^{13}C], and [6-^{13}C]glucose input results in no change in output glyceraldehyde 3-phosphate labeling when the extent of reversibility varies. For example, the labeling of [3-^{13}C]glyceraldehyde 3-phosphate resulting from [6-^{13}C]glucose input is shown in Figure 4-7 as a function of P and a. The fractional labeling in this case does not depend on the extent of reversibility but rather on the net flow through the pentose phosphate pathway due to the loss of CO_2.

The previous plots illustrate the effects of reaction reversibility when the extent of reversibility is the same for all nonoxidative pathway reactions. Since these extents can vary independently, their individual effects on label distribution was further investigated. There are four adjustable parameters in this case, (P, a_4, a_5, and a_6), and pictorial representations of the numerical variation studies are shown in Figures 4-8 through 4-11 for the case where P is fixed and two of the extents of reversibility are identical. The data shown here are for [1-^{13}C]glucose feeding with P equal to 0.50. Although varying P does affect carbon labeling (as shown

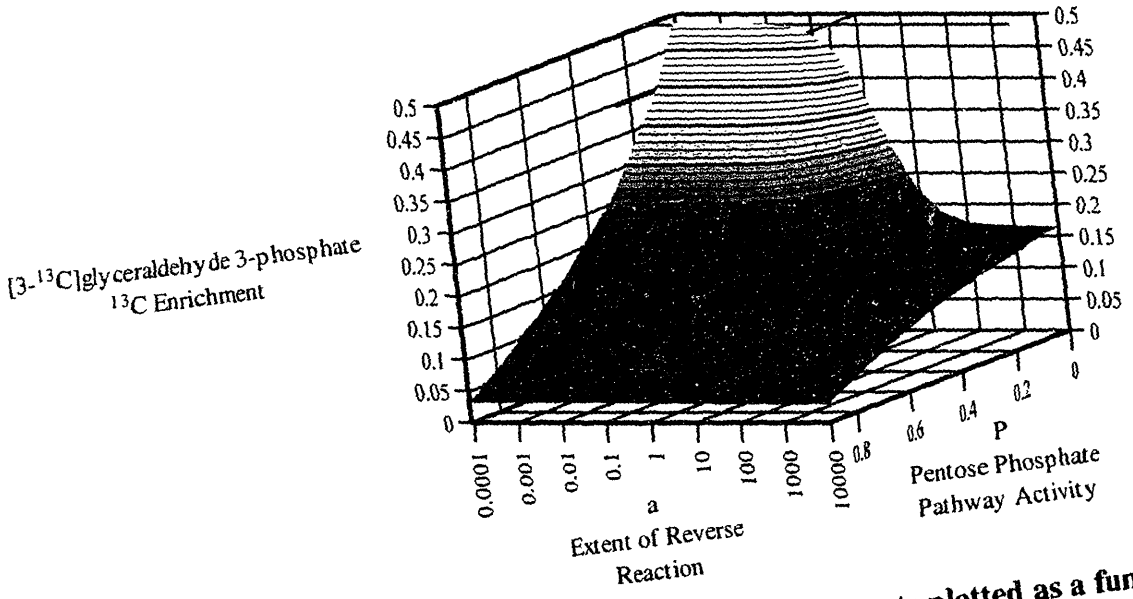

Figure 4-6. [3-^{13}C]glyceraldehyde 3-phosphate fractional enrichments plotted as a function of P and a (a_4=a_5=a_6) resulting from [1-^{13}C]glucose input. The fractional enrichment decreases as P increases and low P values result in the largest variability in fractional enrichment due to reaction reversibility.

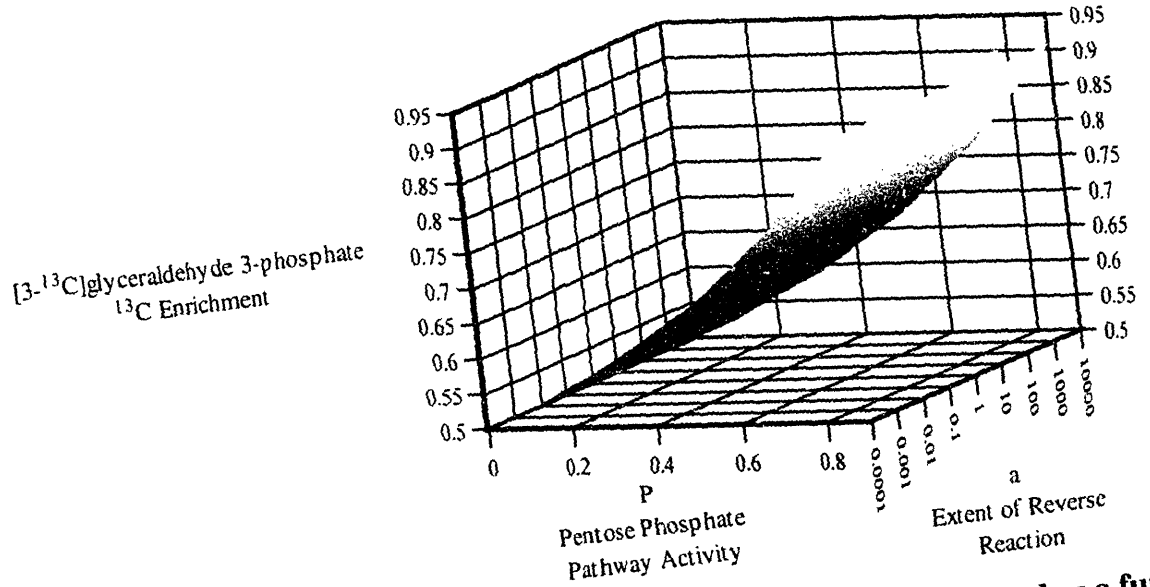

Figure 4-7. [3-^{13}C]glyceraldehyde 3-phosphate fractional enrichments plotted as a function of P and a (a_4=a_5=a_6) resulting from [6-^{13}C]glucose input. The fractional enrichment varies only as a function of P, and label is not scrambled to other metabolite carbons (i.e. only one metabolite carbon is labeled). However, when the reversibilities are not equal (i.e. $a_4 \neq a_5 \neq a_6$) the fractional enrichment can vary even though the label is still not scrambled to other metabolite carbons (data not shown).

previously in Figure 4-6), this effect is not shown in Figures 4-8 through 4-11. In general, a lower value for P results in greater label variation.

The determination of three extents of reversibility requires that a minimum of three label measurements be obtained. It is not a priori obvious which label enrichment measurements would provide the most information in resolving a set of three reaction reversibilities. The determination of the particular label enrichments that optimize the observability of reaction reversibilities is a separate problem that is not addressed in this paper. Here we limit our investigation to a variational study where the effect of reversibilities on different metabolite enrichments is presented. Figure 4-8 illustrates the results for the expected labeling of [6-^{13}C]Hex6P. The curves of this plot show the resulting ^{13}C enrichment when one extent of reversibility is varied while the other two are held fixed at the indicated value. For example, the leftmost curve shows the variation in [6-^{13}C]Hex6P when a_4 is varied from 0.0001 to 10000 while a_5 and a_6 both equal zero. The three sets of curves illustrate the effects that each individual transketolase and transaldolase reaction reversibility can have on labeling. The figure also shows some problems that could arise when one attempts to experimentally determine these reversibilities. The relative flatness of the a_6 curves suggests that the measurement of the enrichment of this metabolite would not be particularly valuable in determining a_6 accurately. Also, the similarity between the curves for a_4 and a_6 points out that some difficulty could arise in distinguishing between these two variables with this particular measurement.

Figure 4-9 shows carbon enrichment values for [1-^{13}C]Pen5P and Figure 4-10 shows values for [5-^{13}C]Pen5P. Figure 4-9 shows that this particular carbon enrichment measurement would lead to difficulties in differentiating a_4 from a_5 but might be helpful in determining a_6. Figure 4-10 illustrates that small differences result when the three extents of reaction

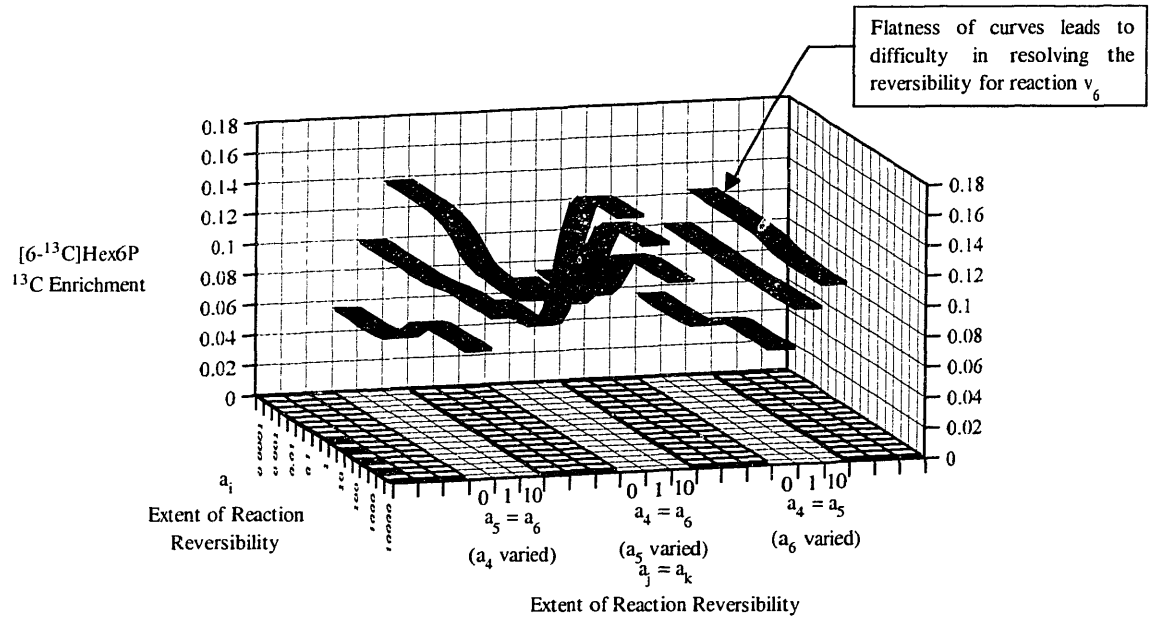

Figure 4-8. [6-^{13}C]Hex6P fractional enrichments plotted as a function of a_i with P equal to 0.50 resulting from [1-^{13}C]glucose feeding. For each curve, one extent of reaction reversibility is varied while the other two are fixed at the specified values. For this case, varying a_6 results in small changes in enrichment, and differences between variations in a_4 and a_6 may be difficult to resolve. Varying a_5, however, results in different behavior helping to resolve this reaction reversibility.

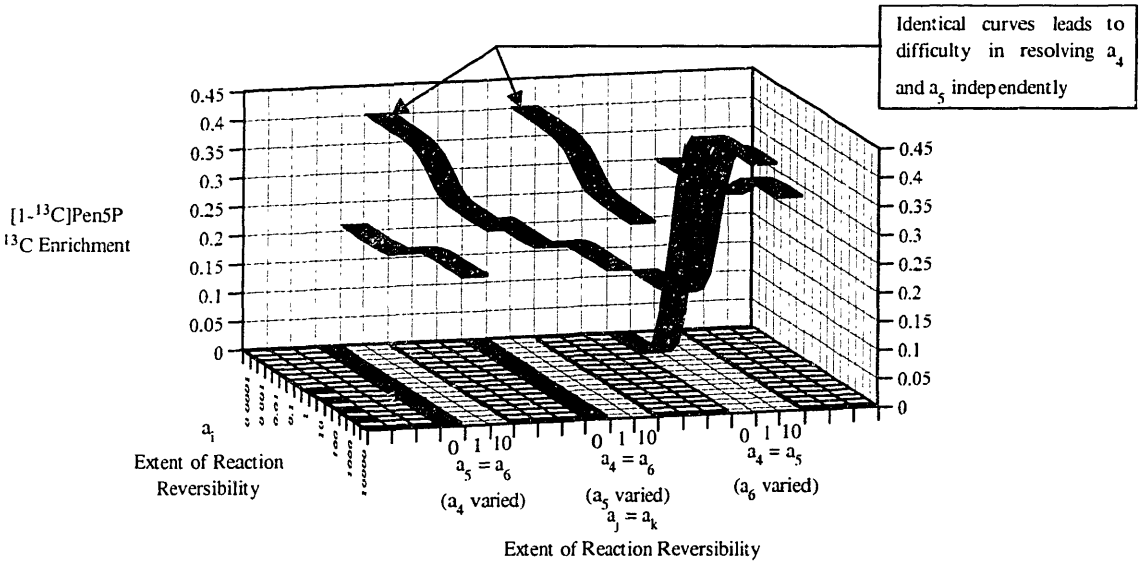

Figure 4-9. [1-^{13}C]Pen5P fractional enrichments plotted as a function of a_i with P equal to 0.50 resulting from [1-^{13}C]glucose feeding. For each curve, one extent of reaction reversibility is varied while the other two are fixed at the specified values. For this case, variances in a_4 and a_5 lead to identical or overlapping curves which leads to difficulty in resolving these reversibilities individually. The fact that varying a_6 leads to a different set of curves aids in the determination of this reversibility.

reversibility are varied separately. Therefore, the information content if Pen5P label measurements is not particularly high and could lead to inaccurate reversibility estimates.

A key metabolite in this pathway is erythrose 4-phosphate (Ery4P). Although Ery4P is difficult to isolate and analyze with NMR, the labeling of this metabolite can be determined indirectly through aromatic amino acid analysis since Ery4P is a precursor in the biosynthesis of these amino acids (Szyperski, 1995). Figure 4-11 illustrates the effects of varying each extent of reversibility on [4-^{13}C]Ery4P enrichment. The carbon enrichment of this metabolite shows significant dependence on reversibility extents, with little curve overlap. This indicates that this measurement is quite valuable in the determination of accurate extents of reaction reversibility.

The above figures illustrate the effects reversible reactions can have on metabolite carbon label fractional enrichment. These effects become particularly important when the overall flux through the pathway is low but the reversible reactions carry a high exchange flux. In such cases, ignoring carbon label scrambling brought about by reaction reversibility in the pentose phosphate pathway would affect the determination of the fluxes in other parts of the metabolic network such as the tricarboxylic acid cycle, and lead to discrepancies between model predictions and experimental data. The variational studies also show that the reversibility extent and accuracy of flux determination depend on the particular choice of metabolite carbon enrichments measured. For example, [6-^{13}C]Hex6P and [4-^{13}C]Ery4P are particularly important measurements due to the fact that they are sensitive to variations in each of the reversible reactions. On the other hand, [1-^{13}C] and [5-^{13}C]Pen5P are not as useful, but they could still be used along with other metabolite carbon enrichment values, such as [3-^{13}C]Gra3P, to add redundancy to the data set and help determine the three extents of reversibility with a higher degree of accuracy.

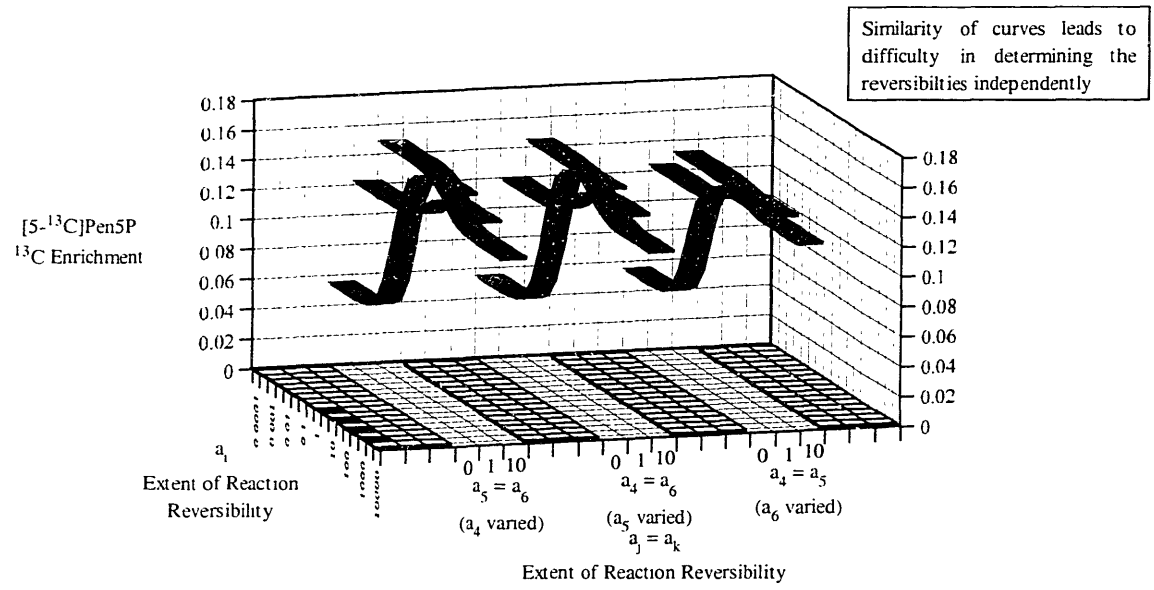

Figure 4-10. [5-^{13}C]Pen5P fractional enrichments are plotted as a function of a_i with P equal to 0.50 resulting from [1-^{13}C]glucose feeding. For each curve, one extent of reversibility is varied while the other two are fixed at the specified values. In this case, nearly all of the curves are identical and overlap leading to virtually no way to determine individual reversibilities.

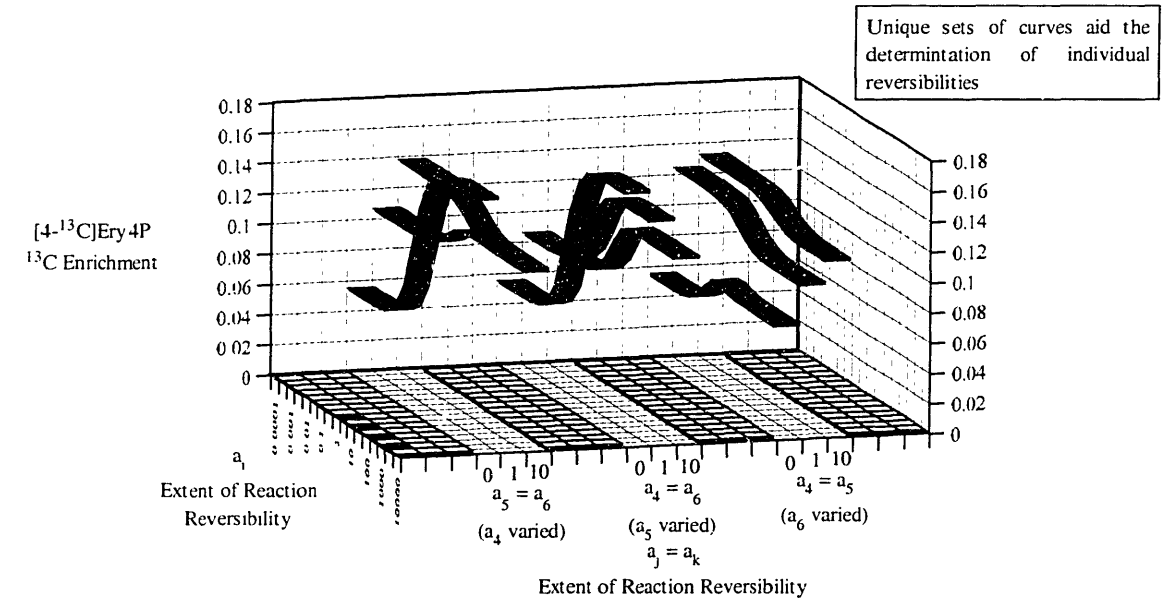

Figure 4-11. [4-^{13}C]erythrose 4-phosphate fractional enrichments are plotted as a function of a_i with P equal to 0.50 resulting from [1-^{13}C]glucose feeding. For each curve, one extent of reversibility is varied while the other two are fixed at the specified values. For this case, variations in each of the three reversibilities results in curves that all differ helping to resolve these reversibilities. This demonstrates that [4-^{13}C]Ery4P is a key enrichment measurement and should be included in the experimental measurement data set if one wants to calculate accurate reversibility values.

A similar exercise can be performed for the use of other labeled substrates in analyzing the pentose phosphate pathway. For example, in the case for [2-^{13}C]glucose feeding, large ^{13}C enrichments are localized in [5-^{13}C]Hex6P, [2-^{13}C]Pen5P, [4-^{13}C]Pen5P, and [3-^{13}C]Ery4P. In addition, variations in [5-^{13}C]Hex6P and [3-^{13}C]Ery4P enrichments are also valuable due to their different response to each of the non-oxidative reaction reversibilities (data not shown) which is a result similar to that obtained for these two metabolites with [1-^{13}C]glucose feeding.

Comparison with literature data. The method presented in this paper yields theoretical predictions that are in agreement with those of other models in the literature such as that of Wiechert et al. (Wiechert and de Graaf, 1997a) for glyceraldehyde 3-phosphate and erythrose 4-phosphate labeling obtained upon xylose feeding to cultures of *Zymomonas mobilis* (data not shown). In addition, this method was applied to the analysis of several sets of published ^{14}C specific activity and ^{13}C fractional enrichment data for Hex6P, Pen5P, Ery4P, and Gra3P metabolite carbons. Although these data sets do not contain the ideal set of enrichment measurements for Hex6P and Ery4P described previously, one can still obtain estimates of reaction reversibility. These data sets covered a wide range of tissue types and cell culture conditions. We omitted data involving the analysis of gluconeogenesis, such as that from rat liver, due to the fact that the reversibility of reaction v_2 introduced by gluconeogenesis involves the addition of another variable in the model.

In two studies (Hostetler et al., 1966; Landau and Katz, 1964), the distribution of ^{14}C in glycogen from rat epididymal adipose tissue and goosefish islet cells incubated with [2-^{14}C]glucose was tabulated. Tables 4-1 and 4-2 show the specific activities of each glycogen (Hex6P) carbon atom relative to the C-2 glycogen label. The value for P was estimated using equation 4.18 and variations of equation 4.18 due to the limited metabolite data. Assuming no

Table 4-1. Rat epididymal adipose tissue ^{14}C label data. ^{14}C label data for Hex6P (glycogen) from rat epididymal adipose tissue supplied with either a high (Ins^+) or low insulin concentration (Ins^-) and with [2-^{14}C]glucose substrate. Experimental values are compared with model predictions assuming no reversibility and reversibility for transketolase and transaldolase reactions (Landau and Katz, 1964). At low insulin concentration, P = 0.13; at high insulin concentration, P = 0.23.

Method	Insulin	Relative ^{14}C specific activity of Hex6P at					
		C-1	C-2	C-3	C-4	C-5	C-6
Experimental	low	15.2	100	12.8	1.9	13.9	2.9
	high	30.7	100	17.9	3.5	14.8	5.3
Model: no reversibility							
(a_4=a_5=a_6=0.0)	low	20.6	100	11.5	0.6	5.4	1.1
	high	31.5	100	18.7	1.5	8.1	2.5
Model: reversibility							
(a_4=0.5, a_5=0.2, a_6=0.0)	low	18.8	100	15.8	2.1	13.4	2.5
(a_4=0.8, a_5=0.08, a_6=0.0)	high	30.5	100	20.9	2.7	13.1	4.0

Table 4-2. Goosefish islet cell ^{14}C label data. ^{14}C label data for Hex6P (glucose polysaccharide) from goosefish islet cells supplied with [2-^{14}C]glucose. Experimental values compared with model predictions assuming no reversibility and reversibility for transketolase and transaldolase reactions (Hostetler et al., 1966). P = 0.075.

Method	Relative ^{14}C specific activity of Hex6P at					
	C-1	C-2	C-3	C-4	C-5	C-6
Experimental	11.1	100	8.3	1.3	15.0	1.7
Model: no reversibility						
(a_4=a_5=a_6=0.0)	12.0	100	7.0	1.0	3.0	1.0
Model: reversibility						
(a_4=0.005, a_5=0.5, a_6=0.005)	13.0	100	7.2	1.0	15.5	2.0

reversibility, the model underestimates the relative specific activity at C-5 for both studies. In the rat adipose tissue study, a moderate reaction 4 (v_4) extent of reversibility ($a_4 = 0.5$), a smaller reaction 5 (v_5) extent of reversibility ($a_5 = 0.2$), and virtually no reaction 6 (v_6) reversibility results in closer agreement with the experimental data. Also, an insulin effect on the extents of reversibility is revealed. The study with goosefish islet cells shows similar improvement in the resolution of C-5 specific activity with rather low reaction 4 and 6 extents of reversibility ($a_4=a_6=0.005$) and a higher reaction 5 extent of reversibility ($a_5=0.5$). No reversibility estimates were presented in these papers, however, the results of Tables 4-1 and 4-2 show that the agreement of the experimental data improved with the addition of non-zero extents of reaction reversibility.

Another study reported ^{13}C fractional enrichment for several metabolites from steady state *C. glutamicum* chemostat cultures (Marx et al., 1996). Table 4-3 compares the experimental fractional enrichments for erythrose 4-phosphate and glyceraldehyde 3-phosphate with the ones predicted by the model. In this case, the value for P was calculated from the metabolite balance data. Assuming no nonoxidative pathway reversibility, the model is unable to determine values consistent with the experiments, particularly for the C-4 carbon of erythrose 4-phosphate. However, adding reversibility to the model improves the estimates of fractional enrichment, lowers the C-3 value for glyceraldehyde 3-phosphate, and increases the values for the other carbons. The relatively high value of the C-3 carbon enrichment of glyceraldehyde 3-phosphate could be explained by adding another flux from the glyceraldehyde 3-phosphate pool to amino acids synthesis such as serine or glycine, two reactions not covered in the reaction network considered. Note that the extents of reversibility are all different, and that the measurement of erythrose 4-phosphate carbon atom fractional enrichment is particularly useful

Table 4-3. *C. glutamicum* ^{13}C label data. ^{13}C label data for Ery4P and Gra3P intermediates taken from *C. glutamicum* growing in a chemostat culture with [1-^{13}C]glucose substrate. Experimental values compared with model predictions assuming no reversibility and reversibility for transketolase and transaldolase reactions (Marx et al., 1996). The corresponding reversibility values calculated by Marx et al. (1996) for this study were comparable to those presented here with values of 0.23 for a_5, 0.0 for a_6, and 0.20 for P (scaled to the same flux basis used here) compared to our value of 0.22. However, the value for a_4 was 9.74 which deviated somewhat from our value of 0.5, and possible sources for this deviation are discussed in Results.

Method	Metabolite	Metabolite carbon atom			
		C-1	C-2	C-3	C-4
Experimental	Ery4P	2.5	2.0	1.9	15.3
	Gra3P	2.7	2.6	26.3	-
Model: no transketolase and transaldolase reversibility					
(a_4=a_5=a_6=0.0)	Ery4P	0.0	0.0	0.0	5.2
	Gra3P	0.0	0.0	32.4	-
Model: transketolase and transaldolase reversibility					
(a_4=0.5, a_5=0.1, a_6=0.2)	Ery4P	3.7	0.9	0.3	15.6
	Gra3P	1.9	0.6	31.0	-

Table 4-4. *E. coli* ^{14}C label data at slow growth conditions. ^{14}C label data for Hex6P and Pen5P from *E. coli* at slow growth conditions supplied with [2-^{14}C]glucose substrate. Experimental values compared with model predictions assuming no reversibility and reversibility for transketolase and transaldolase reactions (Katz and Rognstad, 1967). The reversibility values calculated by Katz and Rognstad (1967) are comparable to those presented here with a value of 0.06 for the transaldolase reaction (a_5), a value of 0.05 for the transketolase reactions (a_4 and a_6), and an identical value of 0.02 for P.

Method	Metabolite	Metabolite carbon atom				
		C-1	C-2	C-3	C-4	C-5
Experimental	Hex6P	4	100	4	-	4
	Pen5P	100	107	-	74	-
Model: no reversibility	Hex6P	4	100	2	-	1
(a_4=a_5=a_6=0.0)	Pen5P	100	2	-	1	-
Model: reversibility	Hex6P	4	100	2	-	3
(a_4=0.05, a_5=0.03, a_6=0.05)	Pen5P	100	111	-	68	-

due to the low fractional enrichments of C-1 and C-2 for glyceraldehyde 3-phosphate. In other words, one could not calculate accurate reversibilities based on the low glyceraldehyde 3-phosphate fractional enrichment values without adding the erythrose 4-phosphate measurements. In addition, the reversibility results shown here are fairly consistent with those calculated by Marx et al. (Marx et al., 1996) for this study (see Table 4-3). The approximately ten-fold difference in the values for a_4 is most likely due to the fact that the ribose metabolites were treated individually by Marx et al. (Marx et al., 1996) and not as one pool, and this would affect reversibilities involving the reactions with these metabolites, particularly for reaction a_4.

Finally, the data of a study that measured polysaccharide glucose and RNA ribose labeling in *E. coli* cultures incubated with [2-^{14}C]glucose under different growth conditions were analyzed (Katz and Rognstad, 1967). Tables 4-4, 4-5, and 4-6 show the specific activities of each polysaccharide glucose carbon atom relative to the C-2 label and each ribose carbon atom relative to the C-1 label. In these cases, the value for P was determined from the metabolite balance data. Again, these tables show that the addition of reaction reversibility dramatically improves the agreement of the experimental data with values calculated using the model. Also, the ribose measurements increased the redundancy of the system improving the resolution of the data. For example, using the hexose carbon atom specific activities alone cannot resolve all reaction reversibilities due to the low enrichment values calculated for C-1, C-3, and C-5. However, the addition of the C-2 and C-4 specific activities from ribose 5-phosphate measurements improved the resolution of flux determination by providing additional measurements with high specific activities. In addition, the reversibilities calculated by Katz and Rognstad (Katz and Rognstad, 1967) are comparable to those calculated here (see Tables 4-4, 4-5, and 4-6).

Table 4-5. *E. coli* ^{14}C label data at log growth phase. ^{14}C label data for Hex6P and Pen5P from *E. coli* at log growth phase supplied with [2-^{14}C]glucose substrate. Experimental values compared with model predictions assuming no reversibility and reversibility for transketolase and transaldolase reactions (Katz and Rognstad, 1967). The reversibility values calculated by Katz and Rognstad (1967) are comparable to those presented here with a value of 0.06 for the transaldolase reaction (a_5), a value of 0.12 for the transketolase reactions (a_4 and a_6), and a value of 0.08 for P, compared to our value of 0.09.

Method	Metabolite	Metabolite carbon atom				
		C-1	C-2	C-3	C-4	C-5
Experimental	Hex6P	15	100	10	-	8
	Pen5P	100	53	-	48	-
Model: no reversibility	Hex6P	15	100	8	-	4
(a_4=a_5=a_6=0.0)	Pen5P	100	8	-	4	-
Model: reversibility	Hex6P	16	100	8	-	10
(a_4=0.105, a_5=0.065, a_6=0.11)	Pen5P	100	57	-	37	-

Table 4-6. *E. coli* ^{14}C label data at stationary phase. ^{14}C label data for Hex6P and Pen5P from *E. coli* at stationary phase supplied with [2-^{14}C]glucose substrate. Experimental values compared with model predictions assuming no reversibility and reversibility for transketolase and transaldolase reactions (Katz and Rognstad, 1967). The reversibility values calculated by Katz and Rognstad (1967) are comparable to those presented here with a value of 0.71 for the transaldolase reaction (a_5), a value of 0.46 for the transketolase reactions (a_4 and a_6), and a value of 0.13 for P, compared to our value of 0.16.

Method	Metabolite	Metabolite carbon atom				
		C-1	C-2	C-3	C-4	C-5
Experimental	Hex6P	24	100	17	-	24
	Pen5P	100	150	-	97	-
Model: no reversibility	Hex6P	24	100	14	-	6
(a_4=a_5=a_6=0.0)	Pen5P	100	14	-	6	-
Model: reversibility	Hex6P	26	100	25	-	25
(a_4=0.6, a_5=0.8, a_6=0.6)	Pen5P	100	147	-	82	-

4.5.4 Conclusions

A variety of methods have been employed in the past to determine pentose phosphate pathway fluxes. One method assumed that pentose phosphate pathway flux equals that required for ribose carbon skeletons for DNA and RNA biosynthesis (Xie and Wang, 1994c; Zupke and Stephanopoulos, 1995a). Another method used the ratio of specific activities of metabolite carbons resulting from the addition of [1-^{14}C] and [6-^{14}C]glucose to calculate pentose phosphate pathway activity (Katz and Wood, 1963; Katz and Wood, 1960; Kingsley-Hickman et al., 1990; Larrabee, 1989; Willis et al., 1986). A third method used ^{13}C labeling to determine the amount of pentose phosphate pathway flux in cells under low growth conditions and assumed that the flux equaled the amount needed for biosynthesis with no scrambling due to this pathway (Mancuso et al., 1994; Sharfstein et al., 1994). All of these methods may be accurate under certain conditions (such as low growth rates) but in general, they only represent the net fluxes through the corresponding pathways. These approaches are not general and do not take into account the resulting label redistribution caused by reaction reversibility which could lead one to calculate incorrect fluxes in other parts of the metabolic network.

The general metabolic reaction network model presented here includes not only overall carbon redistribution balances but also accounts for varying extents of reaction reversibilities. This general approach applied to the pentose phosphate pathway illustrated that varying extents of reaction reversibility can have a dramatic influence on fractional enrichment data. In addition, the accuracy of reversibility calculation depends on the choice(s) of specific metabolite carbon enrichment measurement as illustrated with the [6-^{13}C]Hex6P and [4-^{13}C]Ery4P enrichment values in the variational study for [1-^{13}C]glucose feeding.

Fractional enrichment measurements of intermediate metabolites present at small concentrations may be difficult to obtain due to low sensitivity of NMR spectroscopic measurements. A compound usually produced in larger amounts in cultured cells is lactate which could be used to obtain an analyzable NMR spectrum. Lactate carbon atoms are all derived from the pyruvate pool which is usually formed from glycolysis and thus glyceraldehyde 3-phosphate. However, it is also possible that a fraction of the lactate production is the result of glucose carbon cycling from pyruvate via anapleurotic reactions into the tricarboxylic acid cycle and then back into pyruvate via the malic enzyme. Therefore, in order to properly account for lactate labeling, one needs to account for the tricarboxylic acid cycle recycle labeling effect added to the lactate carbons. This analysis can be done using [4-^{13}C], [5-^{13}C], and [6-^{13}C]glucose, since the pentose phosphate pathway does not scramble these labeled carbon atoms in a particular metabolite, although fractional enrichment values for the labeled carbon atoms may vary (data not shown). In other words, each metabolite would have one labeled carbon atom with a variable fractional enrichment. Using the carbon enrichment labeling of the [1-^{13}C], [2-^{13}C], and [3-^{13}C]lactate carbon atoms, the tricarboxylic acid recycle effect can be calculated using a procedure described in (Klapa et al., 1999; Park, 1996; Park et al., 1999; Park et al., 1997).

When applied to literature data sets, the modeling approach was successful in explaining the appearance of label on several metabolite carbon atoms. This was demonstrated with data sets for the rat adipose tissue and goosefish islet cells in which the high experimental specific activity at the C-5 carbon in the analyzed glycogen was explained by introducing reaction reversibility to the model. The need for reaction reversibility was also clearly shown in the analysis of the *C. glutamicum* and *E. coli* data sets. Finally, the variability in the extents for all

of these data sets suggested that each transketolase and transaldolase reaction may have a different extent of reversibility depending on the cell type, medium environment, or culture growth conditions.

5. METABOLIC FLUX IN CHINESE HAMSTER OVARY CONTINUOUS CULTURE

5.1 Introduction

Two of the most important parameters in metabolic pathway analysis are the flux through various biochemical reactions and the distribution of this flux at key nodes within a biochemical reaction network. The accurate calculation of these fluxes is required in order to elucidate relations between metabolic fluxes and physiological states. Metabolic flux analysis was applied to elucidate these relations for Chinese hamster ovary cells at different growth rates for several continuous culture steady states. These various steady states are representative of the bioreactor environments and cellular physiological states encountered under batch and fed-batch culture conditions. A low residence time (high growth rate) correlates with the initial time points of a batch or fed-batch culture, whereas a high residence time (low growth rate) correlates with the later stages of batch or fed-batch culture. In addition, the low growth rates correlate with the higher cellular death rates observed during the late stages of a batch or fed-batch culture. Therefore, the analysis of the cellular physiology encountered in continuous culture steady states can yield a significant amount of information concerning the cellular control of metabolic flux distribution occurring in various bioreactor environments. Furthermore, this information could be applied in not only process design but also in the modeling of batch or fed-batch processes.

The cellular and environmental conditions that result in metabolic flux and flux distribution variations as well as those that trigger apoptosis were analyzed under steady state conditions. In addition, protein product glycosylation was investigated, and these results are discussed elsewhere in Nyberg et al. (Nyberg et al., 1999b). Specifically, the cellular physiological state was characterized not only through measurements of viability but also through the calculation of metabolic fluxes and variations of flux distribution around the

pyruvate branchpoint. This metabolite was chosen due to the fact that it is the most important branchpoint in metabolism as demonstrated through theoretical analysis of the central carbon metabolism network (Simpson et al., 1999). The results indicated that metabolic flux distribution around pyruvate fluctuates as a function of the cellular growth rate with a higher TCA cycle and respiration activity occurring at the lower growth rates. At these low growth rates, the onset of lactate consumption coincided with the rapid rise in the cellular death rate. These results correlate with the metabolic changes that occur over the course of a fed-batch and illustrate the metabolic regulation occurring as cells attempt to satisfy energetic and biosynthetic requirements as well as the flexibility of the pyruvate branchpoint. In addition, these results indicate that an operating window of growth rates exists for this cell line where cell death can be minimized, and this result could be utilized in the design of a batch or fed-batch culture process.

5.2 Results

The continuous culture runs for the Chinese hamster ovary cell line involved four steady states operated under glucose limiting conditions and one glutamine limited steady state. These reactor runs were initially operated in batch mode and then switched to continuous mode. The culture was determined to be at steady state when the cell density, viability, and key metabolite production rates did not vary for more than 10% for 48 hours. The specific cell growth rates and death rates were calculated using equations 4.4 and 4.5, and the results for the four glucose limited steady states and one glutamine limited steady state are shown in Figure 5-1. As the residence time increased (dilution rate decreased), the specific growth rate decreased while the specific death rate increased. Furthermore, at high dilution rates, large changes in the growth rate resulted in only minor changes in the death rate. This contrasts with the lower dilution rates

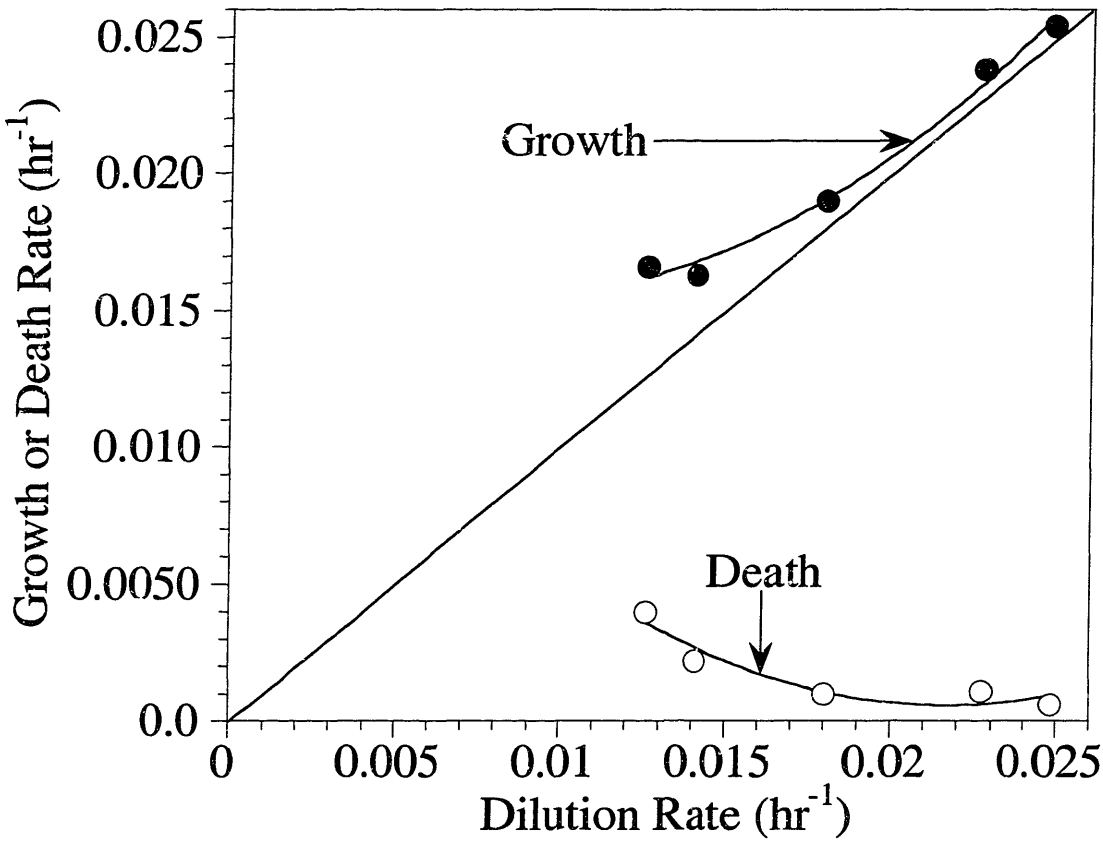

Figure 5-1. Specific growth and death rates versus dilution rate. The specific growth and death rates for the Chinese hamster ovary cell continuous cultures were determined using equations 4.4 and 4.5. As the dilution rate decreased, the death rate increased resulting in lower viabilities at these higher residence times.

which showed large increases in the death rates with only minor changes in the growth rates. This phenomenon has been described in the literature before (Hayter et al., 1993; Lee et al., 1995). Metabolite production and consumption rates were calculated using equation 4.7 and are summarized in Table 5-1 along with the calculated biomass demands. A significant amount of cell aggregation was observed, particularly at the low dilution rates, and the dry cell weight was measured in an effort to obtain accurate biomass concentrations. The errors presented in the table are the propagated errors that include not only metabolite measurement errors but biomass concentration and dilution rate errors as well. The cellular consumption of peptides was measured due to the presence of 2.5 g/L of peptide hydrolysate in the medium (Nyberg et al., 1999a). In addition, the biosynthesis demands for each amino acid were considered in the calculation of each of these values. Therefore, the final values are the metabolite production and consumption rates directly affecting the metabolic network shown in Figure 4-1.

The consistency of the data was evaluated by calculating the consistency index values (h) listed in Table 5-2 as described previously (Nyberg et al., 1999a; Zupke and Stephanopoulos, 1995a). The first and third glucose limited steady states as well as the glutamine limited steady state initially failed the consistency check. However, these data sets became consistent upon the elimination of specific measurements. In particular, the glucose limited steady state became consistent after the elimination of the oxygen measurement. Furthermore, the third glucose limited and the glutamine limited steady states became consistent upon the elimination of the leucine consumption rate. The error in the leucine consumption rate was connected to the OUR and CER measurements and TCA cycle flux as described in Nyberg et al. (Nyberg et al., 1999a). The final calculated metabolic fluxes were obtained for these data sets after the elimination of each of these inconsistent measurements.

Table 5-1. Measured metabolite production and consumption rates (mmole/g_{DCW} d). These values were calculated taking into consideration the biosynthesis demand for amino acids and other metabolites. Positive values indicate metabolite production whereas negative values indicate metabolite consumption.

Metabolite	Steady State Glc-limited 1	Steady State Glc-limited 2	Steady State Glc-limited 3	Steady State Glc-limited 4	Steady State Gln-limited
Glucose	-2.71±0.15	-1.71±0.10	-1.28±0.04	-1.27±0.06	-8.14±0.35
Lactate	0.87±0.35	0.22±0.09	0.04±0.11	-0.08±0.02	9.19±0.49
CO_2	15.89±1.37	17.23±1.30	14.15±0.77	12.82±0.85	18.68±1.15
O_2	-20.54±1.46	-15.52±1.30	-13.76±0.76	-12.70±1.04	-16.02±1.09
Ala	0.52±0.04	-0.17±0.02	-0.16±0.02	-0.22±0.02	0.07±0.03
Asn	-0.25±0.02	-0.23±0.03	-0.21±0.02	-0.19±0.02	-0.26±0.03
Asp	0.00±0.02	-0.06±0.02	0.00±0.02	-0.01±0.02	-0.19±0.03
Gln	-2.31±0.14	-1.67±0.10	-1.25±0.06	-1.18±0.07	-0.04±0.03
Glu	0.05±0.02	-0.02±0.01	0.08±0.02	0.10±0.01	-0.27±0.03
Gly	0.09±0.04	0.06±0.03	0.17±0.03	0.22±0.05	-0.05±0.04
Ile	-0.06±0.02	-0.11±0.02	-0.07±0.01	-0.07±0.01	-0.13±0.02
Leu	-0.15±0.03	-0.29±0.02	-0.21±0.01	-0.22±0.02	-0.34±0.03
Lys	0.01±0.11	0.06±0.05	-0.01±0.05	0.01±0.14	-0.04±0.05
Pro	0.27±0.03	0.09±0.03	0.04±0.02	0.04±0.07	0.02±0.06
Ser	0.36±0.03	0.19±0.02	0.15±0.02	0.15±0.02	0.06±0.04
Thr	0.05±0.02	0.04±0.01	0.06±0.02	0.08±0.01	0.04±0.02
Val	-0.01±0.04	-0.12±0.02	-0.07±0.02	-0.07±0.02	-0.13±0.02
Biomass					
AcetylCoA	4.296	4.296	4.296	4.296	4.296
a-KG	-0.354	-0.354	-0.354	-0.354	-0.354
CO_2	-0.035	-0.035	-0.035	-0.035	-0.035
G6P	0.248	0.248	0.248	0.248	0.248
GAP	0.226	0.226	0.226	0.226	0.226
NADH	-0.346	-0.346	-0.346	-0.346	-0.346
OAA	0.094	0.094	0.094	0.094	0.094
R5P	0.188	0.188	0.188	0.188	0.188

Table 5-2. Calculated consistency index values. Consistency index (h) values were calculated to determine the consistency of the metabolite production and consumption rate data sets. Values lower than the χ^2 distribution value (90% confidence interval, 2 degrees of freedom) indicate that the data set was consistent. The three data sets that were inconsistent were modified through the elimination of the specified measurements resulting in consistent data sets (90% confidence interval, 1 degree of freedom).

Steady State	h	χ^2	Pass / Fail
Glc-limited 1	22.04	4.60	Fail
-OUR	0.60	2.71	Pass
Glc-limited 2	0.02	4.60	Pass
Glc-limited 3	13.84	4.60	Fail
-leucine	0.03	2.71	Pass
Glc-limited 4	1.31	4.60	Pass
Gln-limited 1	6.53	4.60	Fail
-leucine	0.08	2.71	Pass

Metabolic fluxes for the network in Figure 4-1 are listed in Table 5-3 for each of the five steady states. The four glucose limited steady states demonstrated that as the specific growth rate was decreased, several key metabolic fluxes varied uniquely as shown in Figure 5-2. The flux of pyruvate into the TCA cycle via pyruvate dehydrogenase (PDH) decreased, but at a rate lower than that for the influx of pyruvate from glycolysis. This variation in the slopes of the best-fit lines in Figure 5-2 indicates that the flux distribution around pyruvate changes as a function of growth rate with the TCA recycle flux showing the least amount of variation with the growth rate. Figure 5-3 illustrates these flux distribution changes more clearly, and figure 5-3b shows values for the ratios of several calculated metabolic fluxes around the pyruvate branchpoint. As mentioned previously, pyruvate is a key branchpoint in central carbon metabolism linking glycolysis with the TCA cycle, overflow metabolism, and transamination reactions. As mentioned in chapter four, it has been shown through theoretical analysis to be the main link metabolite in this biochemical reaction network (Simpson et al., 1999). Plotted in figure 5-3b are the ratios of the sum of the glycolytic flux (reaction 3) plus the TCA recycle flux (reaction 12) divided by the TCA cycle inlet flux (reaction 6) as a function of specific growth rate. For this ratio, deviations from the value of unity are indicative of waste metabolite production (lactate and alanine). Therefore, high values of the ratio correspond to a large amount of carbon influx, secretion of large amounts of lactate and alanine, and a small carbon flux entering the TCA cycle. Lower values, however, correspond to more efficient utilization of pyruvate for energy generation in the TCA cycle. As the dilution and specific growth rates decreased for the four glucose limited steady states, the pyruvate ratio decreased indicating a flux distribution shift around pyruvate. This shift involves the shuttling of more pyruvate carbon into the TCA cycle as opposed to being converted to lactate. The two lowest steady states were

Table 5-3. Calculated metabolic fluxes (mmole/g viable DCW). The metabolic fluxes were calculated using equation 4.11 and the data listed in Table 5-1.

	Reaction	Steady State Glc-lim 1	Steady State Glc-lim 2	Steady State Glc-lim 3	Steady State Glc-lim 4	Steady State Gln-lim
1	Glc → G6P	4.96	4.05	3.80	4.26	13.67
2	G6P → 2 GAP	4.52	3.62	3.37	3.82	13.24
3	GAP → Pyr	7.98	6.42	5.56	6.23	26.22
4	Pyr → Lac	1.89	0.51	0.11	-0.27	15.44
5	G6P → $Biomass_{R5P}$ + CO_2	0.19	0.19	0.19	0.19	0.19
6	Pyr → AcCoA + CO_2	9.53	11.50	10.37	11.95	12.55
7	Pyr + Glu → αKG + Ala	0.95	-0.41	-0.47	-0.75	0.12
8	OAA + AcCoA → αKG + CO_2	6.03	9.24	8.17	10.68	10.33
9	αKG → SuCoA + CO_2	10.02	13.40	11.88	14.58	11.18
10	SuCoA → Fum	10.05	13.85	12.08	14.79	11.55
11	Fum → OAA	10.05	13.85	12.08	14.79	11.55
12	OAA → Pyr + CO_2	4.38	5.18	4.44	4.70	1.89
13	Gln → Glu	4.67	4.51	4.33	4.60	0.50
14	Glu → αKG	2.31	4.29	3.50	3.78	1.12
15	GAP + Glu → Ser + αKG	0.66	0.45	0.46	0.49	0.11
16	GAP + Glu → Gly + αKG	0.17	0.15	0.49	0.70	-0.09
17	Lys → 2 AcCoA + 2 CO_2	-0.05	-0.14	0.04	0.30	0.07
18	Ile → AcCoA + SuCoA	0.11	0.25	0.19	0.23	0.22
19	Leu → 3 AcCoA	0.27	0.69	0.61	0.73	0.57
20	Glu → Pro	0.49	0.20	0.12	0.08	0.03
21	Thr → SuCoA	-0.09	-0.10	-0.19	-0.26	-0.06
22	Val → SuCoA + CO_2	0.01	0.29	0.20	0.24	0.21
23	OAA + Gln → Asn + αKG	-0.45	-0.54	-0.62	-0.65	-0.44
24	OAA + Glu → Asp + αKG	0.00	-0.13	0.00	-0.03	-0.32
25	G6P → $Biomass_{G6P}$	0.25	0.25	0.25	0.25	0.25
26	GAP → $Biomass_{GAP}$	0.23	0.23	0.23	0.23	0.23
27	AcCoA → $Biomass_{AcCoA}$	4.31	4.29	4.30	4.28	4.30
28	$Biomass_{\alpha KG}$ → αKG	0.35	0.35	0.35	0.35	0.35
29	OAA → $Biomass_{OAA}$	0.09	0.09	0.09	0.09	0.09
30	CO_2 → $Biomass_{CO2}$	-0.22	-0.22	-0.22	-0.22	-0.22
31	NADH → $Biomass_{NADH}$	5.38	5.38	5.38	5.37	5.38
32	0.5 O_2 + 3 ADP + NADH → 3 ATP + NAD^+	40.40	56.32	50.43	63.56	55.09
33	0.5 O_2 + 2 ADP + $FADH_2$ → 2 ATP + FAD	10.39	14.94	13.12	16.29	12.63

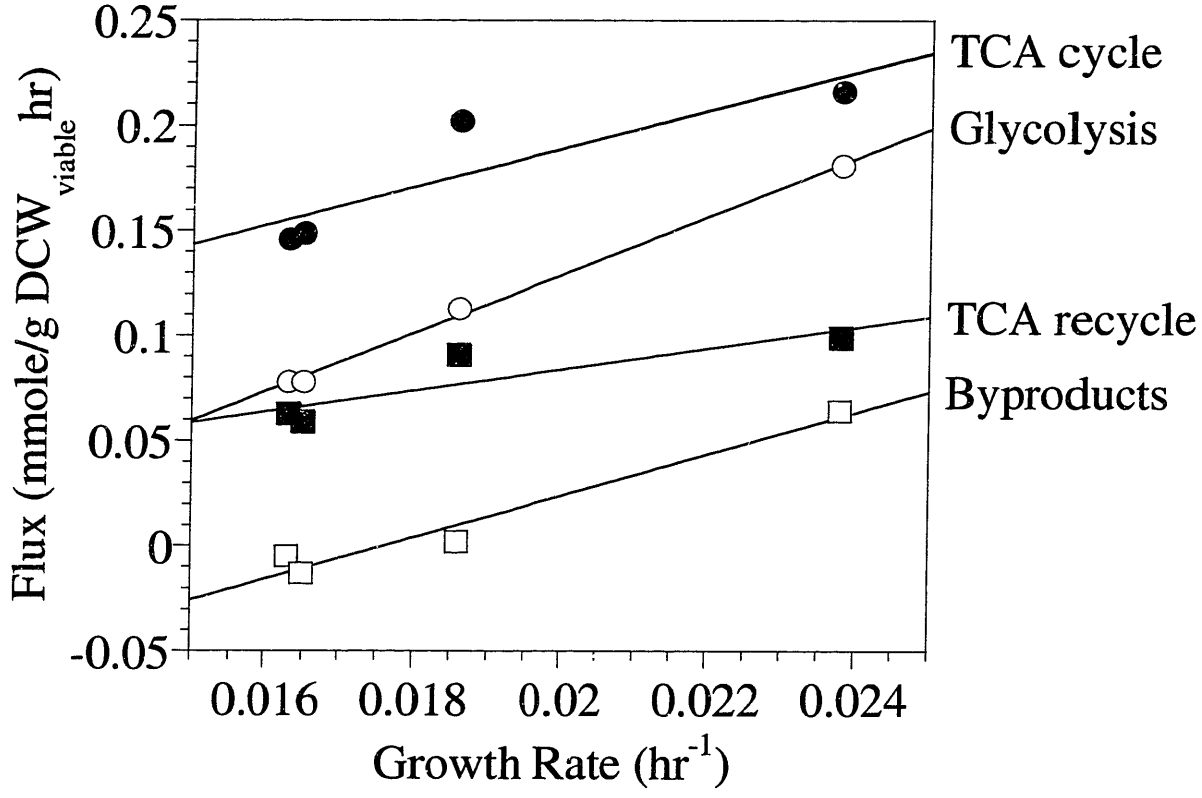

Figure 5-2. Calculated metabolic fluxes (mmole/g_{DCW} hr) versus growth rate. Metabolic fluxes decrease as the growth rate decreases. However, these fluxes decrease at different rates, and the glycolytic metabolic flux drops faster than the TCA cycle flux.

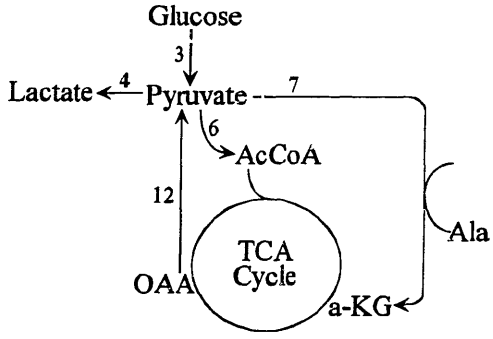

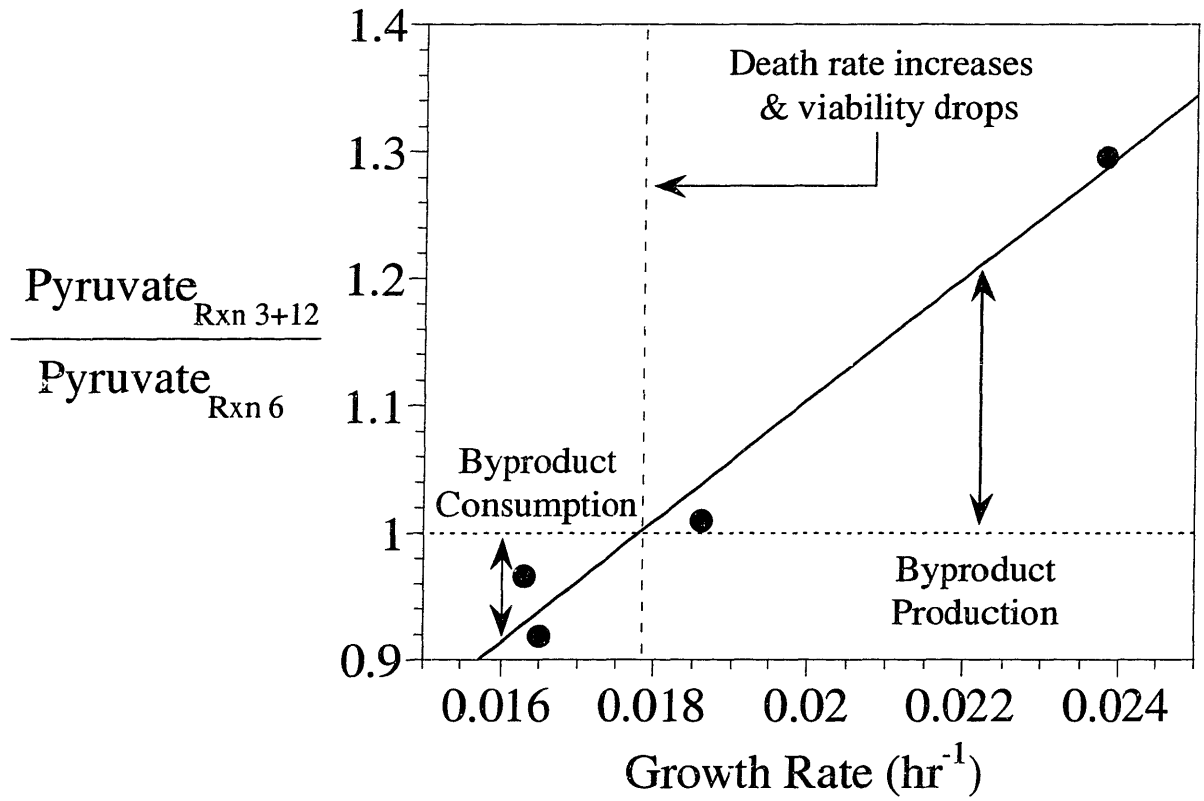

Figure 5-3a,b. Metabolic flux distribution around the pyruvate branchpoint. The values plotted in (5-3b) are the ratio of the sum of glycolytic flux (reaction 3) and the TCA recycle flux (reaction 12) divided by the TCA cycle inlet flux (reaction 6), (reactions shown in 5-3a). Deviations from unity represent waste metabolite (lactate and alanine) production. High values of the ratio indicate a condition of high waste metabolite production, whereas lower values indicate more efficient utilization of pyruvate carbon. The metabolic flux distribution around pyruvate shifted with a higher fraction of pyruvate flowing into the TCA cycle as the growth rate decreased. The condition of lactate consumption (ratio less than 1.0) coincided with a noticeable increase in the death rate and decrease in culture viability.

also situations in which the medium lactate was consumed with a significant increase in the cellular death rate (pyruvate flux ratio less than unity; Figure 5-3b). This net lactate consumption was a result of the fact that the peptide hydrolysate present in the medium contained a small amount of lactate.

The glutamine limited steady state resulted in a higher glucose consumption and lactate production with a higher glycolytic activity as demonstrated by the inefficient metabolism as measured using the technique described in Figure 5-3. The ratio described in Figure 5-3 was calculated to be 2.23 or almost twice the value for the high growth rate steady state under glucose limited conditions. Glucose limitation clearly has a stronger effect on the flux redistribution around pyruvate.

5.3 Discussion

The data presented in this chapter demonstrate that cells underwent changes in their metabolic flux distribution and physiological state in response to progressively lower dilution and growth rates until reaching a point of high cellular death. At the progressively lower growth rates, the utilization of pyruvate carbon became more efficient with more pyruvate flowing into the TCA cycle for respiration and biomass production. This adaptation enabled the cells to maintain energy production as well as meet the requirements for cell biosynthesis.

These results match the behavior observed in batch and fed-batch cultures. At high growth rates, a significant amount of lactate is produced indicating that the TCA cycle is not extremely active and does not demand much pyruvate carbon for energy production. However, over the course of a culture, the lactate to glucose ratio decreases indicating that metabolism is becoming more efficient with more pyruvate carbon flowing into the TCA cycle (Glacken et al., 1986; Hansen and Emborg, 1994; Hassell et al., 1991; Lanks and Li, 1988; Xie, 1997). Feeding

low amounts of glucose and glutamine substrate also results in a lowered lactate to glucose ratio indicating that TCA cycle demand for carbon is a major determinant for byproduct production as demonstrated in the comparison between the glucose and glutamine limited steady states (Glacken et al., 1986; Ljunggren and Häggström, 1994; Xie, 1997). In addition, lactate consumption correlates with the time in a culture at which the cell death rate becomes significant (Xie, 1997).

These results reveal an operating window one should maintain when growing this cell line. Cells should be maintained at a growth rate that is not too high which results in inefficient metabolism but also not too low resulting in cell death. In addition, the fact that flux distribution can change significantly around pyruvate as a function of both the growth rate and the culture limiting substrate indicates the flexibility of this metabolic node. However, the pyruvate node is not completely flexible due to the extensive regulation of the pyruvate dehydrogenase complex (PDH) (Behal et al., 1993). Therefore, this node could be classified as a weakly rigid node that is dominated by PDH activity (Stephanopoulos and Vallino, 1991). PDH is one of the most complex enzymes known, and the PDH enzyme complex consists of sixty subunits, three different enzyme groups, and several separate regulatory proteins and requires five different coenzymes (Lodish et al., 1995). PDH is regulated through separate enzymes involving both a kinase (inactivates PDH) and a phosphatase (activates PDH) that are in turn regulated by NADH, ATP, pyruvate, and acetyl CoA. Figure 5-4 illustrates the enzymes around the pyruvate branchpoint. Lactate dehydrogenase, malic enzyme, pyruvate kinase, and transaminase are not nearly as regulated as pyruvate dehydrogenase. The flux distribution around pyruvate in cultured mammalian cells appears to be dominated by the activity of PDH. Typically, only a minimal amount of pyruvate is allowed through PDH resulting in excess pyruvate flowing through lactate

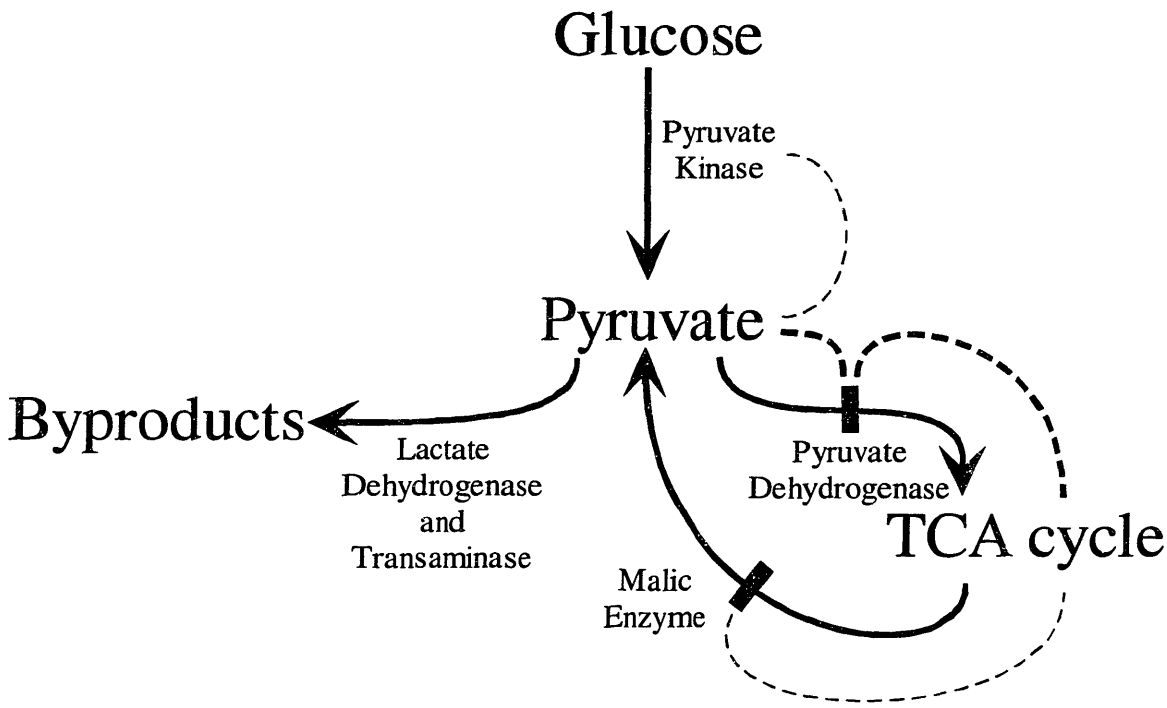

Figure 5-4. Pyruvate branchpoint flexibility. The pyruvate branchpoint is a weakly rigid branchpoint. A significant amount of the regulation around pyruvate occurs at the pyruvate dehydrogenase complex, and this enzyme dominates the partitioning of metabolic flux.

dehydrogenase. However, since the TCA cycle generates a significant amount of energy due to the more efficient respiration process, enhancing the metabolic flux to the TCA cycle in the pyruvate branchpoint could result in increased cellular energy and biomass production.

Engineering the metabolic flux distribution around this branchpoint would be a difficult if not impossible task. Even with enzymes that are easy to transfect and overexpress within a cell line, metabolic engineering oftentimes results in little enhancement of the desired metabolic flux (Bailey, 1999). An easier solution would be to define cell culture operating conditions that would cause the cells to increase their PDH activity while continuing to grow at a high rate. This form of inverse metabolic engineering involves the identification of environments that result in a desired phenotype, and this strategy has proven to be an effective method to enhance desired traits in cultured cell lines (Bailey et al., 1996).

6. STEADY STATE MULTIPLICITY IN HYBRIDOMA CONTINUOUS CULTURE

6.1 Introduction

The previous chapter demonstrated the importance of the pyruvate branchpoint in the identification of cellular phenotypes associated with efficient metabolic patterns. The PDH enzyme was identified as a potential site for metabolic engineering techniques. However, inverse metabolic engineering could provide a more useful method for enhancing this cellular flux by identifying operating conditions that lead to enhanced PDH activity.

Metabolic flux analysis was applied to elucidate the physiological state of hybridoma cells at different continuous culture steady states. Of particular interest is the observed steady state multiplicity, whereby drastically different cell concentrations were observed under the same dilution rate. The specific steady state obtained depended on the operating path that was followed in reaching the steady state. Metabolic flux analysis applied to these multiple steady states provided a framework for the rational integration of a multitude of metabolic rate data and also showed that cell concentration multiplicity was the result of physiological state multiplicity, as measured by the fraction of carbon flux shuttled into the TCA cycle for energy generation. Elucidation of cellular physiological states provided the basis for designing operating and cell strain selection strategies to reproduce the high efficiency physiological states in industrial cell applications.

6.2 Results

The total and viable cell concentrations, as well as the dilution rate for the continuous culture run are presented in Figure 6-1. Cell physiology of each of the five steady states was characterized by analyzing the last few data points in each of the sections marked as A, B, C, D and E on Figure 6-1. After the reactor run was initiated, the dilution rate was set at 0.04 hr^{-1}. At

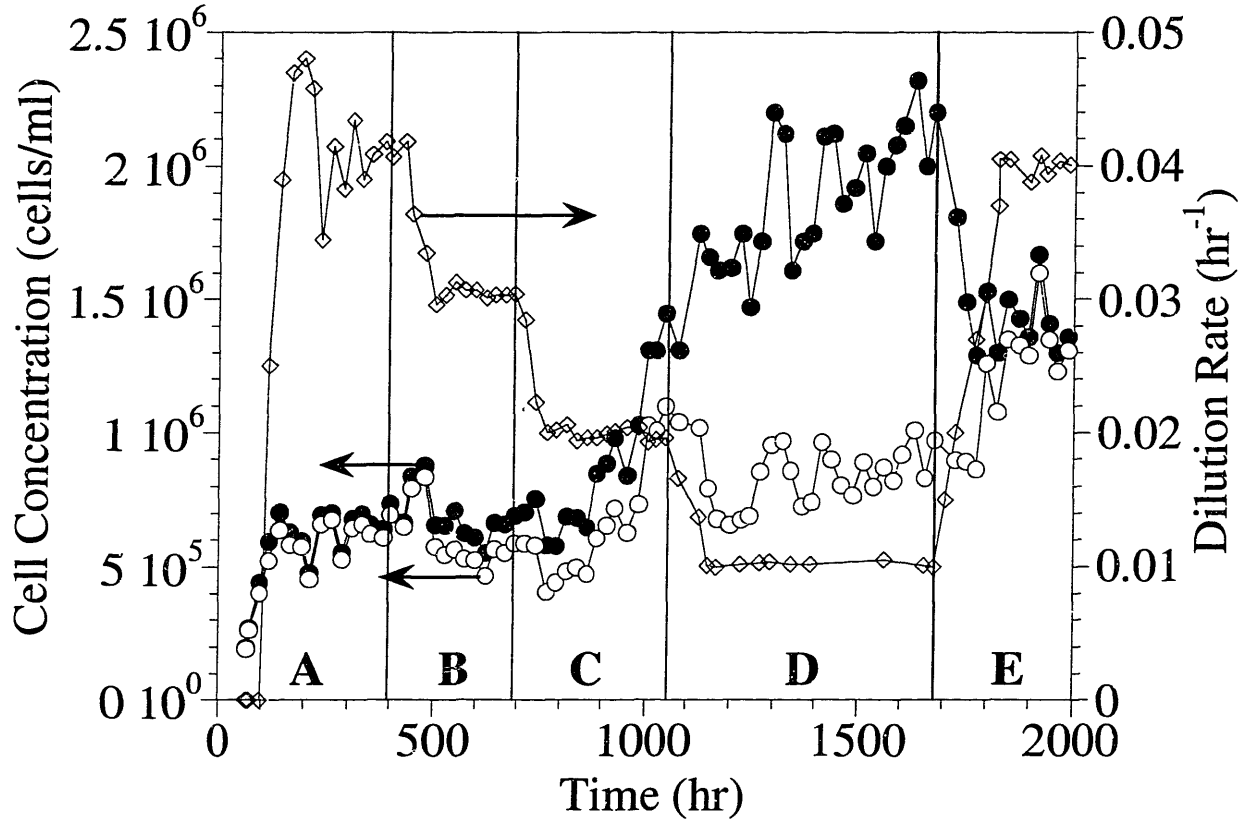

Figure 6-1. Cell concentration and dilution rate versus time. Viable (open circles) and total (closed circles) cell concentrations for the hybridoma continuous culture run as well as the dilution rate for each time period. The five sections marked A, B, C, D, and E represent the five time periods with different dilution rates. Flux analysis was carried out for the last few data points in each time period.

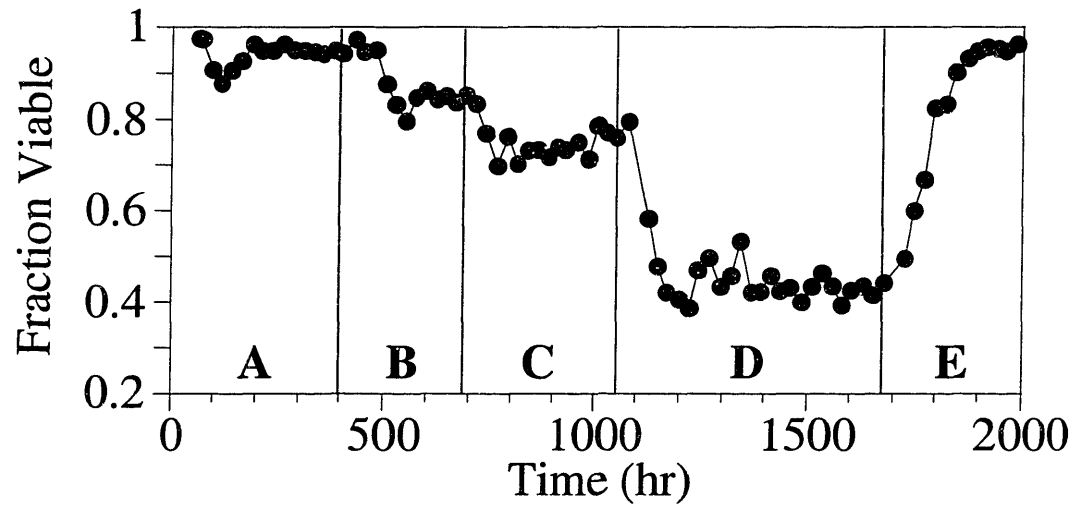

Figure 6-2. Cell viability versus time for each time period. The five sections marked A, B, C, D, and E represent the five time periods with different dilution rates. Flux analysis was carried out for the last few data points in each time period.

each dilution rate, the reactor was determined to be at steady state after five residence times as it satisfied the steady state criteria previously mentioned. The dilution rate was decreased in increments of 0.01 hr^{-1} for each of the next three steady states after a steady state had been reached. At the end of the period corresponding to a dilution rate of 0.01 hr^{-1}, the dilution rate was stepped back up to 0.04 hr^{-1} over a period of approximately 100 hours. The viable cell density ranged from $5*10^5$ to $9*10^5$ cells/ml in the first four steady states (A, B, C, and D) and increased further to $1.3*10^6$ cells/ml upon return to a dilution rate of 0.04 hr^{-1} in the last steady state (E). Even though the dilution rates for steady states A and E were the same, the viable cell concentrations for steady state E were approximately two-fold higher compared to steady state A. Therefore, the culture can reach different viable cell concentrations at the same operating conditions, indicating steady state multiplicity. Figure 6-2 shows the cell viabilities for the various steady states. As the dilution rate decreases, the viability drops, ranging from 95% to approximately 42% at the lowest dilution rate examined. Upon stepping the dilution rate back up to 0.04 hr^{-1}, the viability returned to 95% similar to that obtained at the first steady state (A).

The specific cell growth rates and death rates calculated from equations 4.4 and 4.5 for the five steady states are shown in Figure 6-3. As the dilution rate decreased, the specific growth rate decreased while the specific death rate increased. At a hybridoma steady state, a condition of abortive proliferation eventually is reached where cell growth is exactly balanced by cell death and cell dilution at steady state as described previously by Chung et al. (Chung et al., 1998) for this cell line. Most of the death occurring at the low dilution rates was by apoptosis as shown in Figure 6-4. Most of the apoptotic cells were found to be in the late apoptotic phase (data not shown) which explains the agreement between the fraction of apoptotic cells measured by acridine orange / ethidium bromide with the fraction of dead cells determined by trypan blue.

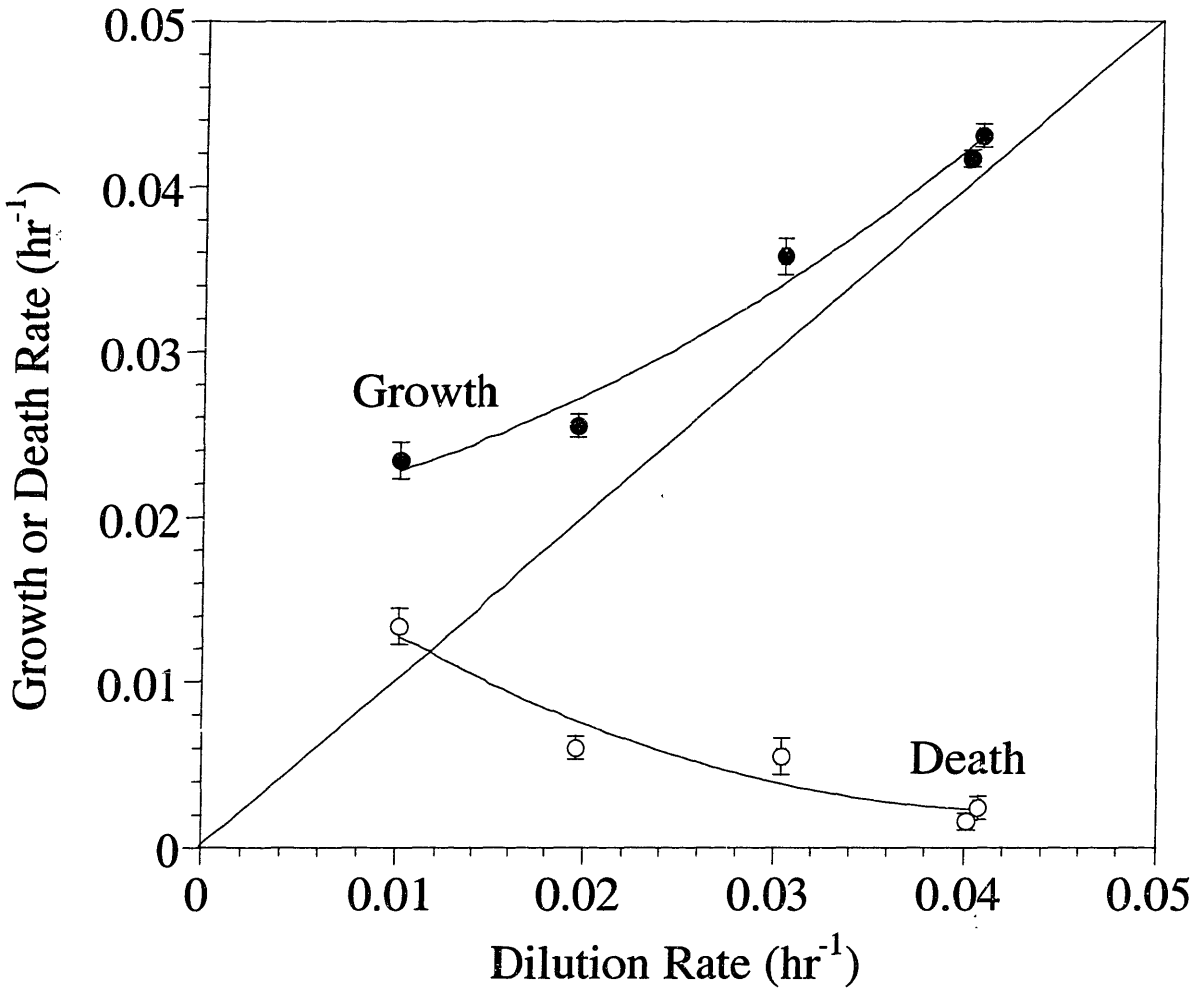

Figure 6-3. Specific growth and death rates versus dilution rate. The specific growth and death rates were determined using equations 4.4 and 4.5. As the dilution rate decreased, the death rate increased resulting in lower viabilities at these higher residence times.

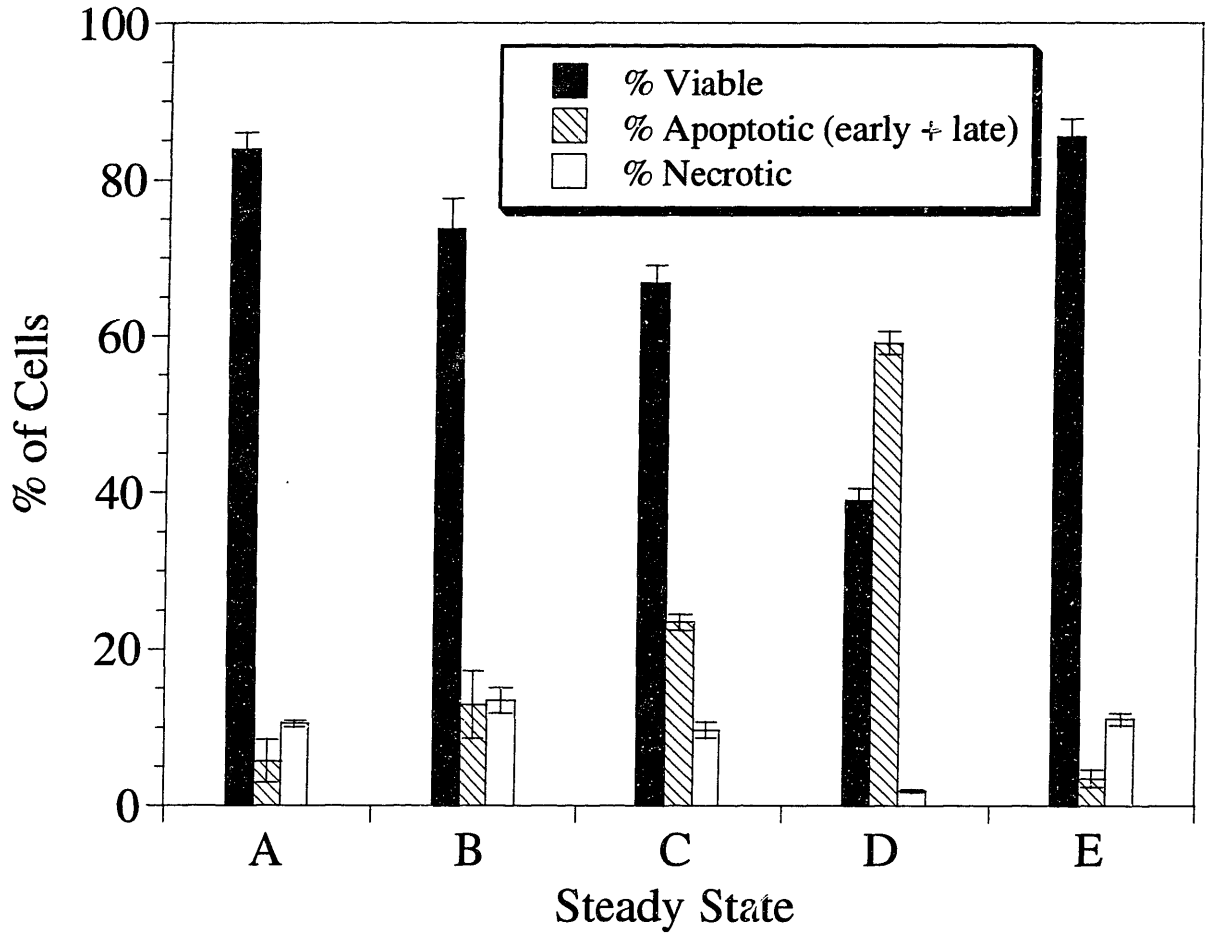

Figure 6-4. Acridine orange / ethidium bromide stain for each steady state. Nearly identical death characteristics were observed for steady states A and E. Also, apoptosis was the predominant type of death for the low growth rate steady states.

The specific productivity of IgG is shown in Figure 6-5. An intermediate dilution rate (steady state B) yielded the largest specific productivity compared to the other steady states. As the dilution rate was reduced to 0.02 and further to 0.01 hr^{-1}, the specific productivity also decreased and remained low, even after the dilution rate had been increased back to 0.04 hr^{-1} (steady state E). Even though the specific productivity was lower compared to steady state A, the final product concentration was higher for steady state E due to the higher cell concentration at this steady state (data not shown). The observation of an increasing specific productivity at lower dilution rates has been recorded (Linardos et al., 1991). However, in the case of CRL-1606 cells, a maximum specific productivity is obtained at an intermediate growth rate. One possible explanation may be that previous work did not investigate dilution rates and cell viabilities as low as the one presented here. However, the maintenance of the low specific productivity upon return to the high dilution rate steady state of 0.04 hr^{-1} was never observed in previous continuous culture experiments. The fact that in the experiment reported here the specific productivity was not found to be a function of the specific growth rate suggests that metabolism and other factors may play a role in IgG productivity.

Metabolite production and consumption rates calculated using equation 4.7, as well as calculated biomass demands are summarized in Table 6-1. The errors presented in the table are the propagated errors that include not only metabolite measurement errors but cell concentration and dilution rate errors as well. In addition, the biosynthesis demands for each amino acid were considered in the calculation of each of these values. Therefore, the final values are the metabolite production and consumption rates directly affecting the metabolic network shown in Figure 4-1.

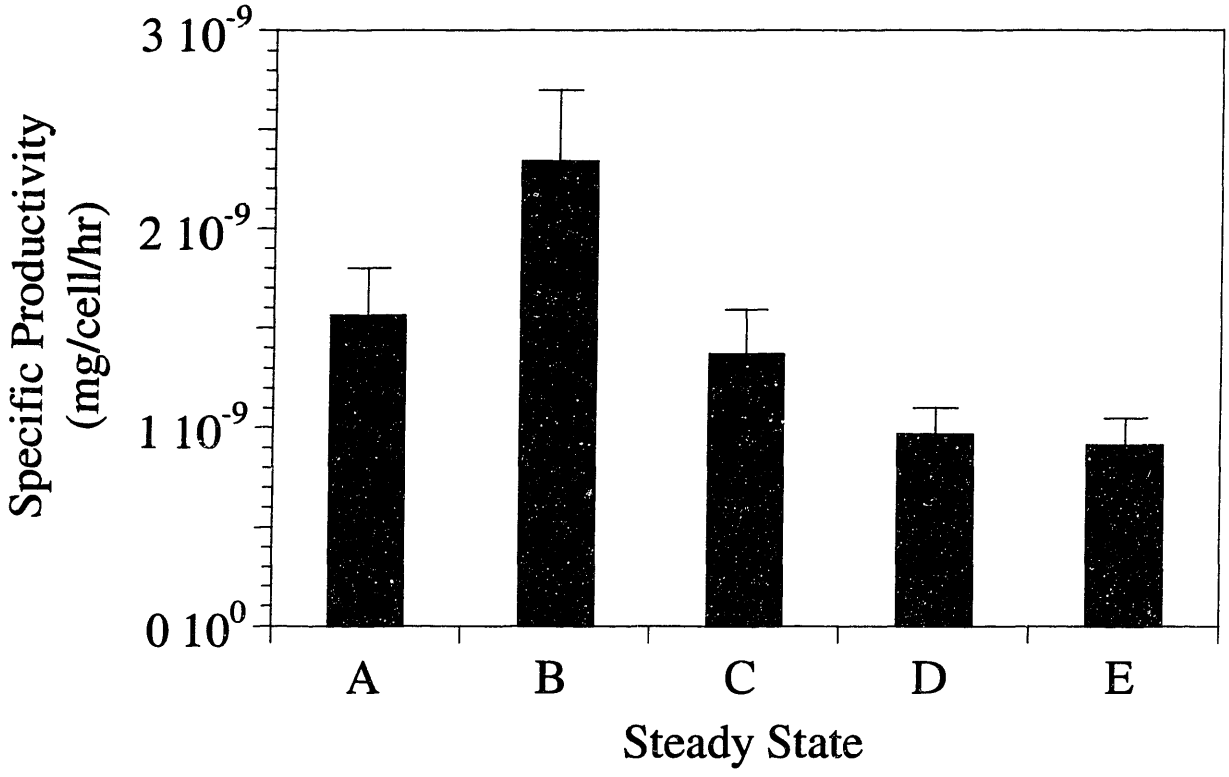

Figure 6-5. Specific productivity of the IgG product for each steady state. A maximum specific productivity was achieved at the intermediate growth rate in steady state B. The subsequent reduction in specific productivity observed at the lower growth rates was maintained at the last steady state (E). However, the final product concentration was higher in steady state E as compared to steady state A due to the differences in cell density (data not shown).

Table 6-1. Measured metabolite production and consumption rates (*10^{-10} mmole/viable cell/hr). These values were calculated taking into consideration the biosynthesis demand for amino acids and other metabolites. Positive values indicate metabolite production whereas negative values indicate metabolite consumption.

Metabolite	Steady State A	Steady State B	Steady State C	Steady State D	Steady State E
Glucose	-3.54±0.32	-3.62±0.52	-1.81±0.20	-1.21±0.15	-3.89±0.37
Lactate	6.71±0.61	7.23±0.79	2.70±0.31	1.63±0.14	5.71±0.54
CO_2	2.28±0.21	3.57±0.41	3.40±0.41	3.02±0.24	3.10±0.31
O_2	-2.69±0.24	-3.41±0.39	-3.92±0.47	-3.54±0.28	-3.53±0.36
Ala	0.13±0.01	0.12±0.01	0.03±0.00	0.01±0.00	0.06±0.01
Asn	-0.04±0.03	-0.04±0.03	-0.02±0.01	-0.01±0.01	-0.03±0.02
Asp	0.00±0.00	-0.01±0.02	0.01±0.00	0.00±0.00	-0.02±0.01
Gln	-0.38±0.10	-0.35±0.09	-0.12±0.03	-0.06±0.02	-0.21±0.05
Glu	0.01±0.01	-0.05±0.02	0.03±0.00	0.01±0.00	-0.04±0.01
Gly	0.07±0.00	0.05±0.01	0.02±0.00	0.01±0.00	0.00±0.00
Ile	-0.13±0.04	-0.14±0.03	-0.08±0.01	-0.05±0.01	-0.11±0.02
Leu	-0.12±0.04	-0.13±0.04	-0.08±0.02	-0.05±0.01	-0.10±0.02
Lys	-0.09±0.10	-0.16±0.09	-0.05±0.03	-0.03±0.02	-0.10±0.05
Pro	-0.02±0.11	-0.03±0.10	-0.03±0.03	-0.02±0.02	-0.04±0.05
Ser	-0.02±0.03	-0.02±0.02	-0.02±0.01	-0.02±0.01	-0.08±0.02
Thr	-0.03±0.03	-0.05±0.02	-0.01±0.01	-0.02±0.01	-0.02±0.01
Val	-0.10±0.03	-0.11±0.02	-0.05±0.01	-0.04±0.01	-0.08±0.02
Biomass					
AcetylCoA	0.66±0.05	0.55±0.06	0.39±0.04	0.36±0.02	0.64±0.06
a-KG	-0.12±0.01	-0.10±0.01	-0.07±0.01	-0.07±0.00	-0.12±0.01
CO_2	0.01±0.00	0.01±0.00	0.01±0.00	0.01±0.00	0.01±0.00
G6P	0.05±0.00	0.04±0.00	0.03±0.00	0.03±0.00	0.05±0.00
GAP	0.06±0.00	0.05±0.01	0.03±0.00	0.03±0.00	0.05±0.00
NADH	0.83±0.06	0.69±0.07	0.49±0.05	0.45±0.03	0.80±0.07
OAA	0.04±0.00	0.04±0.00	0.03±0.00	0.02±0.00	0.04±0.00
R5P	0.07±0.01	0.06±0.01	0.04±0.00	0.04±0.00	0.07±0.01

The consistency of the data was evaluated by calculating the consistency index values (h) listed in Table 6-2 as described previously (Nyberg et al., 1999a; Zupke and Stephanopoulos, 1995a). All of the consistency indexes passed the χ^2 distribution test with a 90% confidence interval indicating that all data sets are consistent and unlikely to contain gross measurement errors.

Metabolic fluxes for the network in Figure 4-1 are listed in Table 6-3 for each of the five steady states. At the first four steady states (A, B, C, and D), as the specific growth rate was decreased, the glycolytic flux decreased. Additionally, the flux of pyruvate into the TCA cycle increased, but the flux of glutamine was reduced. The consumption of branched chain amino acids (lysine, isoleucine, and leucine) was reduced as well at the lower growth rates.

Flux distributions varied for the different steady states, and Figure 6-6 shows values for the ratios of several calculated metabolic fluxes around the pyruvate branchpoint. Plotted in Figure 6-6 are the ratios of the sum of the glycolytic flux (reaction 3) plus the TCA recycle flux (reaction 12) divided by the TCA cycle inlet flux (reaction 6) as a function of specific growth rate. High values of this ratio represent a large amount of carbon influx with the secretion of large amounts of lactate and alanine. Only a small amount of carbon flux enters the TCA cycle. Conversely, lower values represent the more efficient metabolic states with high TCA cycle activity. As the dilution and specific growth rates decreased at the first four steady states, the pyruvate ratio decreased indicating a flux distribution shift around pyruvate shuttling more pyruvate carbon into the TCA cycle as opposed to being converted to lactate. Upon return to a high dilution rate at the fifth steady state (E), cells maintained this efficient utilization of pyruvate in contrast to the physiology observed at steady state A. The fact that more pyruvate was shuttled into the TCA cycle for steady state E as opposed to being converted to lactate as in

Table 6-2. Calculated consistency index values. Consistency index (h) values were calculated to determine the consistency of the metabolite production and consumption rate data sets. Values lower than the χ^2 distribution value (90% confidence interval) indicate that the data set was consistent.

	h	χ^2	Pass / Fail
Steady State A	0.68	4.60	Pass
Steady State B	0.74	4.60	Pass
Steady State C	0.43	4.60	Pass
Steady State D	2.10	4.60	Pass
Steady State E	3.93	4.60	Pass

Table 6-3. Calculated metabolic fluxes (*10^{-10} mmole/viable cell/hr). Metabolic fluxes calculated using equation 4.11 and the data listed in Table 6-1.

	Reaction	Steady State A	Steady State B	Steady State C	Steady State D	Steady State E
1	Glc → G6P	3.53	3.63	1.81	1.21	3.84
2	G6P → 2 GAP	3.38	3.52	1.73	1.16	3.56
3	GAP → Pyr	6.64	6.98	3.42	2.29	7.03
4	Pyr → Lac	6.72	7.24	2.70	1.62	5.74
5	G6P → $Biomass_{R5P}$ + CO_2	0.08	0.06	0.04	0.03	0.12
6	Pyr → AcCoA + CO_2	0.36	0.59	0.89	0.81	1.15
7	Pyr + Glu → αKG + Ala	0.13	0.12	0.03	0.01	0.09
8	OAA + AcCoA → αKG + CO_2	0.42	0.66	1.06	0.96	0.91
9	αKG → SuCoA + CO_2	0.86	1.25	1.21	1.06	1.06
10	SuCoA → Fum	1.11	1.50	1.37	1.23	1.12
11	Fum → OAA	1.09	1.52	1.36	1.21	1.07
12	OAA → Pyr + CO_2	0.59	0.97	0.21	0.16	-0.02
13	Gln → Glu	0.38	0.42	0.12	0.05	0.14
14	Glu → αKG	0.16	0.40	0.04	0.03	0.03
15	GAP + Glu → Ser + αKG	-0.01	-0.02	-0.01	-0.01	-0.05
16	GAP + Glu → Gly + αKG	0.08	0.04	0.03	0.02	0.03
17	Lys → 2 AcCoA + 2 CO_2	0.12	0.10	0.09	0.09	0.09
18	Ile → AcCoA + SuCoA	0.13	0.11	0.10	0.08	0.07
19	Leu → 3 AcCoA	0.12	0.10	0.09	0.08	0.06
20	Glu → Pro	-0.01	-0.03	-0.03	-0.02	0.00
21	Thr → SuCoA	0.03	0.05	0.01	0.02	-0.01
22	Val → SuCoA + CO_2	0.10	0.09	0.07	0.07	0.05
23	OAA + Gln → Asn + αKG	-0.03	-0.06	-0.01	0.01	0.02
24	OAA + Glu → Asp + αKG	0.02	-0.03	0.02	0.02	0.02
25	G6P → $Biomass_{G6P}$	0.06	0.04	0.03	0.02	0.10
26	GAP → $Biomass_{GAP}$	0.06	0.05	0.03	0.03	0.08
27	AcCoA → $Biomass_{AcCoA}$	0.67	0.55	0.39	0.36	0.66
28	$Biomass_{\alpha KG}$ → αKG	0.10	0.12	0.06	0.05	0.06
29	OAA → $Biomass_{OAA}$	0.07	0.01	0.05	0.05	0.09
30	CO_2 → $Biomass_{CO2}$	0.03	-0.01	0.02	0.03	0.03
31	NADH → $Biomass_{NADH}$	0.83	0.70	0.48	0.44	0.80
32	0.5 O_2 + 3 ADP + NADH → 3 ATP + NAD^+	3.79	4.97	6.08	5.49	5.64
33	0.5 O_2 + 2 ADP + $FADH_2$ → 2 ATP + FAD	1.58	1.90	1.73	1.55	1.39

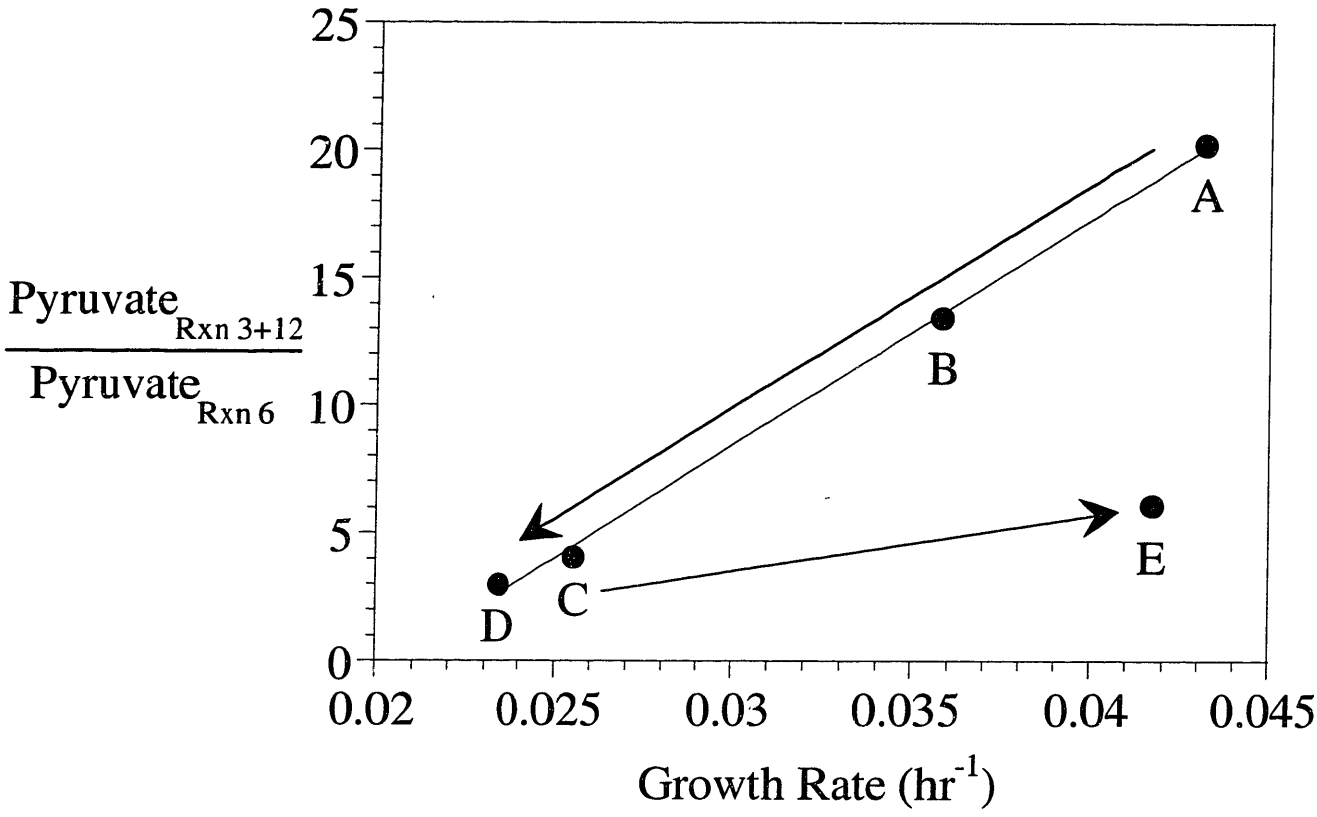

Figure 6-6. Metabolic flux distribution around the pyruvate branchpoint. The values plotted in (6-6) are the ratio of the sum of glycolytic flux (reaction 3) and the TCA recycle flux (reaction 12) divided by the TCA cycle inlet flux (reaction 6). Deviations from unity represent waste metabolite (lactate and alanine) production. High values of the ratio indicate a condition of high waste metabolite production, whereas lower values indicate more efficient utilization of pyruvate carbon. For the first four steady states when the growth rate was progressively reduced, the metabolic flux around pyruvate was redistributed in favor of more efficient metabolism. This efficient metabolism was maintained during the subsequent increase in growth rate to the final steady state (E).

steady state A, explains the nearly two-fold increase in cell concentration for steady state E. In addition, less branched chain amino acids and glutamine were metabolized in the TCA cycle for steady state E as compared to steady state A. In short, flux analysis reveals a more efficient utilization of substrate carbon associated with steady state E which was reached after the cells were first adapted to lower growth rate conditions.

6.3 Discussion

The data presented in this chapter demonstrate that two steady states can be obtained for the same dilution rate, exhibiting similar specific growth rates and cell viabilities but drastically different cell densities and metabolic flux distributions. After the first high dilution steady state (A), cells underwent changes in their metabolic flux distribution in response to progressively lower dilution and growth rates until reaching a point of near abortive proliferation (D). At the progressively lower growth rates, the utilization of pyruvate carbon became more efficient with more pyruvate flowing into the TCA cycle. This adaptation enabled the cells to maintain energy production as well as meet the requirements for cell biosynthesis at the last high dilution steady state (E). This efficient metabolic pattern was maintained resulting in a higher cell density.

The observation of multiple steady states with different metabolic flux distributions was observed previously by Hayter et al. (Hayter et al., 1992a). This glucose limited continuous culture of Chinese hamster ovary (CHO) cells was grown under varying glucose concentrations. The first and last steady state sections of the run were performed at a glucose concentration of 2.75mM. Although the glucose uptake rates for these two sections were similar, the specific lactate production rates differed by nearly a factor of two. This demonstrates that this cell line also underwent a metabolic shift to a metabolically more efficient state where less glucose substrate carbon was released as lactate. Although the cell densities in these two cases did not

vary by a significant amount, this may have been due to the low growth rate and the fact that these cultures were glucose limited and unable to consume higher amounts of this substrate for biomass production.

The metabolic shifts observed in the reported continuous culture run could be due to a favorable genetic mutation, a change in the genetic expression of particular metabolic enzymes, or a change in the regulation of these enzymes. A favorable genetic mutation causing the higher cell concentration and metabolic flux redistribution is highly unlikely due to the rather long time period it would take for a favorably mutated cell to become a noticeable fraction of the reactor cell population. For example, if an identically favorable mutation occurred in one of every 10^7 cells (a high mutation rate) that resulted in a growth rate advantage of 20% over the wild-type cell line, 100 cell doublings would be required in order for the cell population to reach a contamination level of 10%. This value increases to 199 doublings for a 10% growth rate advantage. For the continuous run reported, doubling times ranged from 16 hours to 30 hours yielding a total of approximately 70 cell doublings before reaching steady state E. In addition, since selection in chemostats typically results after cells have grown for several hundred generations (Dykhuizen and Hartl, 1983), the hypothesis that the cells in this study underwent a favorable random mutation around the pyruvate branchpoint is unlikely.

The metabolic shift could also be due to a phenomena connected to asymmetric cell division. At the low viability steady state (D), for every cell that divides, approximately one of the two daughter cells must die before it can divide. One could hypothesize that the dividing cell does not equally distribute its cellular resources to the two daughter cells but rather it favors one over the other following a stochastic process. An unequal distribution of mitochondria could aid in the maintenance of the culture cell population at the expense of the culture viability under the

more stressful environmental conditions. This increase in population heterogeneity could be used as a way for cell populations to increase their chances for survival at the expense of individual cell survival by attaching critical cell survival parameters to a stochastic genetic regulatory mechanism that is induced under stressful conditions. Unequal mitochondrial inheritance has been observed for a variety of cell types (McConnell et al., 1990; Rappaport et al., 1998; Smirnova et al., 1998). This would also explain the increase in mitochondrial or TCA cycle activity at the lower dilution rates. At the second high growth rate steady state (E), a cell subpopulation with this history of adaptation to higher mitochondrial activity could maintain this physiology as a result of the population now expressing a new genetic regulatory state (McAdams and Arkin, 1999).

The operation pathway followed to reach steady state E suggests potential feeding strategies and fed-batch reactor operations to achieve high cell densities. Typically, fed-batch cultures are run under glucose and/or glutamine limitation in order to reduce the production of toxic byproducts such as lactate and ammonia. This nutrient limitation results in lower growth rates but more efficient substrate utilization with lower conversion of glucose into lactate (Xie and Wang, 1994c). Alternatively, the results from this paper suggest that an initial adaptation phase in a fed-batch could be used as a means of shifting cells to a more efficient state of pyruvate utilization. After this adaptation is achieved, the cells could then be grown under conditions of higher nutrient concentrations at a higher growth rate resulting in the maintenance of the lower lactate production but with a higher viable cell concentration. This new approach toward fed-batch operations may prove to enhance not only industrial cell culture performance but fundamental knowledge concerning cell behavior and metabolism as well.

The utilization of bioreactor operating conditions to induce the appearance of a desired phenotype differs from the typical approach used in metabolic engineering to achieve modified flux distributions. In this case, the cell concentration was doubled and flux distribution was altered dramatically without the transfection of any enzyme involved in the altered metabolic branchpoint. The success of this type of inverse metabolic engineering could be applied in other situations where knowledge about the metabolic network regulatory architecture could allow for the perturbation and adaptation of cells that express more desirable phenotypes without using transfection techniques. In addition, knowledge concerning the physiological characteristics of desirable phenotypes could also be used in the isolation of subpopulations that express these desirable traits, and this strategy was employed in the experimental work covered in the next chapter.

7. MITOCHONDRIAL MEMBRANE POTENTIAL SORTED SUBPOPULATIONS

7.1 Introduction

The continuous culture steady state multiplicity results indicate that the enhancement of TCA cycle activity and the flux through PDH could be beneficial for cultured mammalian cells resulting in increased culture viable cell concentrations and viabilities. The observed changes in metabolic flux distribution that involved a higher production of energy generated through the oxidative phosphorylation pathway and a higher production of biomass were hypothesized to be reproducible under either batch or fed-batch culture conditions. The oxidative phosphorylation respiratory chain located in the inner mitochondrial membrane is a significant contributor to cellular energy production, and therefore, the characterization of mitochondrial activity was hypothesized to be a strategic cellular target for the development of novel strategies aimed at improving viable cell concentration and culture viability.

The characterization of oxidative phosphorylation and TCA activity along with the metabolic flux distribution around the pyruvate branchpoint requires metabolic flux analysis calculations that need accurate gas exchange measurements (OUR and CER). These flux analysis techniques, however, require extensive amounts of experimental and computational effort. In addition, obtaining accurate redundant gas exchange measurements under transient culture conditions is extremely difficult (Bonarius et al., 1995; Stephanopoulos et al., 1998; Zupke and Stephanopoulos, 1995a). Therefore, a quicker technique was developed in order to obtain data that characterize the physiological state of mitochondria *in-vivo*. Since oxidative phosphorylation is driven by the proton-motive force across the inner mitochondrial membrane, the mitochondrial membrane potential (MMP; $\Delta\Psi_m$) was used as a measure of the mitochondrial

physiological state. This membrane potential was experimentally determined using the commonly used lipophilic cationic dye, Rhodamine 123 (Rh123). FACS techniques provided a quick and simple method for obtaining membrane potential values for a significant number of cells in culture resulting in a statistically significant measure of mitochondrial physiology. Fluorescent dye characterization of $\Delta\Psi_m$ has been used extensively in a large number of cell lines for mitochondrial membrane potential measurement and mitochondrial physiology analysis (Bereiter-Hahn and Vöth, 1994; Chen, 1988; Petit et al., 1990). Unlike other dyes that stain mitochondrial membrane potential such as JC-1 and $DiOC_6$ (see Literature Review), Rh123 has a low toxicity at low concentrations, enabling one to stain cells and then perform long-term experiments on these stained cells (Bereiter-Hahn and Vöth, 1994; Chen, 1988).

Cells with different mitochondrial physiologies, as determined through the measurement of $\Delta\Psi_m$, were hypothesized to have different cellular physiologies. The experimental strategy designed to test this hypothesis consisted of several stages. The first stage involved the development of a staining procedure using Rhodamine 123 and then checking the dye specificity by subjecting stained cells to mitochondrial membrane uncouplers. The second stage involved the separation of a population of stained cells using FACS techniques in order to obtain several subpopulations of cells that varied in their mean mitochondrial membrane potential as determined using Rh123. The third stage involved the development of methods for killing cells through apoptosis induced through specific mechanisms. The mitochondrial membrane potential sorted subpopulations were subjected to these apoptosis inducers, and the apoptotic death was characterized both morphologically through the measurement of apoptosis related chromatin condensation and also biochemically through the measurement of caspase-3 enzymatic activity. In addition, cytochrome *c* was added to cytosolic extracts obtained from these apoptotic cells in

order to obtain more insight concerning the differences between the mechanisms of apoptosis for the various mitochondrial membrane potential sorted subpopulations.

The results from these experiments demonstrated that a population of wild-type cells contains subpopulations that vary in their resistance to apoptosis. Furthermore, these apoptosis resistant subpopulations could be separated based on their mitochondrial membrane potential with significant differences between the measured membrane potentials being maintained even after numerous generations. The differences in apoptosis resistance involved not only morphological variances as demonstrated by their different chromatin condensation kinetics but also biochemical variances as shown by their different caspase-3 enzymatic activities.

7.2 Results

7.2.1 Staining for Mitochondrial Membrane Potential

The hybridoma cells were stained with a final concentration of 2 μg/ml Rhodamine 123 for 10 minutes, washed with PBS, and analyzed on a FACS machine according to the procedure described in Materials and Methods. An example histogram of the resulting cellular fluorescence is shown in Figure 7-1. The histogram of an unstained control showed a distribution of fluorescence values between 1 and 10 (mean fluorescence of approximately 3 to 4) whereas the stained cells resulted in a distribution of values centered above 1,000 (Figure 7-1). In cultures with a high dead cell fraction, as measured using the trypan blue dye exclusion method, a smaller peak was observed that had a fluorescence value distribution lower than the viable fraction (Figure 7-1). The appearance of this lower dead cell peak has been observed previously (Ferlini et al., 1995). The mitochondrial membrane potential was the driving force

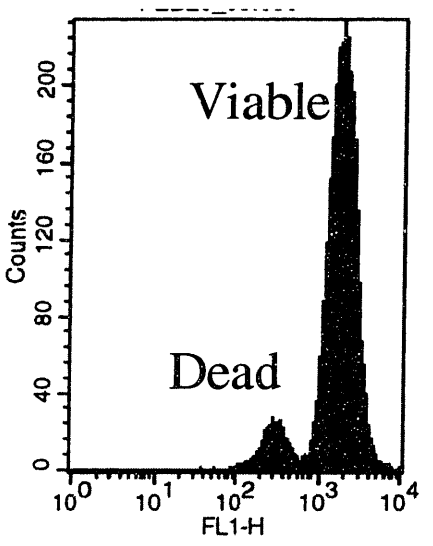

Figure 7-1. Rhodamine 123 staining of mitochondrial membrane potential. The hybridoma cells were incubated with Rh123, washed, and then analyzed on a FACS. The resulting histogram of fluorescence values is shown. A dead cell peak is observed in cultures with a low viability as measured using the trypan blue dye exclusion method.

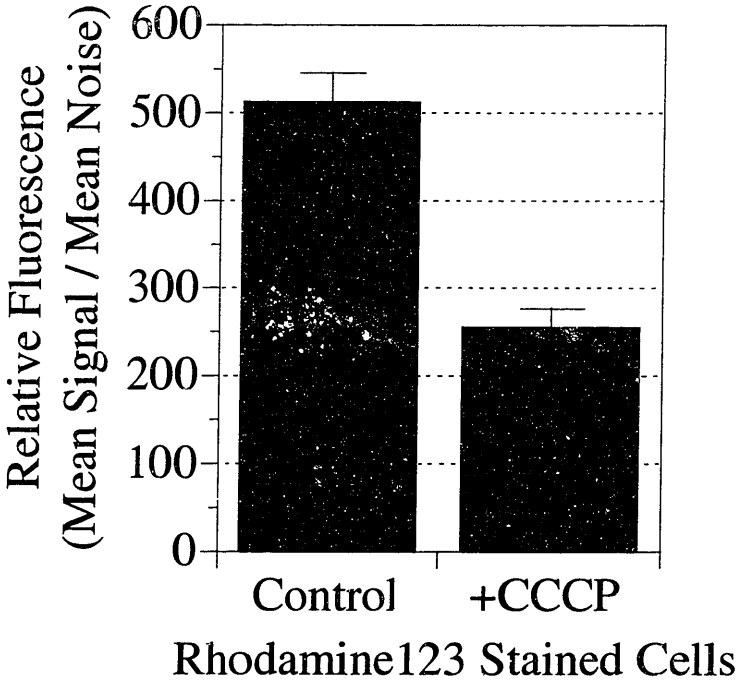

Figure 7-2. Rhodamine staining of mitochondria subjected to a membrane potential uncoupler (CCCP). The hybridoma cells were subjected to CCCP for 10 minutes and then stained with Rh123. The resulting histograms of fluorescence values showed a dramatic drop in Rh123 uptake indicating the specificity of Rh123 for mitochondrial membrane potential.

behind the cellular uptake of Rhodamine 123 as demonstrated in Figure 7-2. A dramatic loss of Rh123 uptake was observed when the cultured cells were incubated with a specific mitochondrial membrane uncoupler, carbonyl cyanide *m*-chlorophenylhydrazone (CCCP), for 10 minutes at a working concentration of 2 μg/ml. This result has been repeatedly shown in the literature for this uncoupler as well as for a variety of other mitochondria specific depolarizing agents (Chen, 1988; Emaus et al., 1986; Juan et al., 1994). Furthermore, researchers have analyzed compounds that collapse the mitochondrial proton gradient (Δp) and hyperpolarize the electrochemical potential ($\Delta\Psi_m$) which result in an increased uptake of Rh123. This result demonstrates that this stain serves primarily as an indicator of the mitochondrial membrane potential ($\Delta\Psi_m$) component of the proton motive force (Emaus et al., 1986).

Although Rh123 can be used to determine the overall cellular mitochondrial activity and membrane potential, it can not effectively distinguish between an increase in either the specific mitochondrial activity or the overall mitochondrial mass. Other stains such as 10-n-nonyl acridine orange are not incorporated according to the electrochemical potential but rather through interactions with specific mitochondrial membrane proteins and lipids. Although not used in this research, these stains could be used to determine these other mitochondrial parameters in order to obtain more detailed data describing mitochondrial physiology (Benel et al., 1989).

7.2.2 Sorting Cells Based on Mitochondrial Membrane Potential

The low toxicity of Rh123 enables one to separate and then grow cells stained with this dye. The Rh123 stained hybridoma cells were separated into various subpopulations using a FACS (FACSCAN, Becton Dickinson) based on their individual fluorescence values (Figure 7-3). These sorted mixed-culture cell subpopulations were passaged for several generations until enough cells were grown to permit the freezing of several vials for cell bank storage. These

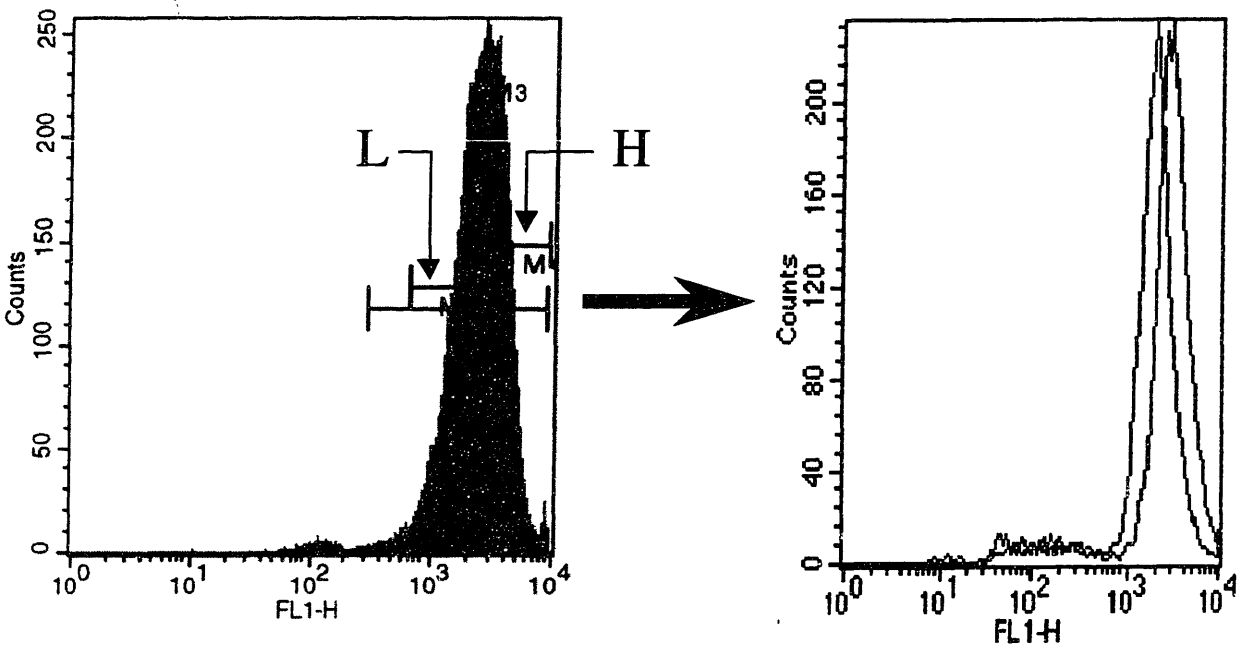

Figure 7-3. FACS sorting of cells separated based on mitochondrial membrane potential. The hybridoma cells were stained for mitochondrial membrane potential using Rh123 and then separated into subpopulations using FACS. Here, the low (L) and high (H) fractions each represent approximately 15% of the total population. These sorted cells were passaged for numerous (10-20) generations and then restained with Rh123. The resulting histogram of fluorescence values showed a distinct difference between the two subpopulations with respect to mitochondrial membrane potential.

passaged cells maintained a significant mitochondrial membrane potential fluorescent staining differential, as measured by restaining with Rh123, even after passaging for approximately 10-20 generations. The sorted cell populations were named high (H) and low (L) with respect to their mean fluorescent values when stained with Rh123. Additional enrichment was also performed on these high and low populations in an effort to increase their mean Rh123 fluorescence staining differential by resorting them in a FACS. In other words, the high fraction from the high subpopulation (H) was separated and passaged, and this resulted in even higher mean Rh123 fluorescence values and mitochondrial membrane potential differentials.

The cell populations were analyzed not only for their mean Rh123 fluorescence values but also for their cell cycle and DNA content properties as well. Table 7-1 lists the results for cells that were stained with propidium iodide and then analyzed using FACS to determine the cell cycle properties for both the high (H) and low (L) populations. These cells were all taken from cultures that were growing at mid-exponential phase. Although the two subpopulations listed in Table 7-1 had Rh123 mean fluorescence values that differed by over one third, the cell cycle values were virtually identical. In addition, no differences in DNA content were observed (data not shown) indicating that the observed differences in Rh123 staining could not be attributed to cell cycle variances or the appearance of multiple chromosomes.

7.2.3 Apoptosis Induction

Apoptosis is the primary cause of death for cultured mammalian cells (Goswami et al., 1999; Mercille and Massie, 1994; Mosser and Massie, 1994; Simpson et al., 1998). Therefore, the Rh123 sorted subpopulations were characterized for their differences in resistance to apoptosis as determined by their responses to incubation with specific apoptosis inducers. A mitochondria specific apoptosis inducer, rotenone, and another more commonly used apoptosis

Table 7-1. Comparison of cell cycle data for MMP sorted subpopulations. Cells stained with propidium iodide were examined using FACS. The high (H) and low (L) staining subpopulations had similar cell cycle characteristics indicating that these cells do not vary significantly in their DNA content or cell cycle. The relative fluorescence (mean signal to noise ratio) for the high subpopulation was 39% higher than that for the low subpopulation.

Cell Cycle Phase	Low (L)	High (H)
G_0/G_1	24.5 ± 0.5	24.5 ± 0.9
G_2/M	13.6 ± 0.6	12.5 ± 0.3
S	61.9 ± 1.1	63.1 ± 1.1

inducer, staurosporin, were both utilized in these experiments. Numerous electron transport chain inhibitors have been implicated in apoptosis induction (Kroemer et al., 1995; Susin et al., 1998; Wertz and Hanley, 1996)], and rotenone specifically inhibits the NADH dehydrogenase complex (Krippner et al., 1996; Stryer, 1988; Wertz and Hanley, 1996). Staurosporin is another potent apoptosis inducer that is believed to inhibit protein serine / threonine kinases that affect protein phosphorylation and survival factor signaling (Wertz and Hanley, 1996). The wild-type unsorted hybridoma cells were subjected to each of these inducers, and the resulting kill curves are shown in Figure 7-4 along with their point of action in the mitochondria related apoptosis pathway. The viable and apoptotic fractions were differentiated by determining the degree of chromatin condensation shown using the acridine orange and ethidium bromide stain described in Materials and Methods. Since these compounds induce apoptosis within a few hours, they can be used in experiments that are aimed at determining specific differences between apoptotic death mechanisms and kinetics in various cell populations. This method contrasts with long-term experiments which are subject to variable culture conditions in which additional inducers of apoptotic death exist such as glucose and amino acid nutrient limitation or growth factor depletion. Since the cells for these apoptosis induction experiments were taken from mid-exponential growth cultures, these additional apoptosis inducing factors can be ruled out as significant sources of apoptosis, leaving the apoptosis inducers as the primary source of the observed apoptotic cell death. This was supported by the fact that virtually no apoptotic death was observed in the uninduced control cultures.

Figure 7-5 illustrates a more specific quantitation of the effect of rotenone on viable cells (determined using the trypan blue exclusion method). 3-(4,5-dimethylthiazol-2-yl)-2,5-diphenyl tetrazolium bromide (MTT) measures mitochondria dehydrogenase activity and has been

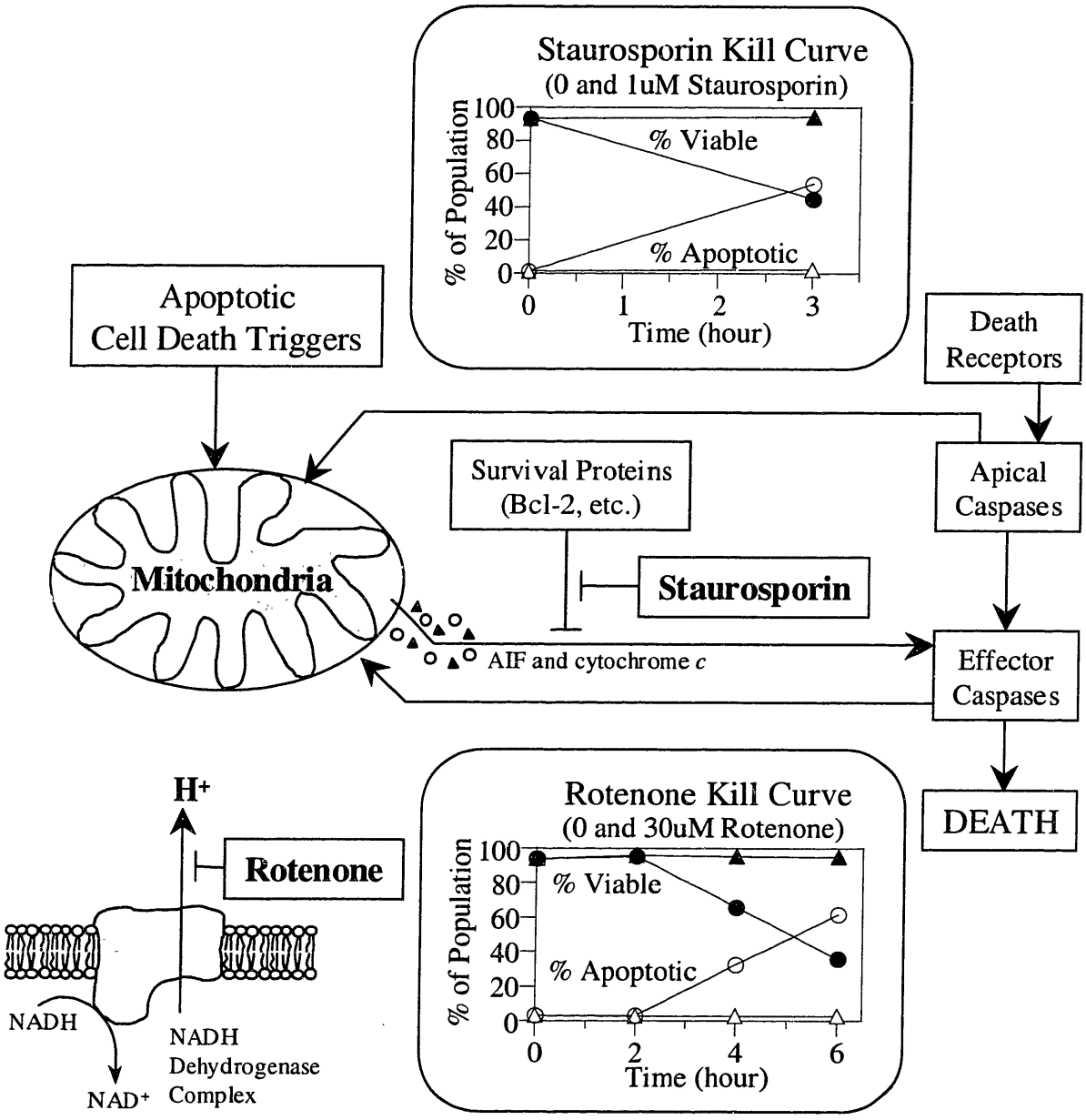

Figure 7-4. Apoptosis induction using staurosporin and rotenone. The hybridoma cells were subjected to these two apoptosis inducers in order to characterize the responses of the Rh123 sorted subpopulations to defined apoptotic stimuli. The specific point of action of each apoptosis inducer within the overall apoptotic pathway is shown in the figure along with the corresponding kill curves.

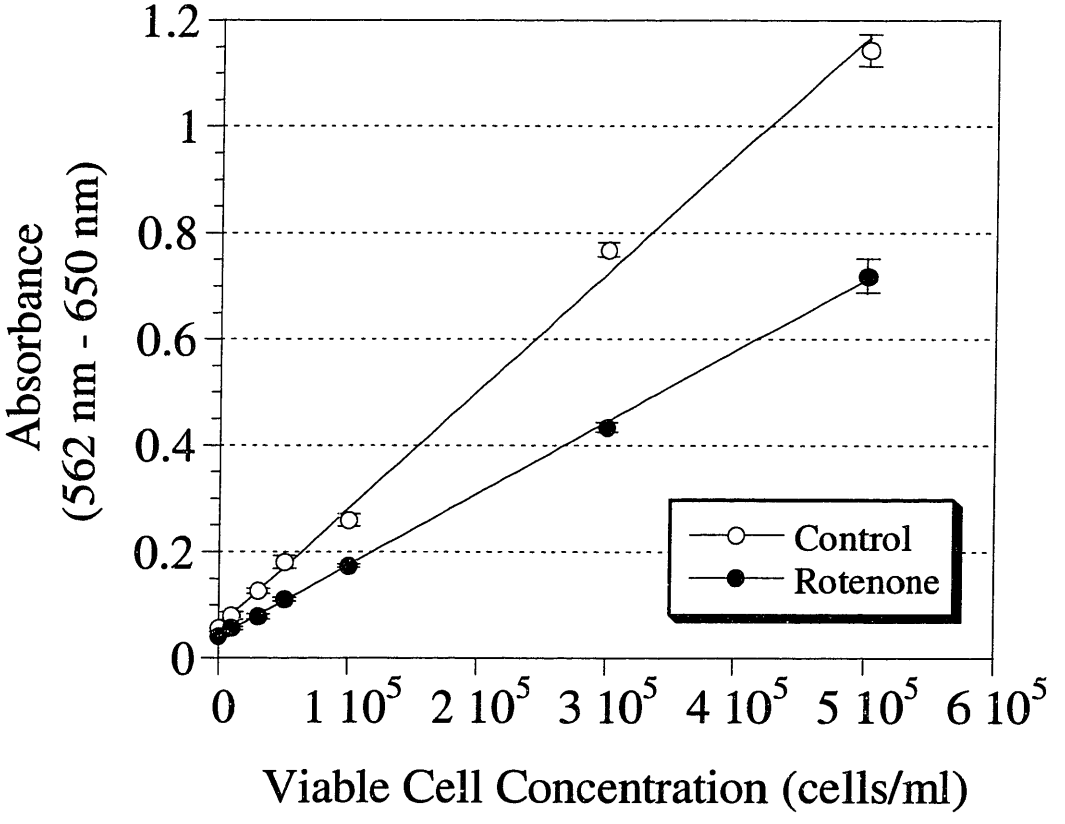

Figure 7-5. MTT measurement of cells undergoing rotenone induced apoptosis. Cells taken from the same culture were incubated either with or without 30 μM rotenone for two hours. The resulting MTT assay measurement of mitochondrial dehydrogenase activity is shown for each of the viable cells concentrations (viability was measured using trypan blue).

used extensively to measure surviving and proliferating cells (Mosmann, 1983; Slater et al., 1963). These results indicate that rotenone caused a dramatic loss of mitochondrial dehydrogenase activity after the cells were incubated with rotenone for only two hours. These results show that mitochondrial dehydrogenase activity was affected by apoptotic death and that the trypan dye exclusion method does not necessarily correlate with the MTT method for cells undergoing apoptosis (Knorr, 1999; Mosmann, 1983).

7.2.4 Characterizing Apoptosis for Mitochondrial Membrane Potential Sorted Cells

The Rh123 sorted hybridoma cell subpopulations were characterized for both key morphological and biochemical features of apoptosis resulting from the apoptotic death inducers. The cell subpopulations were all taken from frozen cell stocks and cultured until they reached mid-exponential phase. The subpopulations were stained for mitochondrial membrane potential using Rh123 and FACS. Then, the apoptosis inducers were added to the cultures (30 μM rotenone and 1 μM staurosporin). Dimethyl sulfoxide (DMSO) was added to the control cultures to account for the DMSO present in the apoptosis inducer stock solutions. The apoptosis related chromatin condensation was assessed at various time points using the acridine orange and ethidium bromide stain. Figure 7-6 shows the compiled results from three separate experiments for the rotenone induced apoptosis with the percentage of viable cells containing intact chromatin plotted versus the mean Rh123 fluorescence signal to noise ratio (S/N) for the various inoculum subpopulations. All of these mean Rh123 fluorescence values refer to the values for the inoculum; no time course of Rh123 uptake was taken for these experiments. Initially, the cultures all started out with a viability of approximately 95%. Even after two hours, no significant differences between the subpopulations were observed. Beginning at four hours, however, a significant deviation between the various subpopulations was observed. After eight

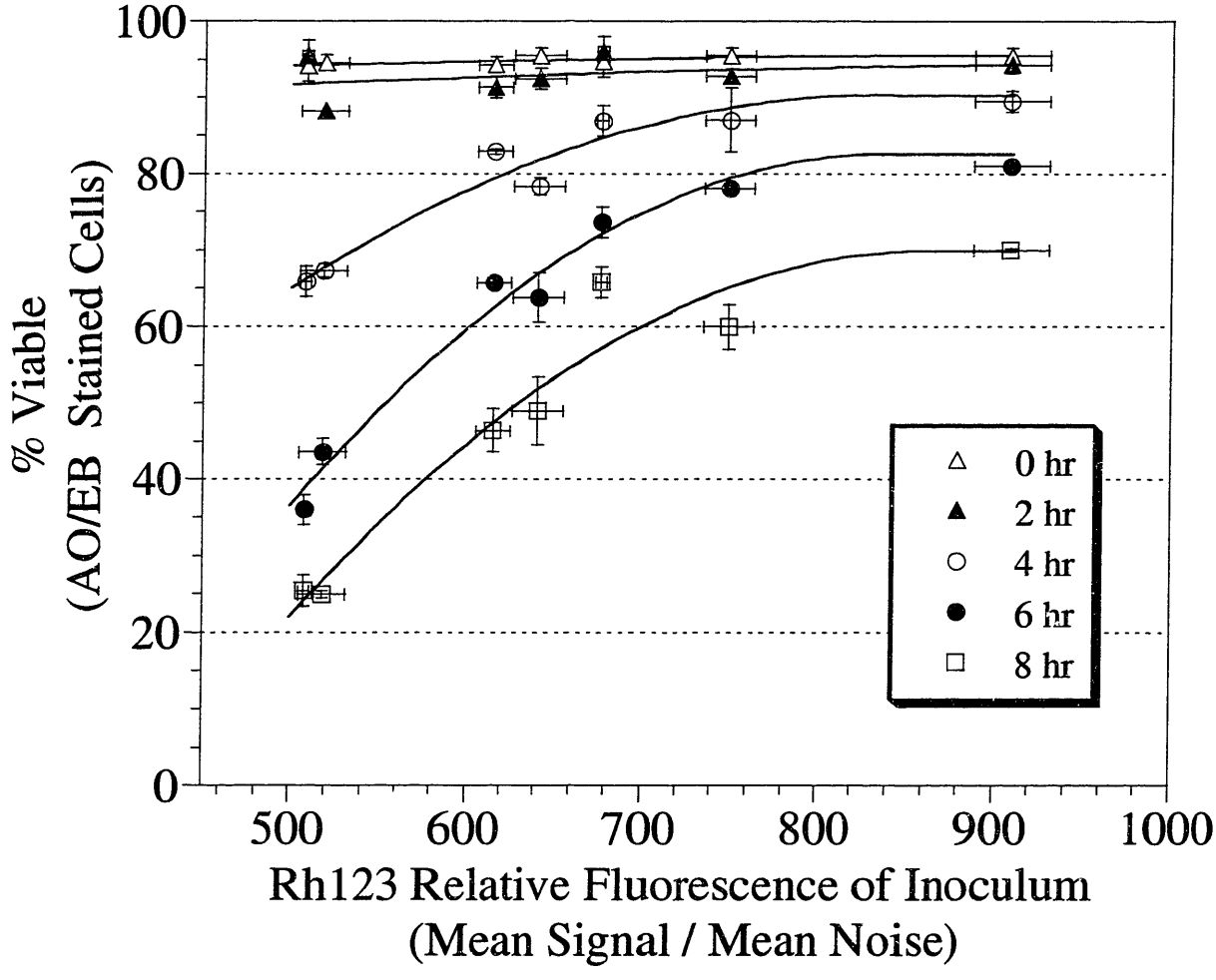

Figure 7-6. Apoptotic death kinetics for Rhodamine 123 sorted subpopulations subjected to 30 μM rotenone. The hybridoma cell subpopulations were stained with Rh123 and then analyzed on a FACS. Then, they were given either rotenone (30 μM) or DMSO (the rotenone stock contained DMSO). The chromatin condensation apoptotic morphology was measured at the indicated time intervals using the acridine orange and ethidium bromide stain. The Rh123 fluorescence values refer to only the initial values taken for the inoculum; no Rh123 fluorescence value time course data was taken. This plot is a compilation of data taken from three separate experiments.

hours, the highest Rh123 staining subpopulation was still 70% viable as compared to the lowest Rh123 staining subpopulation that was only 25% viable. This indicates that subpopulations with a higher mean mitochondrial membrane potential as measured using Rh123 have an enhanced ability to resist apoptotic death. Furthermore, these results were reproducible as demonstrated with the cells subjected to staurosporin induced apoptosis (Figure 7-7). This result indicates that these subpopulations vary in their resistance to multiple apoptosis inducers, and a feature of the apoptotic pathway related to mitochondria physiology may be the source of this resistance.

Effector caspase activity causes the apoptosis related chromatin condensation morphology. Caspase-3 has been shown to be a potent effector caspase that targets a number of specific cellular proteins, causing a significant number of changes associated with apoptotic death. Therefore, biochemical differences between the Rh123 sorted subpopulations were determined by measuring the caspase-3 enzymatic activity. For this experiment, the cells were again taken from the frozen cell stock and cultured until they reached mid-exponential phase. The mean Rh123 fluorescence values were determined using FACS, and then the subpopulations were subjected to each of the apoptosis inducers described previously (30 μM rotenone and 1 μM staurosporin). After several hours (3 hours for staurosporin and 4 hours for rotenone), the cellular apoptotic morphology was determined using acridine orange and ethidium bromide measurement of apoptosis related chromatin condensation, and the results are shown in Table 7-2 for rotenone and Table 7-3 for staurosporin. Then, cytosolic extractions were performed for each set of apoptosis inducers as described in Materials and Methods. The protein content of the extracts was measured using the Bradford assay with a BSA standard. The caspase-3 enzymatic activity was then determined colorimetrically by incubating 50 μg of extract protein with DEVD-pNA and then by measuring the amount of free pNA (cleaved DEVD-pNA substrate). Figure 7-

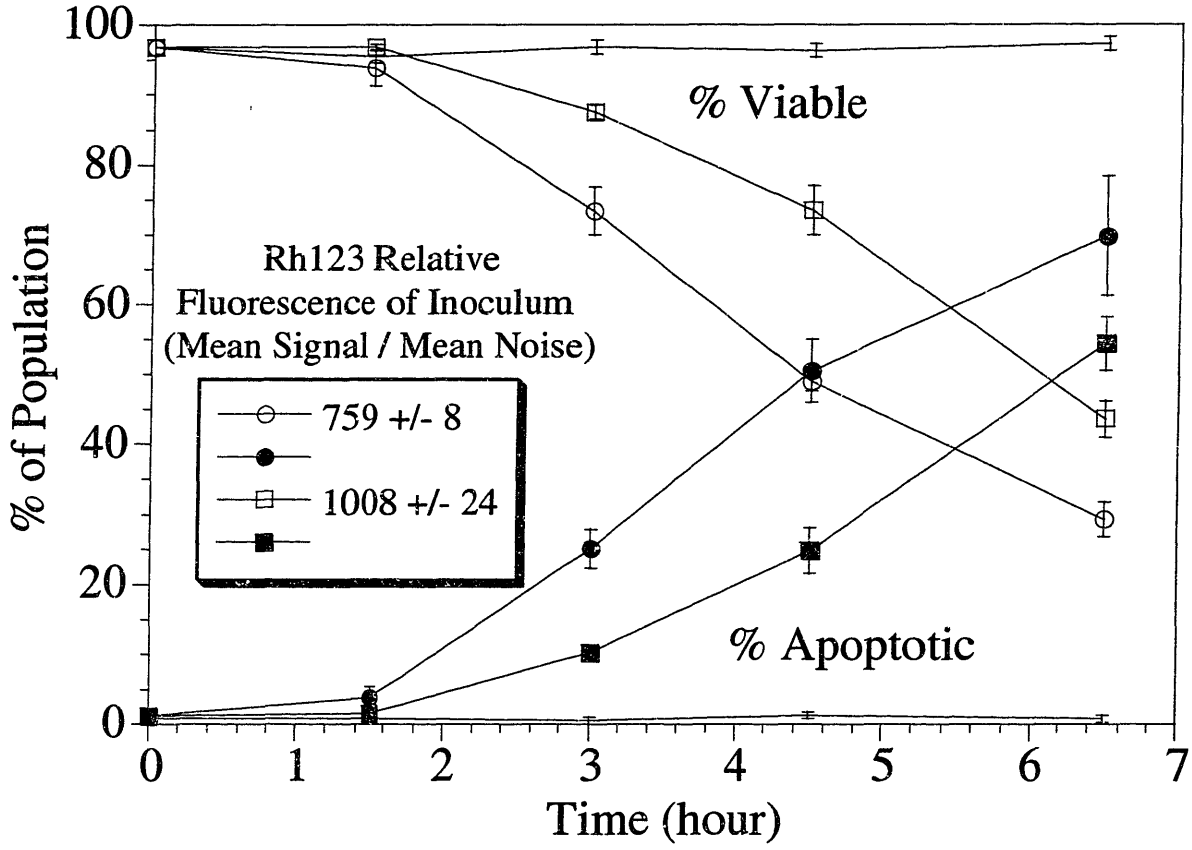

Figure 7-7. Apoptotic death kinetics for Rhodamine 123 sorted subpopulations subjected to 1 μM staurosporin. The hybridoma cell subpopulations were stained with Rh123 and then analyzed on a FACS. Then, they were given either staurosporin (1 μM) or DMSO (the staurosporin stock contained DMSO). The chromatin condensation apoptotic morphology was measured at the indicated time intervals using the acridine orange and ethidium bromide stain. The Rh123 fluorescence values refer to only the initial values taken for the inoculum; no Rh123 fluorescence value time course data was taken. The constant value data points refer to the controls that were not subjected to staurosporin.

Table 7-2. Data for rotenone induced caspase-3 enzymatic activity. Cytosolic extracts were taken from cells subjected to 30 μM rotenone for 4 hours and assayed for caspase-3 activity using DEVD-pNA.

	Low (L)	High (H)
Percent Viable (AO / EB)	76.5	92.5
Rh123 (S/N) (Relative Fluorescence of inoculum)	562	886
Caspase-3 Activity (μmole / hr $\mu g_{protein}$)	3.17	1.10

Table 7-3. Data for staurosporin induced caspase-3 enzymatic activity. Cytosolic extracts were taken from cells subjected to 1 μM staurosporin for 3 hours and assayed for caspase-3 activity using DEVD-pNA.

	Low (L)	High (H)
Percent Viable (AO / EB)	64.5	83.5
Rh123 (S/N) (Relative Fluorescence of inoculum)	562	886
Caspase-3 Activity (μmole / hr $\mu g_{protein}$)	5.38	1.92

8 shows the caspase-3 enzymatic activity results for rotenone induced apoptosis and these data demonstrate a significant difference in the enzymatic activity for this critical caspase. The fact that the z-VAD-fmk inhibited caspase-3 activity matched the activity for the uninduced control indicates that the extraction procedure did not inadvertently cause the activation of any caspase-3 activity. These results were also repeated in the staurosporin induced apoptosis cell extracts, and the caspase-3 enzymatic activity is shown in Figure 7-9. Again, a significant difference in caspase-3 activity is shown for the two Rh123 sorted subpopulations. The specific caspase-3 enzymatic activities are tabulated in Tables 7-2 and 7-3. The specific caspase-3 enzymatic activities differ by nearly three-fold between the two subpopulations. This supports the morphological differences observed previously and provides a more fundamental biochemical basis for these observations.

Additional experiments were also conducted in an effort to determine more fundamental aspects of the observed variance in apoptotic resistance for these Rh123 sorted subpopulations. Since cytochrome *c* has been implicated in the activation of apoptosis and caspase activity (Bossy-Wetzel et al., 1998; Green and Reed, 1998; Krippner et al., 1996), cytochrome *c* (10μM) was added along with dATP (1mM) in order to activate the apoptosome *in-vitro*. Figure 7-10 shows the results for cytochrome *c* induction of capsase-3 activity for various experimental cases. These results indicate that caspase-3 activity was inducible in the control cells, but again this activity was different for each of the Rh123 sorted subpopulations. In addition, extracts taken from the Rh123 sorted cells subjected to rotenone and incubated with cytochrome *c* and dATP did not yield a significant increase in caspase-3 activity.

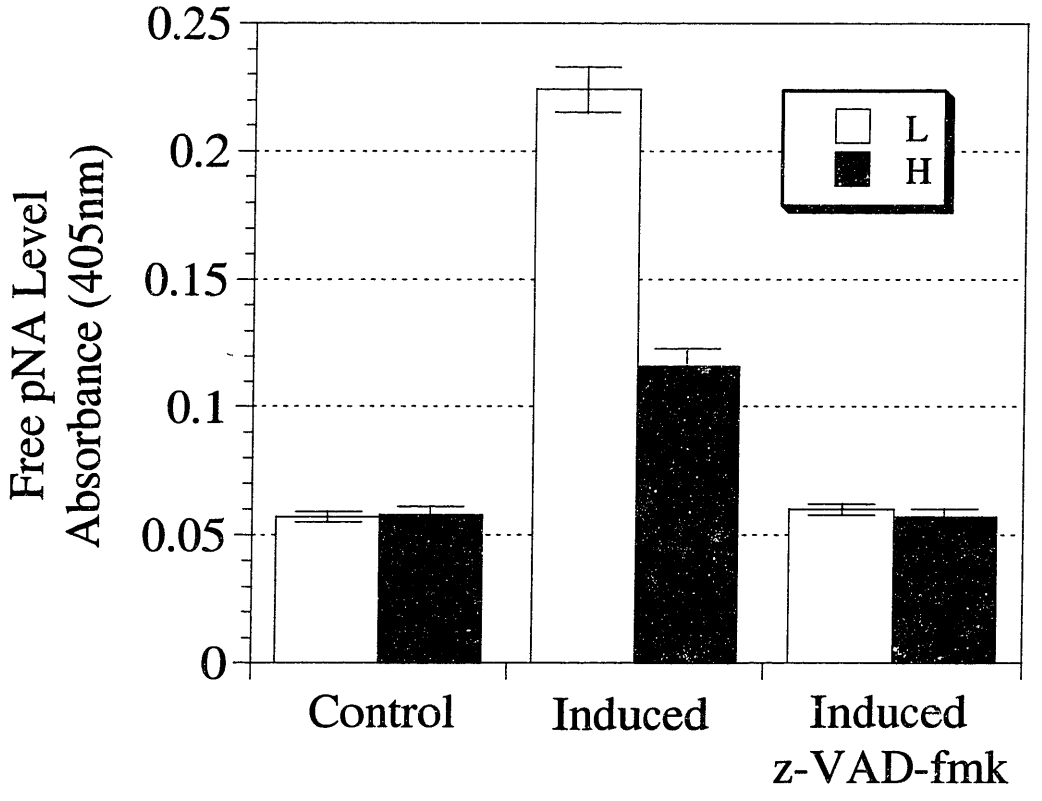

Figure 7-8. Caspase-3 enzymatic activity for Rhodamine 123 sorted subpopulations subjected to 30 μM rotenone. Cytosolic extracts were collected from cells subjected to rotenone. The caspase-3 enzymatic activity was measured using DEVD-pNA substrate incubated with 50 μg of extract protein. The caspase inhibitor, z-VAD-fmk was also added to the apoptosis induced extracts in order to demonstrate the absence of caspase activity in the control.

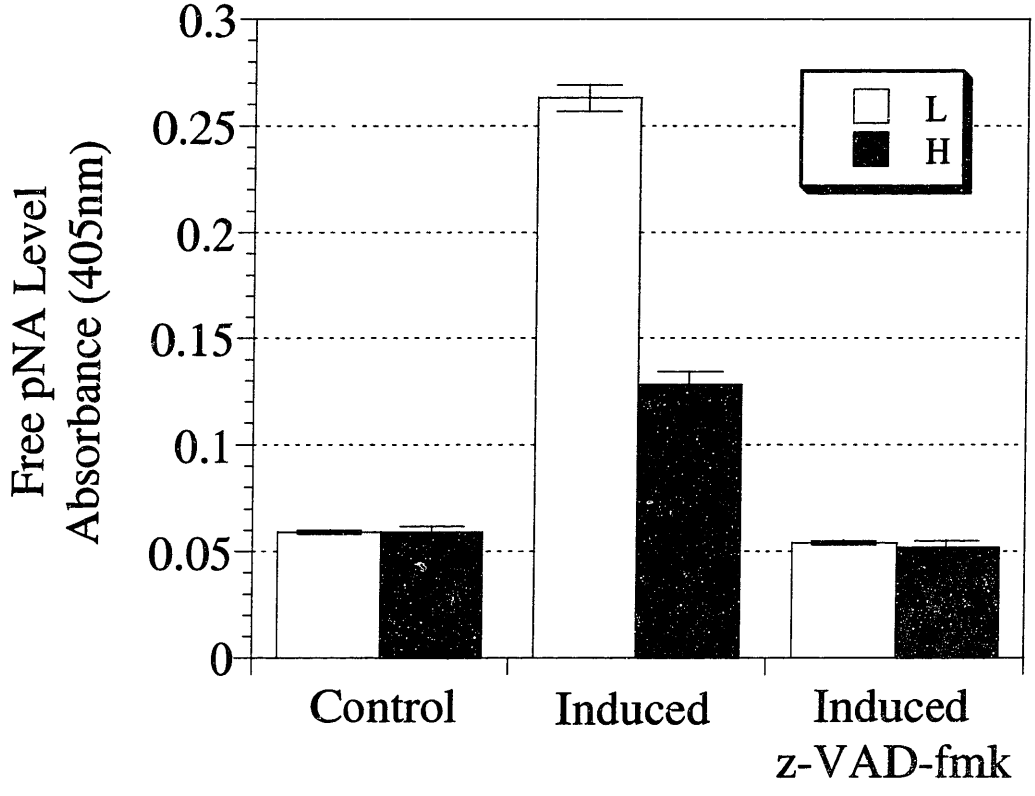

Figure 7-9. Caspase-3 enzymatic activity for Rhodamine 123 sorted subpopulations subjected to 1 μM staurosporin. Cytosolic extracts were collected from cells subjected to staurosporin. The caspase-3 enzymatic activity was measured using DEVD-pNA substrate incubated with 50 μg of extract protein. The caspase inhibitor, z-VAD-fmk was also added to the apoptosis induced extracts in order to demonstrate the absence of caspase activity in the control.

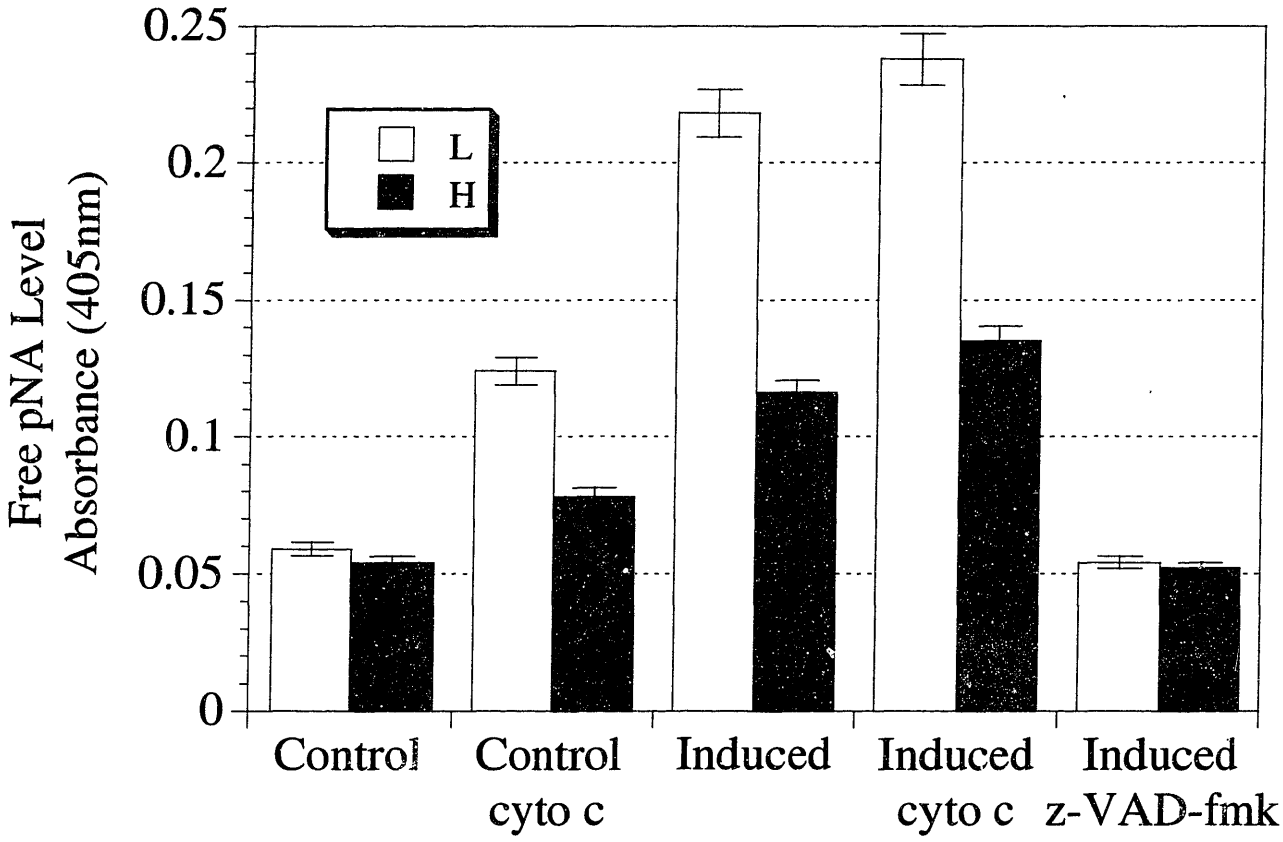

Figure 7-10. Caspase-3 enzymatic activity for Rhodamine 123 sorted subpopulations subjected to 30 μM rotenone, cytochrome *c*, and dATP. Cytosolic extracts were collected from cells subjected to rotenone. Cytochrome *c* (10 μM) and dATP (1 mM) were preincubated with the control and induced extracts before incubation with the DEVD-pNA substrate. Then, the caspase-3 enzymatic activity was measured using DEVD-pNA substrate incubated with 50 μg of extract protein.

7.3 Discussion

Apoptosis is a significant problem for mammalian cell culture (Goswami et al., 1999; Mercille and Massie, 1994; Mosser and Massie, 1994; Simpson et al., 1998). Nutrient limitations, death receptor activation, as well a vast number of other factors all trigger apoptotic cell death (Simpson et al., 1998; Wertz and Hanley, 1996). Previous strategies aimed at preventing apoptotic cell death have involved either eliminating the apoptosis triggers from the culture environment or creating more robust cell lines through the over-expression of antiapoptosis genes. The results from this research suggest an additional strategy. Selecting for subpopulations present within the wild-type subpopulation that are resistant to apoptosis could provide an additional means of reducing apoptosis in culture. As demonstrated in the research presented in this thesis, this selection process could be based on mitochondrial properties. The link between mitochondria and apoptosis has been established in the past several years by a number of researchers (Green and Reed, 1998; Susin et al., 1998). The release of numerous mitochondrial factors, such as cytochrome *c*, procaspases, and AIF, upon stimulation of the apoptosis pathway in addition to the presence of Bcl-2 family members residing in mitochondrial membranes all support the hypothesis that mitochondria play a key role in orchestrating apoptotic death.

The results from this research support the hypothesis concerning the importance of mitochondria in apoptotic death. Cell populations sorted based on mitochondrial membrane potential result in subpopulations that vary in their resistance to apoptosis as determined using both morphological and biochemical measures of apoptosis. The molecular biology behind the differences between these subpopulations was investigated in an effort to determine the exact molecular differences between these subpopulations through cytochrome *c* induction of caspase-

3 activity. The results showed that caspase-3 activity differed even in the uninduced control cells, suggesting an endogenous heterogeneity with respect to base cytosolic levels of procaspase-3 . Mitochondria have been shown to contain a number of procaspases, including procaspase-3, and one hypothesis could be that the increased level of inducible caspase-3 activity in the control extracts was caused by mitochondria with lower membrane potential resulting in the release of procaspase-3. Since the subpopulations originated from a single wild-type culture and were sorted based only on their mitochondrial membrane potential, these variances are likely related to some basic mitochondrial properties. The collapse of the mitochondrial membrane potential and the opening of the mitochondrial permeability transition pore may play a role in the observed differences between these sorted subpopulations (Green and Reed, 1998). Research has shown that the voltage-dependant anion channel (VDAC) switches between an open and closed state when subjected to a 30 mV potential difference (Martinou, 1999). Using equation 2.1, one can approximate the potential differences measured between the mitochondrial membrane potential sorted subpopulations by assuming that the concentration difference is the same as the Rh123 fluorescence signal to noise ratio. For these subpopulations, these values differ by approximately 20 mV, and this suggests that mitochondrial channels could be operating differently for these two subpopulations.

Virtually all cell culture researchers have observed cell death heterogeneity in which certain subpopulations of cells assume the morphological and biochemical features associated with either necrotic or apoptotic death sooner than other subpopulations. Why do these cell subpopulations die faster than others? This question concerning population heterogeneity is not trivial and unimportant. Physiological heterogeneity can result from asymmetric cell division in which membrane proteins and RNA associate with specific cellular regions before cellular

division (Horvitz and Herskowitz, 1992; Jan and Jan, 1998). Furthermore, cells characterized by specific morphological features can vary significantly in their functionality as demonstrated in β-cell responsiveness to glucose levels *in-vitro* (Pipeleers, 1992). Additionally, organisms can create physiological heterogeneous populations even when they are genetically identical and grown in identical environments (Spudich and Koshland, 1976). Theoretical deterministic models have been successfully utilized to explain population heterogeneity in a number of biological systems (Chung and Stephanopoulos, 1996).

Heterogeneity also occurs intracellularly with respect to organelle function. For example, within the same mitochondrial population, various subpopulations with different membrane potentials exist. Under membrane depolarizing conditions, subpopulations of mitochondria have been observed to maintain a high membrane potential despite the appearance of a significant number of depolarized mitochondria. Furthermore, the physiological environment contributes to the appearance of various classes of mitochondria that differ in mitochondrial membrane potential even when size and density changes are considered (Cossarizza et al., 1996; Diaz et al., 1999; Petit et al., 1990).

As was previously shown, the appearance of steady state multiplicity in continuous culture in which drastically different cell concentrations were observed to occur at virtually identical growth rates was attributed to physiological multiplicity as measured through the determination of the metabolic flux distribution occurring around the pyruvate branchpoint. In this section, sorting based on mitochondrial membrane potential led to correlations between physiological heterogeneity, measured using Rh123, and differences in both morphological and biochemical features associated with apoptosis. Heterogeneity clearly plays a significant role in mammalian cell culture and could be utilized in the formulation of novel culture strategies.

8. APPLICATIONS TO FED-BATCH CULTURE

8.1 Introduction

Industrial mammalian cell culture has typically been conducted in batch mode. However, fed-batch cultivation has proven to be a more effective method for increasing the culture cell and product concentrations. This bioreactor operational mode prevents nutrient depletion that oftentimes occurs late in a batch culture. The maintenance of proper nutrient levels allows cells to continue to grow which could result in a higher product concentration. High product titers are desirable not just because of the obvious increase in the amount of product that can be sold but also due to the fact that high product concentrations improve downstream separation process efficiency. This contrasts with other operational modes, such as continuous or perfusion mode, which produce large amounts of product but typically at low concentrations (Hu and Peshwa, 1991; Xie and Wang, 1994c).

Novel strategies have been developed as modifications of the basic fed-batch cultivation mode. Feeding medium concentrates, utilizing stoichiometric feeding protocols, and designing feeding strategies based on cell culture models have all been applied to fed-batch culture processes (Glacken et al., 1989b; Hu and Peshwa, 1991; Pörtner and Schäfer, 1996; Xie and Wang, 1994c). The results from the previous chapters suggest two additional novel strategies for fed-batch culture operation. The multiple steady state continuous culture results dramatically illustrate the potential for mammalian cells to operate at a high growth rate with an increase in efficiency in their utilization of nutrients as demonstrated by the lower lactate production and higher respiration. Therefore, one hypothesis would be that fed-batches that are initially put through an adaptation phase of low nutrient feeding would increase the cellular metabolic efficiency. Then the culture could be switched to a higher feeding rate to increase the growth

rate while maintaining the higher metabolic efficiency. This strategy was tested using a modification of the stoichiometric feeding strategy developed by Xie and Wang (Xie, 1997; Xie and Wang, 1994c). The results clearly show that this new strategy resulted in a higher viable cell concentration, culture viability, specific productivity, and culture product concentration when compared to the conventional stoichiometric feeding method.

The second new fed-batch operational strategy involved using the mitochondrial membrane potential sorted subpopulations in order to increase the culture viable cell concentration. The previous results concerning the Rh123 sorted subpopulations indicate that higher mitochondrial membrane potential subpopulations are able to resist apoptosis when induced by specific factors under short-term conditions. Therefore, these sorted subpopulations were hypothesized to be able to resist the other various apoptosis inducing influences present in a typical cell culture. This strategy was implemented, and the results demonstrated that the cell populations with a higher mitochondrial membrane potential were able to resist the general apoptosis inducing conditions encountered during fed-batch culture. Consequently, these more resistant cell populations reached higher viable cell concentrations and maintained culture viabilities for an extended period of time. These results could provide for a new approach toward culture operation in which inoculums and cultures are analyzed using FACS techniques to determine cellular physiological states that would in-turn dictate the feeding strategy. In addition, this method may also result in culture processes becoming more predictable in terms of knowing relations between cellular death kinetics and cellular physiology.

8.2 Feeding Strategy and Design of Fed-batch Cultures

The first variation of fed-batch operation involved adjusting the feeding during a culture in order to account for altered metabolic behavior with the goal of increasing the culture viable

cell concentration and viability. The fed-batches were labeled 1X, 1X-2X, and 2X in reference to the feeding protocol used for each culture. The 1X fed-batch refers to the control culture that was fed the regular stoichiometric amount as prescribed by Xie (Xie and Wang, 1994c) and Möllborn (Möllborn, 1996). The 2X fed-batch refers to the second control culture that was fed twice the stoichiometric amount. The 1X-2X fed batch refers to the experimental culture that was initially fed the low stoichiometric amount and then later on overfed with twice the stoichiometric amount after the mitochondrial activity was determined to be different for the two 1X and 2X control cultures. The fed batches were all inoculated with cells taken from a common stock and suspended in IMDM medium containing low concentrations of glucose and glutamine: glucose (1X: 1 g/L; 1X-2X: 1 g/L; 2X: 2 g/L) and glutamine (1X: 0.5 mM; 1X-2X: 0.5 mM; 2X: 1.0 mM). In addition to the stoichiometric feeding of nutrients, growth factors were also fed everyday (10 mg/L insulin and 5 mg/L transferrin) in order to prevent the possible degradation of these medium proteins, particularly insulin, as demonstrated by Goswami (Goswami, 1998).

The viable cell concentrations and percent viabilities for these three cultures are shown in Figures 8-1 and 8-2. In addition, the lactate/glucose ratio is shown for time points up to the point at which the feeding rate was switched for the experimental 1X-2X fed-batch. The vertical lines on these two figures refer to the time at which the mitochondrial membrane potential was determined (dashed line) along with the time at which the feeding rate was switched for the 1X-2X fed-batch (solid line). The 2X culture reached the highest viable cell concentration, but this concentration dropped rapidly after reaching this peak. The culture viability was maintained the longest in the 1X-2X fed-batch with a higher viability ranging from 10 to over 40 percent over the 2X culture. The 2X culture also had a higher lactate/glucose ratio as compared to the 1X fed cultures which indicates that these cells growing under low nutrient levels had a more efficient

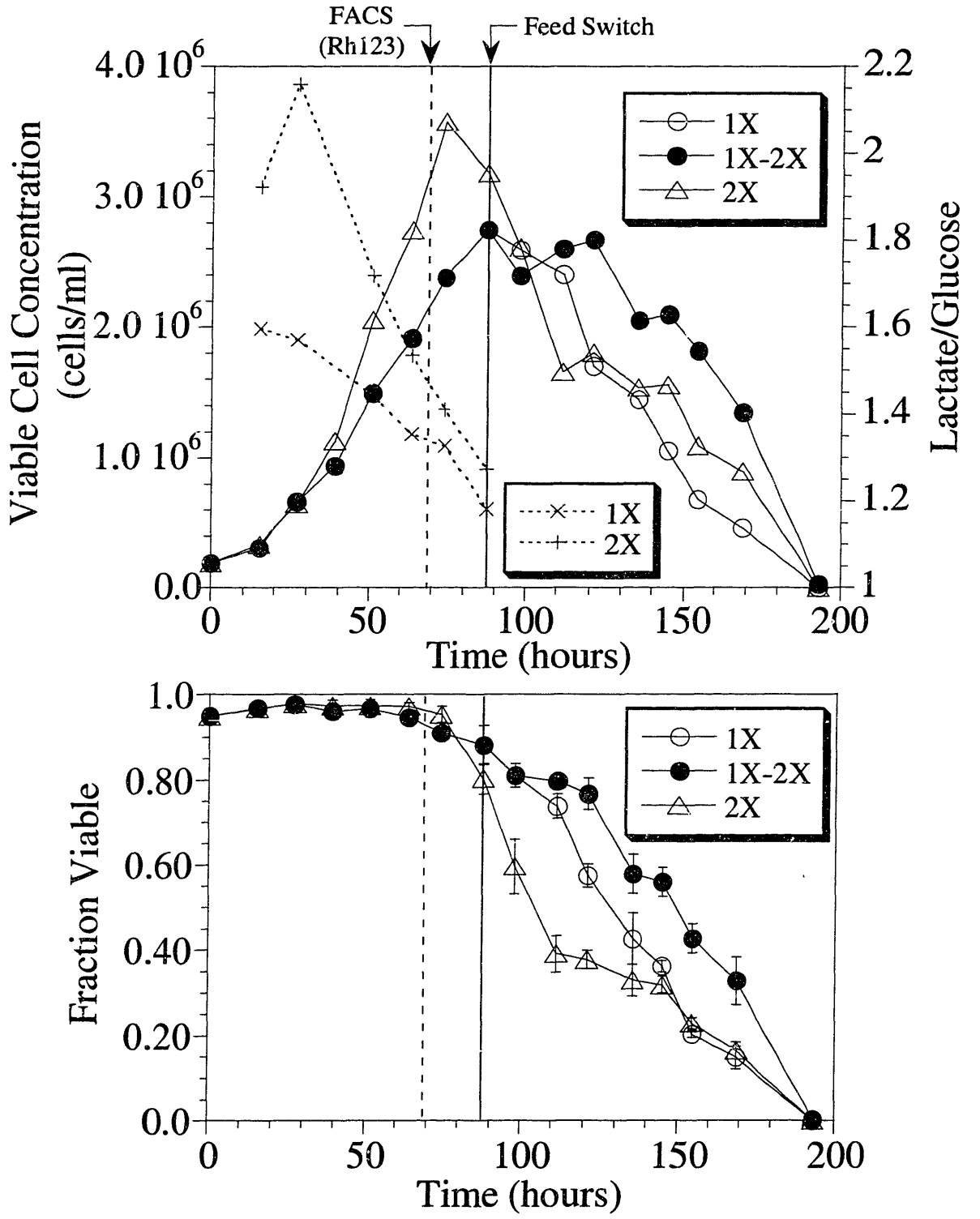

Figures 8-1 and 8-2. Viable cell concentration and percent viability versus time for the feeding strategy test fed-batch. The fed-batch experiment involved two control cultures (1X and 2X) and one experimental (1X-2X) culture. The term "1X" refers to the fed-batch feeding amount prescribed in the stoichiometric feeding protocol (Xie, 1997). The dashed and solid lines refer to the times at which the MMP was measured and the time at which the feeding was switched respectively.

utilization of glucose as compared to the 2X culture. The 1X cultures also had a 20% higher mean Rh123 fluorescent value for the mitochondrial membrane potential as compared to the 2X culture. The Rh123 fluorescence values along with the lactate/glucose ratios suggest that the 2X fed-batch culture had a lower level of mitochondrial activity. The medium used in these fed-batches was relatively rich as compared to other fed-batches, and these differences would most likely increase under leaner medium conditions in the 1X fed-batch culture.

The glucose consumption and lactate production profiles are shown in Figure 8-3. In this figure, the integrated viable cell density is used in order to enable one to visualize the specific consumption and production rates (slopes in the plot). The specific lactate production rate is the highest in the 2X fed-batch at the initial stages of the culture. As the culture progresses, the lactate production profiles all level off, indicating that the cells have all shifted their metabolism. The 1X-2X fed-batch, however, did continue to produce some additional lactate when the feeding rate was switched to the 2X feeding schedule. This indicates that the metabolism of the pre-adapted cells could still switch to a somewhat more inefficient metabolic state for a short period of time. The lactate concentrations for the 1X and 2X all appear to drop indicating lactate consumption. However, the 1X-2X fed-batch does not show a noticeable amount of lactate consumption. The 2X and 1X-2X cultures appear to end with a similar overall yield (lactate/glucose). However, this is misleading due to the fact that lactate was consumed in the 2X culture. The glucose consumption profiles show that the 2X fed-batch consumed the most lactate, but the specific glucose consumption rates all appeared to be similar. The main observation for Figure 8-3 is that the initial behavior of the metabolism for 1X fed-batches differs from the behavior for the 2X fed-batches

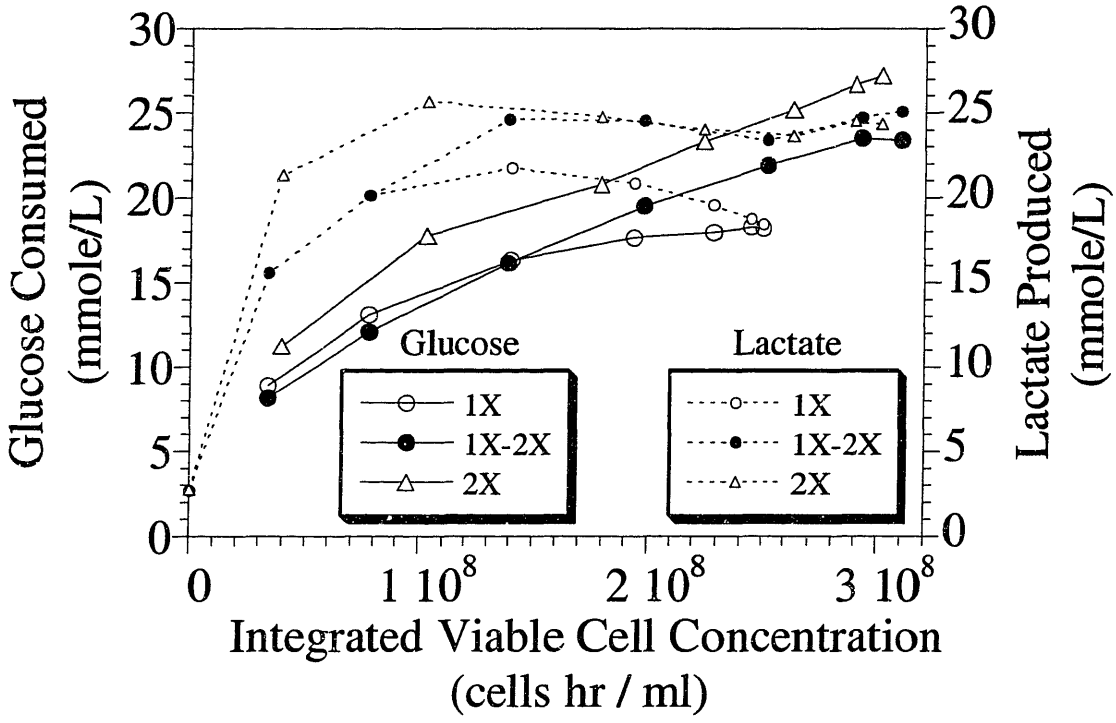

Figure 8-3. Glucose consumption and lactate production versus the integrated viable cell concentration. The fed-batch experiment involved two control cultures (1X and 2X) and one experimental (1X-2X) culture. The term "1X" refers to the fed-batch feeding amount prescribed in the stoichiometric feeding protocol (Xie, 1997).

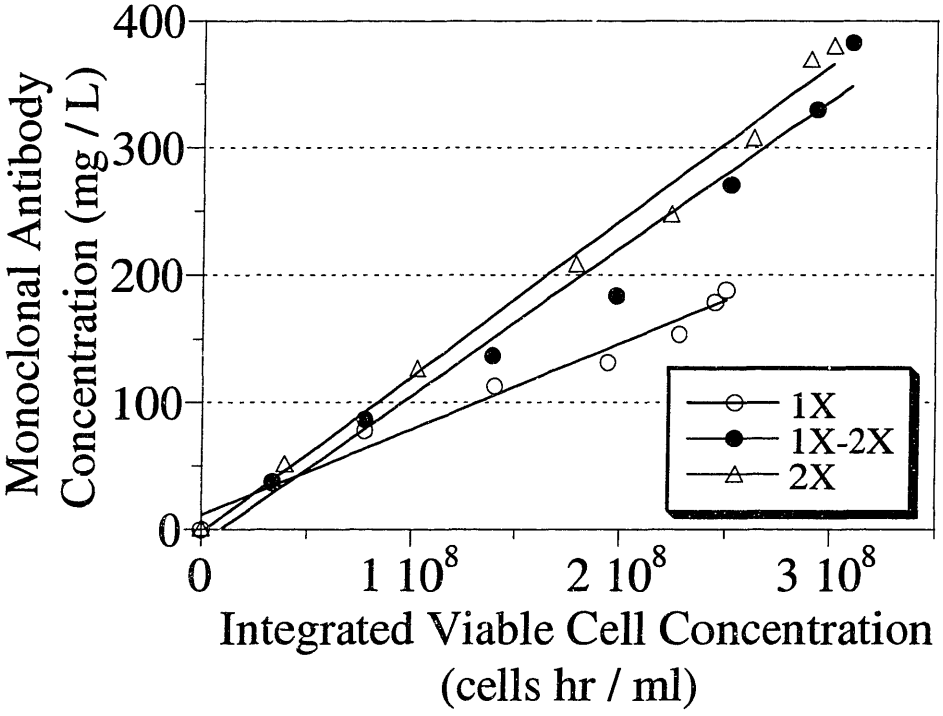

Figure 8-4. Monoclonal antibody concentration versus the integrated viable cell density for the feeding strategy test fed-batch. The fed-batch experiment involved two control cultures (1X and 2X) and one experimental (1X-2X) culture. The term "1X" refers to the fed-batch feeding amount prescribed in the stoichiometric feeding protocol (Xie, 1997).

The monoclonal antibody concentrations versus the integrated viable cell concentrations for the three cultures are shown in Figure 8-4. The antibody concentration reached the highest value of approximately 350 mg/L for both the 2X and 1X-2X cultures as compared to less than 200 mg/L for the 1X culture. In addition, the highest specific antibody productivity occurred in the 2X and 1X-2X fed-batches. The plots are more linear for the 1X and 2X fed-batches when compared to the 1X-2X fed-batch, and this suggests that the switch in feeding rate had a direst influence on the cellular specific productivity.

8.3 Rhodamine 123 Sorted Subpopulations in Fed-batch Culture

In chapter 7, subpopulations with a higher mitochondrial membrane potential, as measured using Rh123, were demonstrated to have a higher resistance to apoptosis induced with various compounds. This enhanced apoptosis resistance was hypothesized to be applicable in fed-batch cell cultivation. The fed-batches were inoculated with cells that had been previously sorted according to their Rh123 fluorescence as described in chapter 7 and Materials and Methods. The initial and supplemental medium for these fed-batches was identical. The initial medium was IMDM with low glucose (2mM) and glutamine (0.5mM) with 8.36 g/L of MOPS to increase the medium buffer capacity (osmolarity adjusted accordingly). The conditioned medium was also identical because it was prepared by mixing the conditioned medium obtained from each of the two Rh123 sorted subpopulation inoculums. The fed-batches were fed according to the stoichiometric feeding protocol. The 1X, 2X, and 1X-2X feeding strategies described previously were all used to determine differences between the behavior for the Rh123 sorted subpopulations.

8.3.1 1X-2X Fed-batches With Rh123 Sorted Subpopulations

The results for the viable cell concentrations and culture viabilities for the 1X-2X fed-batch are shown in Figures 8-5 and 8-6. The cultures labeled L and H refer to the cell populations that have either a low or high mean Rh123 fluorescence value respectively. The fed-batch culture with the higher mitochondrial membrane potential maintained a higher percent viability and reached a higher viable cell concentration as compared to the low membrane potential culture. This viability difference ranged from 10 to 20% and was maintained for a period of almost 70 hours. The error bars on the plots refer not to the measurement error but to the error between duplicate fed-batch cultures containing each subpopulation.

Figure 8-7 shows the mean Rh123 fluorescence values for the fed-batch cultures. The mitochondrial membrane potential difference was maintained between the two cultures for the entire length of the experiment. Also, the membrane potential increased at 90 hours in both sets of cultures. This increase could potentially be attributed to a number of phenomena. However, since this increase occurred after the onset of cell death in the culture, it could be due to the higher death rate of subpopulations that have a lower mitochondrial membrane potential as shown previously in the apoptosis induced death experiments. In other words, over the course of the culture, the cell population was enriched with the higher membrane potential cells that had the lower death rate.

The glucose consumption and lactate production profiles are shown in Figure 8-8. The metabolic behavior for these different fed-batches does not differ significantly from one another. This suggests that the differences in Rh123 staining indicate the ability for a cell population to survive when apoptosis begins. In the fed-batches with different feeding strategies, differences in Rh123 staining were observed, but this data indicates that the reverse may not be true.

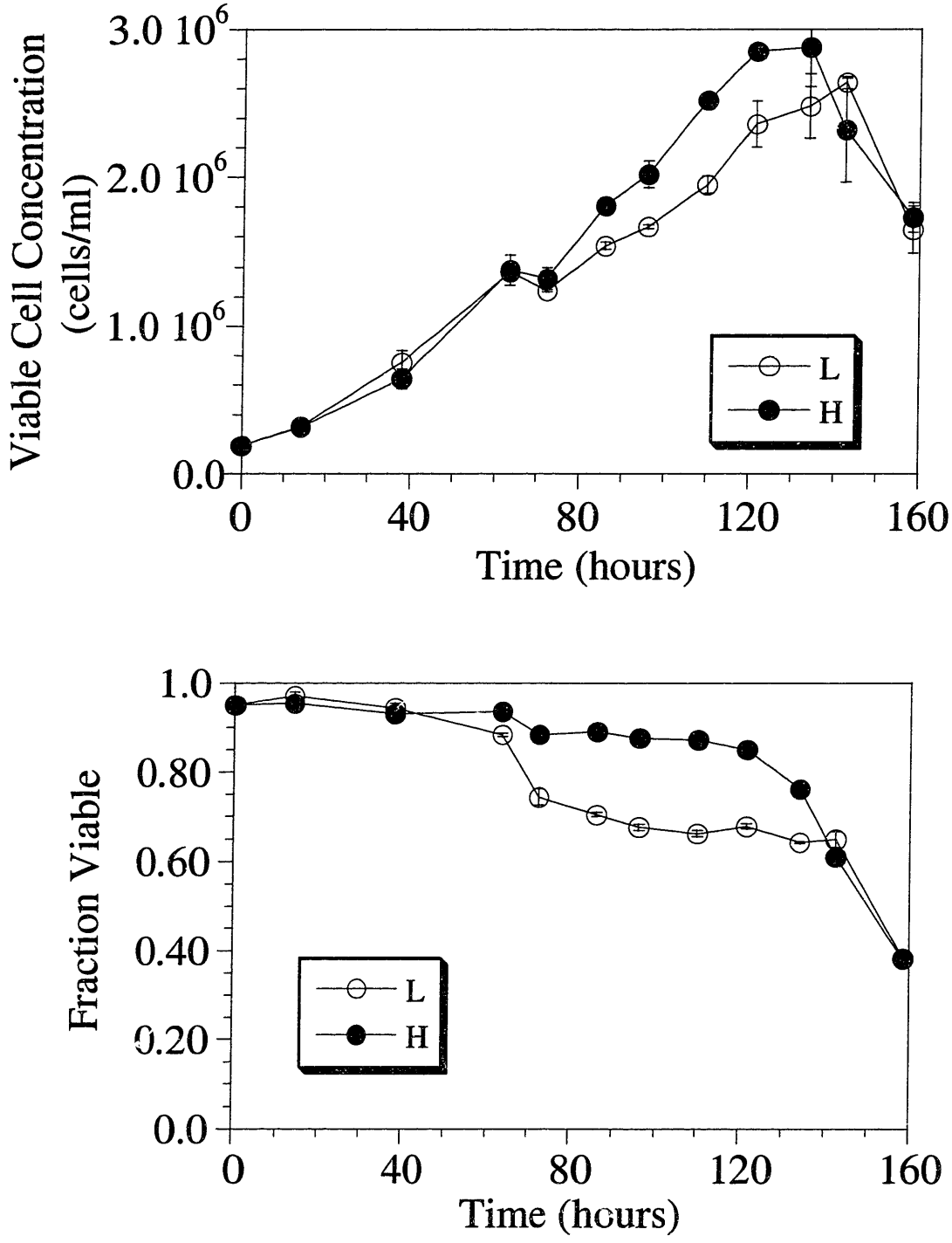

Figures 8-5 and 8-6. Viable cell concentration and percent viability versus time for Rhodamine 123 sorted subpopulations (high (H) and low (L) MMP). The fed-batches were fed according to the 1X-2X feeding protocol.

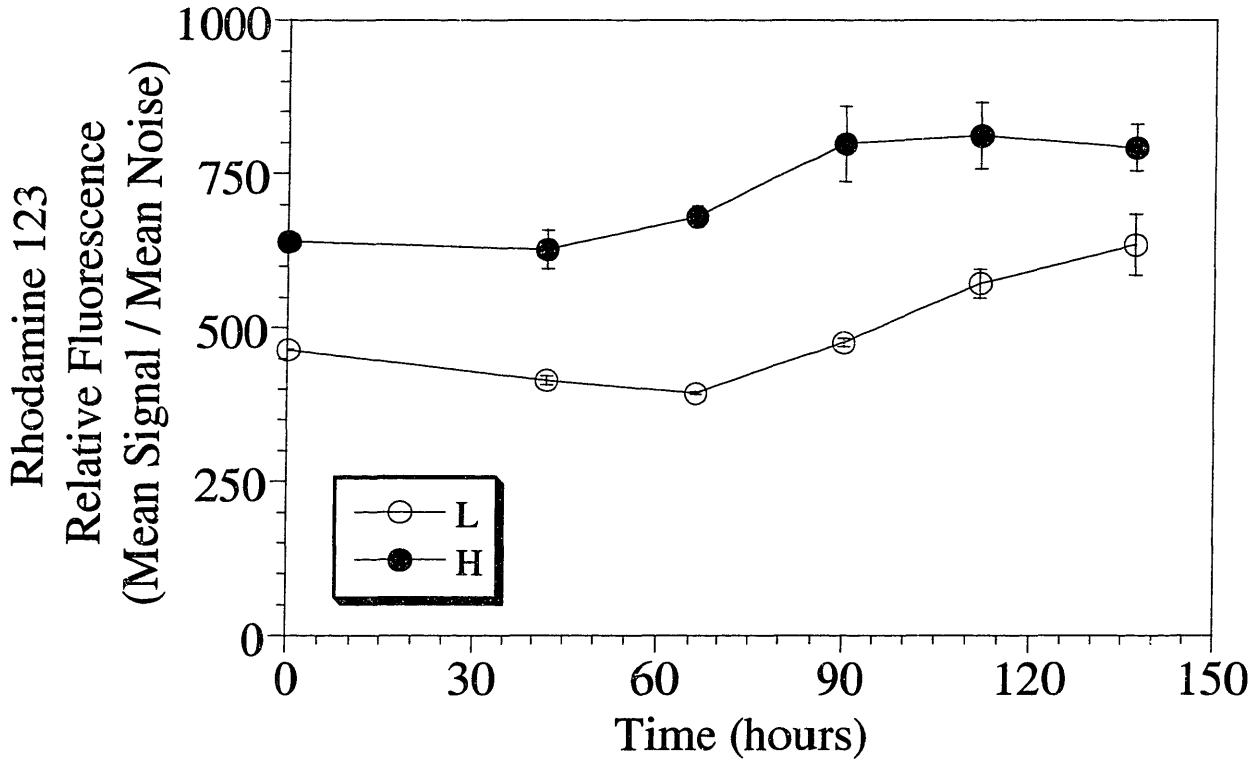

Figure 8-7. Rhodamine 123 relative fluorescence values versus time for Rhodamine 123 sorted subpopulations (high (H) and low (L) MMP). The subpopulation MMP values remained separate over the course of the experiment. In addition, the values increased when the cells began to die.

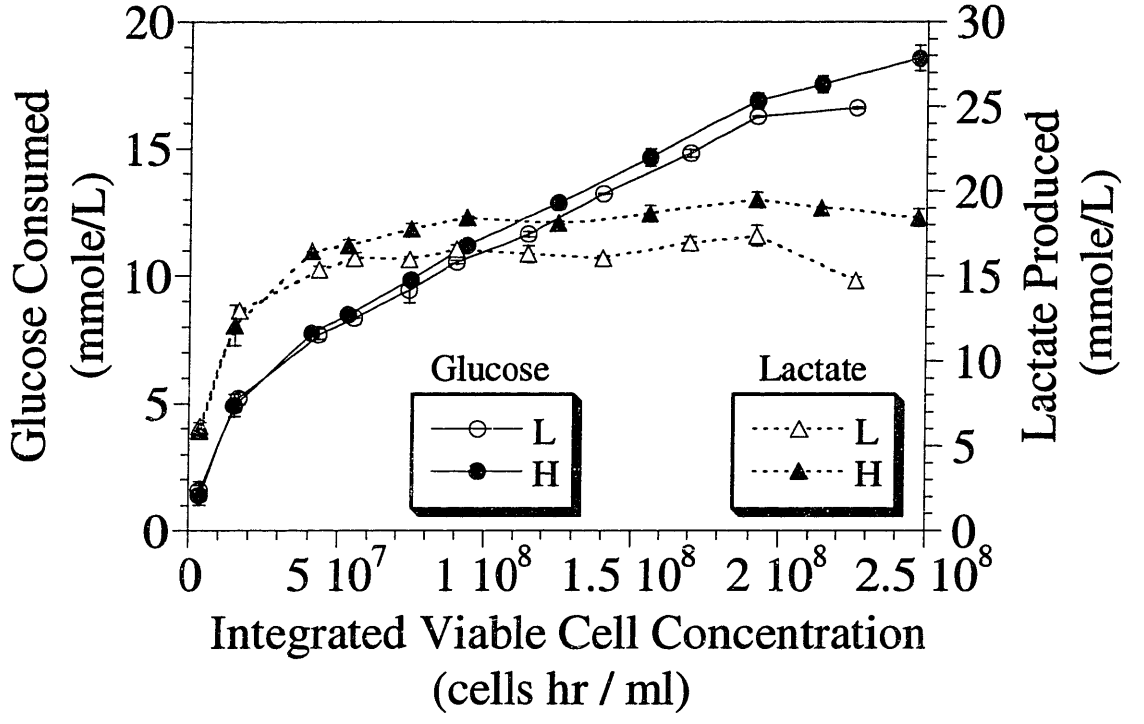

Figure 8-8. Glucose consumption and lactate production versus the integrated viable cell density for Rhodamine 123 sorted subpopulations (high (H) and low (L) MMP). The fed-batches were fed according to the 1X-2X feeding protocol.

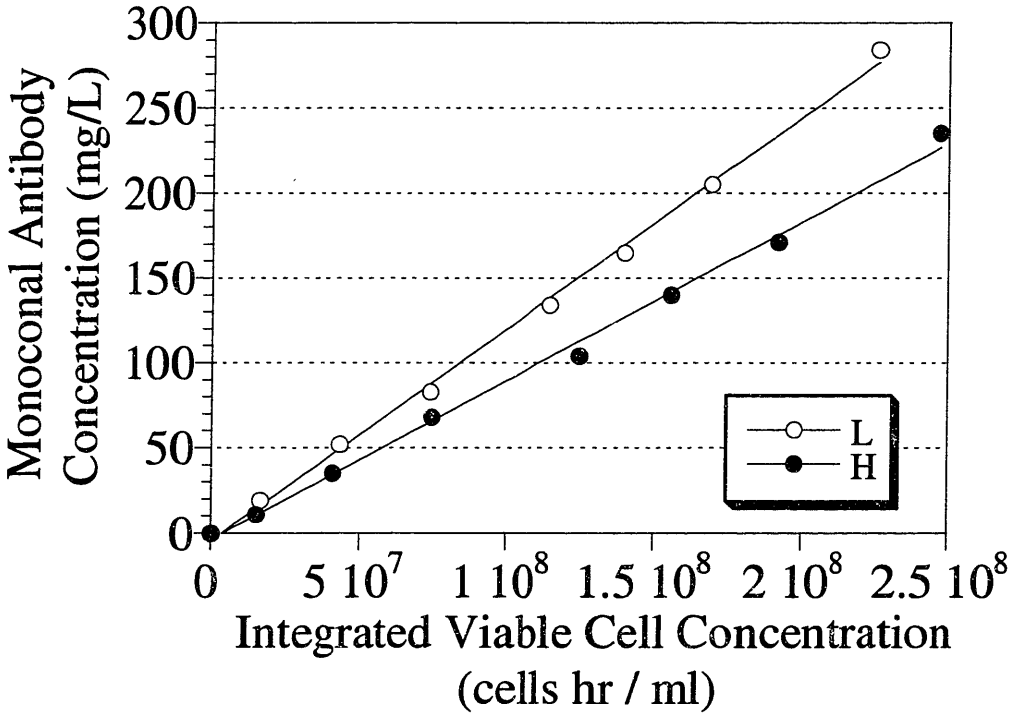

Figure 8-9. Monoclonal antibody concentration versus integrated viable cell density for Rhodamine 123 sorted subpopulations (high (H) and low (L) MMP). The fed-batches were fed according to the 1X-2X feeding protocol. The subpopulation with the higher MMP had a lower productivity.

Although metabolic changes involving mitochondria cause changes in Rh123 staining, these data suggest that even without metabolic changes, the mitochondrial membrane potential could indicate additional physiological properties of the mitochondria that are related to the cell population's response to apoptotic stimuli.

The monoclonal antibody concentrations versus the integrated viable cell concentrations for the 1X-2X fed-batches are shown in Figure 8-9. The specific productivity was higher for the culture containing the low mitochondrial membrane potential subpopulation. This phenomena has been observed previously for this same hybridoma cell line. Chang (Chang, 1994) demonstrated that cultures subjected to sodium butyrate, a known apoptosis inducer, increased their specific productivity despite causing lower viable cell concentrations. A lower growth rate sometimes correlates with an increase in specific productivity. The IgG product from this hybridoma cell is oftentimes approximately 15% of the total protein produced by the cell. One hypothesis could be that these cells shift their protein production away from product protein and into biomass protein in the higher Rh123 staining subpopulations.

8.3.2 1X and 2X Fed-batches With Rh123 Sorted Subpopulations

Additional data were collected for fed-batches conducted using the two control feeding strategies that were described previously in the Feeding Strategy section (8.2). The results for the 1X and 2X fed-batch culture viable cell concentrations and viabilities are shown in Figures 8-10 and 8-12 respectfully. These figures all demonstrate the fact that the culture inoculums with the higher mitochondrial membrane potential subpopulations result in higher culture viable cell concentrations and viabilities as was the case in the 1X-2X fed-batch cultures. Furthermore, the drop in specific monoclonal antibody production was also observed for each fed-batch culture as shown in Figures 8-11 and 8-13.

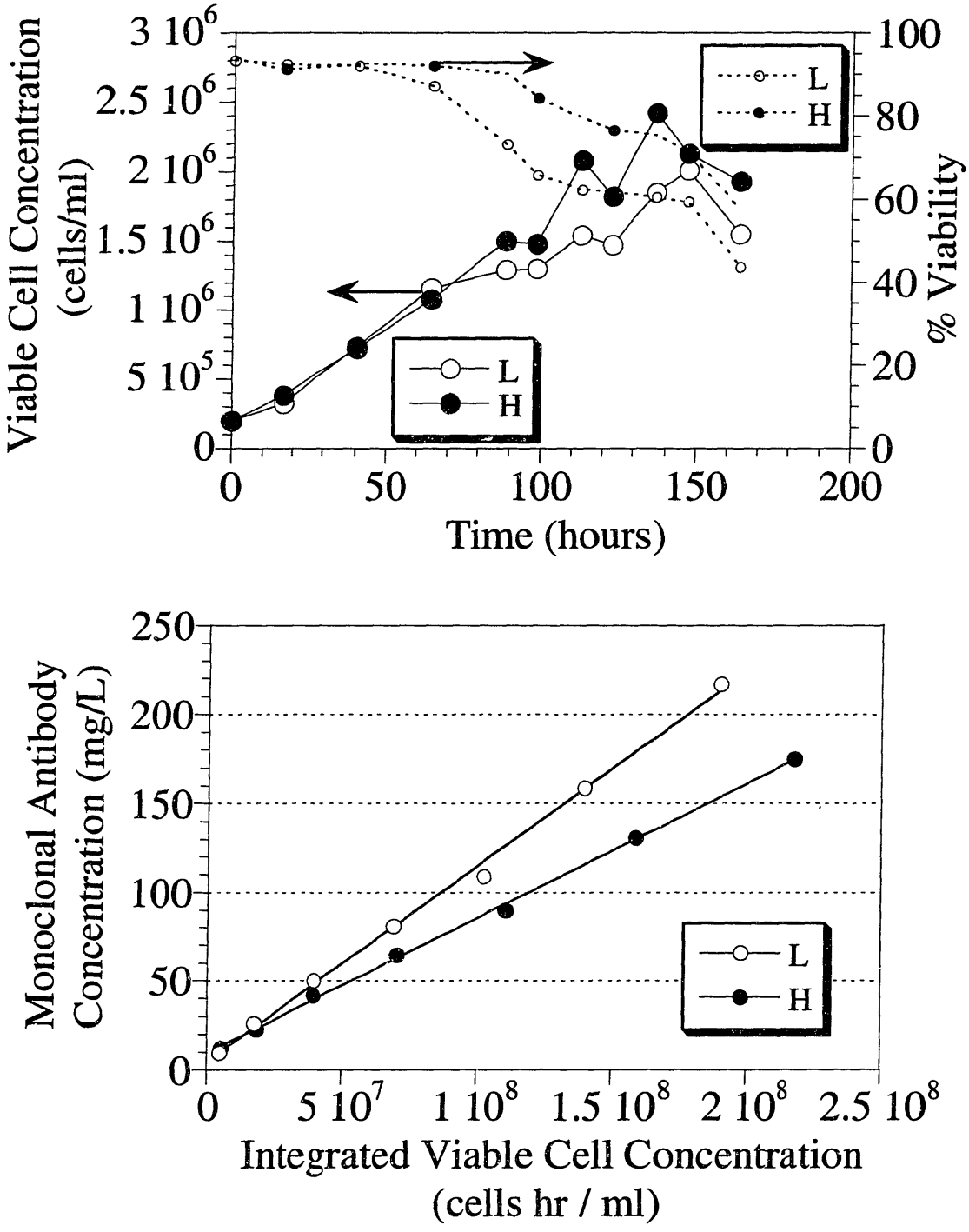

Figures 8-10 and 8-11. Viable cell concentration and percent viability versus time for Rhodamine 123 sorted subpopulations (high (H) and low (L) MMP) along with the monoclonal antibody concentration versus the integrated viable cell density. The fed-batches were fed according to the 1X feeding protocol.

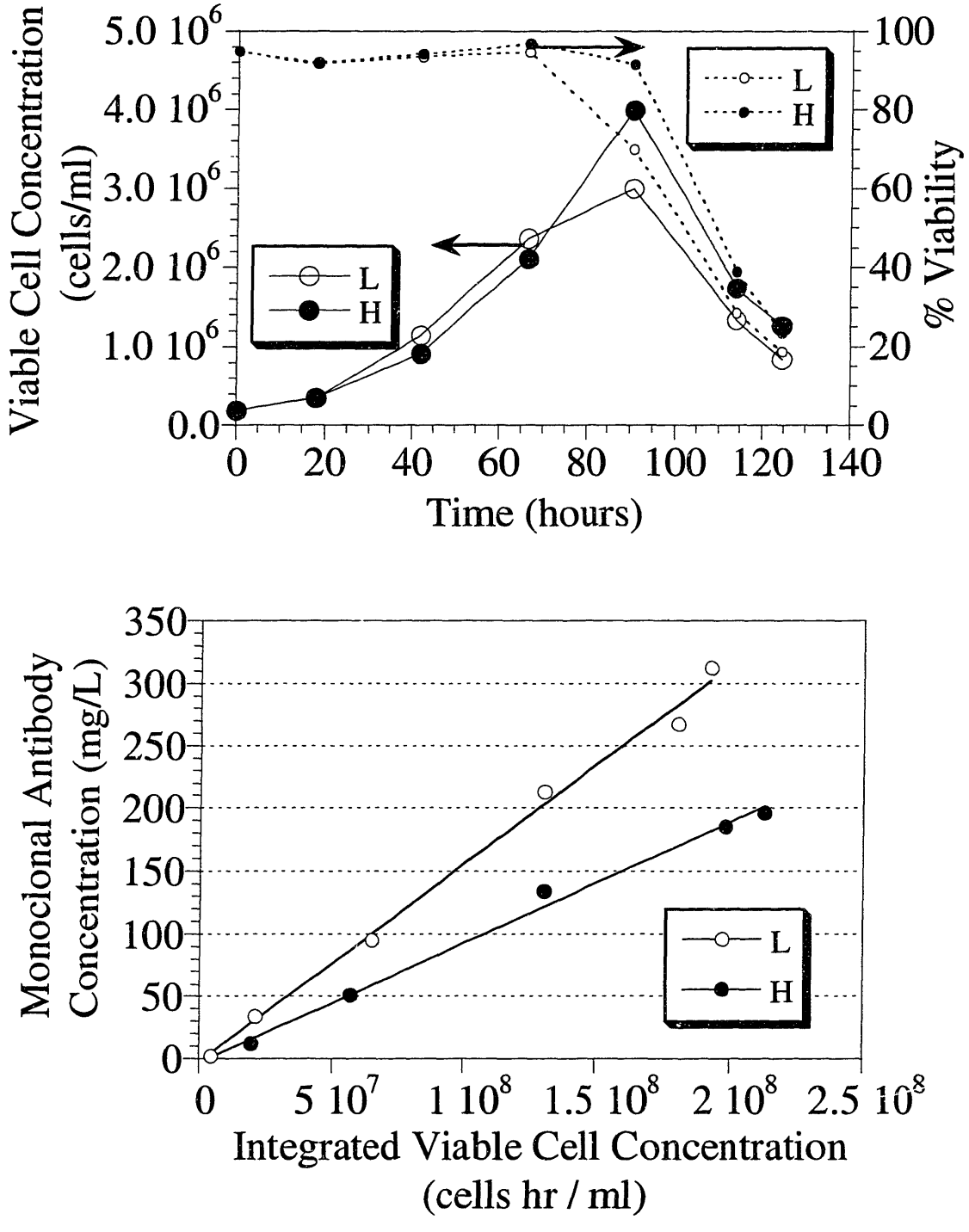

Figures 8-12 and 8-13. Viable cell concentration and percent viability versus time for Rhodamine 123 sorted subpopulations (high (H) and low (L) MMP) along with the monoclonal antibody concentration versus the integrated viable cell density. The fed-batches were fed according to the 2X feeding protocol.

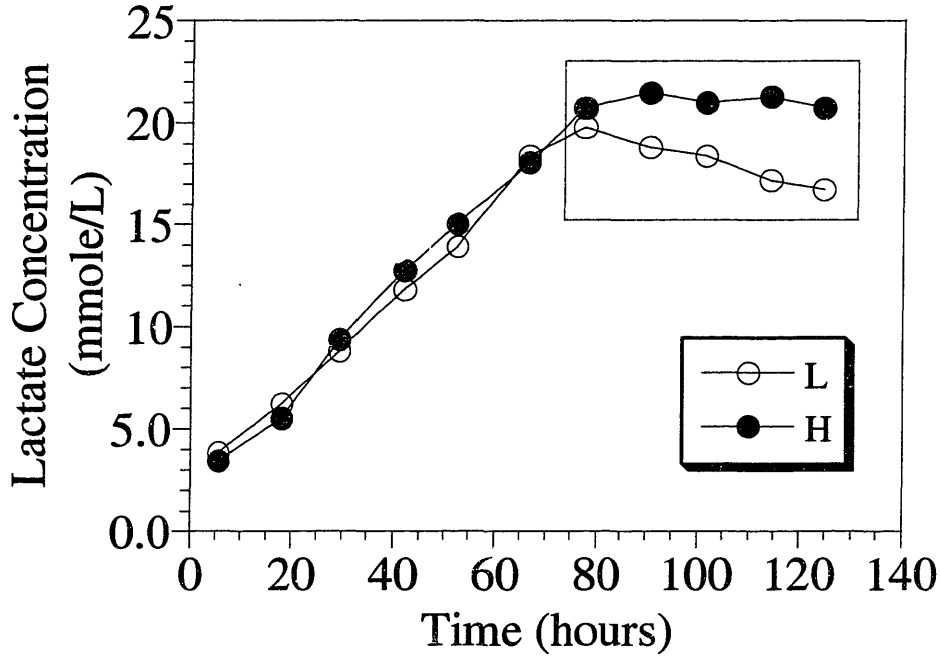

Figure 8-14. Lactate concentration versus time. The fed-batches were fed according to the 2X feeding protocol. The boxed area compares the rates of lactate consumption between the two subpopulations.

In addition, the low mitochondrial membrane potential subpopulations always consumed lactate at the end of cultures unlike the high mitochondrial membrane potential subpopulations. This occurred even when the viability for both subpopulations dropped to approximately the same value. This phenomena was most dramatic in the 2X fed-batch as shown in Figure 8-14. From 80 hours to the end of the culture, the lactate concentration dropped from 20 to 16 mM for the L subpopulation whereas the lactate levels for the H subpopulation remained relatively constant. Lactate consumption has been observed in a number of mammalian cell cultures, and is generally attributed to the onset of cell death in the culture (Bibila et al., 1994; Xie and Wang, 1994c). This observation combined with the observation that cells with a higher mitochondrial membrane potential can resist apoptosis suggest that the mitochondrial integrity changes that occur during apoptosis may be associated with lactate consumption.

8.4 Discussion

A vast number of fed-batch feeding strategies have been proposed for mammalian cell culture over the past twenty years. Controlling fed-batches at low glutamine and glucose levels in order to reduce the build up of lactate and toxic ammonium has been one of the most commons strategies proposed and applied in cell culture (Glacken et al., 1986; Ljunggren and Häggström, 1994). Medium concentrates have also been fed to cultures to improve culture performance (Bibila et al., 1994; Zhou et al., 1995). The stoichiometric feeding protocol developed by Xie and Wang (Xie and Wang, 1994c) and utilized in this work involved reducing the glucose and glutamine concentrations while feeding just the amount of supplemental nutrients required to produce biomass and protein product.

This work presents two new strategies for fed-batch operation. The first strategy involves the optimization of the stoichiometric feeding process by taking into account the changes in

metabolic behavior that occur over the course of a typical fed-batch. The increase in feeding rate resulted in higher viable cell concentrations, viabilities, and productivities, and this indicates that the stoichiometric feeding strategy may in fact lead to cell starvation and suboptimal culture performance. Later in the culture when the metabolic behavior of the cells changes to a more efficient utilization of glucose, cells respond positively to slight overfeeding. In addition, the maintenance of a healthy nutrient level to avoid starvation has a higher priority over the prevention of supposed toxic by-product build-up. Although ammonium is a definite threat to cell survival, researchers should focus on the cellular nutrient needs and not necessarily on lactate build-up.

The second strategy was an extension of the mitochondrial membrane potential sorted cell population results that demonstrated increased resistance to apoptosis. The high Rh123 sorted subpopulations were able to resist the various bioreactor stimuli that cause apoptosis. This adds yet another method one can use to prevent apoptosis in culture. The observations that a wild-type subpopulation contains cells that vary in their resistance to apoptosis may suggest a number of new novel views towards mammalian cell cultures. Heterogeneity will almost inevitably occur in a culture with respect to any number of cellular properties. Physiological heterogeneity could provide a basis for survival in which individual cell survival is not optimized but rather the survival of the cell population is key. A cell population that has a robust ability to survive would demonstrate heterogeneity toward a variety of death inducers with the surviving cells determining the new population's adaptation to new environments. Understanding these variances in responses to various bioreactor environments could be a dramatic step forward in understanding heterogeneity with respect to bioreactor performance. Furthermore, understanding the death kinetics for a given subpopulation may enable researchers to predict the

death rate for a mammalian cell culture. An inoculum with a high mitochondrial membrane potential would be preferred over one with a lower potential, and this physiological parameter could be used as a way to screen for optimal inoculum cultures.

9. CONCLUSIONS AND RECOMMENDATIONS

9.1 Conclusions

The goals outlined in the introduction of this thesis included the desire to contribute to the continual development of quantitative methodologies that analyze complex biological systems and illustrate relations between cellular physiology and behavior. Analyzing metabolic fluxes are not enough for metabolic engineering to become an effective tool for mammalian cell culture analysis, but rather, fluxes must be combined with observations of cellular physiology. Furthermore, all biological systems must be analyzed with the thought that heterogeneity almost undoubtedly exists within these systems. The analysis of multivariable and nonlinear dynamic biological systems must be done within a mathematical framework and not the "mental model" framework that currently dominates much of the biology literature (Bailey, 1999). This thesis employed mathematical techniques to analyze experimental data that was then, most importantly, used to formulate hypothesis concerning relations between mitochondria and cell death.

The findings from this research helped strengthen the field of metabolic flux analysis by showing how this analysis technique can be employed in the quantitation of cellular physiology. The analysis of metabolic pathways formed the basis for much of the work described in this thesis. The theoretical analysis of central carbon metabolism led to the confirmation that pyruvate is the most important flux distribution point within this biochemical reaction network, enabling one to focus efforts on this branchpoint and direct research efforts toward the analysis of factors that affect this branchpoint. Redundant data, collected in the continuous culture experiments from the gas exchange rate measurements, resulted in the ability to not only determine errors within data sets but also to generate confidence in the relevance of these calculated metabolic fluxes to the true physiological and metabolic state of cultured cells. The

mathematical analysis of the pentose phosphate pathway improved upon over forty years of research in which experimental data could be resolved through the recognition that the previous "mental models" and simplified mathematical models could not completely describe this small yet complex part of central carbon metabolism. Furthermore, it demonstrates how a seemingly complex reaction pathway could be simplified through the use of metabolic flux analysis techniques.

Metabolic flux analysis applied to continuous culture experiments using both Chinese hamster ovary and hybridoma cells resulted in numerous conclusions concerning the metabolic and physiological behavior of these cells lines. The ability to use flux analysis to determine the actual flux distribution around pyruvate resulted in the determination of the flux distribution as related to cellular physiology parameters such as the death rate and metabolite production or consumption rates. Factors related to respiration that appeared to correlate with physiology were the common thread throughout this flux analysis research, leading to the hypothesis that respiration, oxidative phosphorylation, and other factors related to mitochondria are critical parameters that contribute to mammalian cell culture physiology.

This conclusion was further supported by the result concerning steady state multiplicity in which cells that were pre-adapted to a high respiratory physiological state were able to maintain this high respiratory flux leading to a dramatic increase in cell density. Since most mammalian cultures are inefficient with respect to their ability to convert glucose into carbon dioxide through the respiratory chain, this finding that cells can become more efficient even when at high growth rates indicates the definite potential for cell cultures to reach more efficient physiological states. In other words, this result shows the potential for cell cultures to

dramatically increase their respiratory capacity. The question now is, how can one reach these efficient metabolic states consistently?

The hypothesis concerning the important role of mitochondria in mammalian cell culture was also supported through the research involving the cell populations sorted based on mitochondrial membrane potential. The fact that cell populations with a higher mean mitochondrial membrane potential resist apoptosis was demonstrated through measurements of both the morphological and biochemical characteristics associated with cells undergoing apoptosis. This result is reasonable since mitochondria have proven to be one of the key players involved in orchestrating the apoptosis mechanism.

Finally, these results were applied in the development of two new strategies for fed-batch operation and design. The first strategy showed that overfeeding cells later in a culture leads to an increase in culture viable cell concentration, viability, and productivity. The second strategy showed that cell populations with a higher mean mitochondrial membrane potential are able to resist apoptosis stimuli encountered in typical bioreactor fed-batch conditions. These results indicate that mitochondrial physiology plays a significant role in cell culture performance.

9.2 Recommendations

Mammalian cell culture modeling and flux analysis should continue to play a significant role not only in the development of bioreactor operations such as for feeding strategy formulation, but also as a means of obtaining a fundamental understanding of biological mechanisms related to cell death and productivity. Previous work using metabolic fluxes has resulted in several novel hypothesis concerning these biological mechanisms. Peptide hydrolysate metabolism and product glycosylation have been two areas of research covered in other work, and the role of mitochondria in mammalian cell culture was covered in this work.

Future work should continue to examine central carbon metabolism flux distribution when cells are subjected to changes in controlled environmental conditions. Typical biological research does not adequately provide an experimental framework through which one can examine the complex multivariate dynamical systems present in biological systems. For example, the effects of a growth factor are almost always conducted in experiments that measure only a few parameters such as gene expression or cell growth. This contrasts dramatically with a continuous culture experiment in which the withdrawal or supplementation of a key medium component provides information concerning the overall physiological effects of these compounds and their relations with central carbon metabolism and enzyme and gene regulatory networks.

Population heterogeneity is also another significant area of research in biochemical engineering that has not been adequately explored. Issues such as genetic instability and bioreactor performance heterogeneity are considered a significant problem in the field of biochemical engineering, and effort should be directed toward solving these issues. FACS is an excellent tool for population heterogeneity hypothesis testing, and it will most likely become a standard piece of equipment for all biotechnology labs. For example, a therapeutic drug undergoing testing may result in little overall stimulation of a target cell population. Through ordinary, whole-population analysis such as gel electrophoresis, true effects that influence a small subpopulation of cells would be masked. FACS could detect these subpopulations, allow one to isolate them, and then allow one to perform additional testing on this cell subpopulation which could lead to the development of a more potent therapeutic. The laser scanning cytometer, the gene chip, and other technologies would also play a major role in this analysis of population heterogeneity leading to more effective therapeutics aimed at a more select cell or

patient subpopulation. The downside to this research will be the now unavoidable truth that heterogeneity exists in places where it was previously either unknown or ignored. Commonly used cell lines will likely show considerable population heterogeneity and this will add another dimension to biological research by requiring not only the specification of the cell line being used but also the exact experimental background of that cell line.

Apoptosis research has made considerable progress in the last few years. The future work in this area, though, is still limitless due to the fact that research in this field is still in the basic discovery stage. The recent understanding that mitochondria play a fundamental role in the apoptotic mechanism still leaves scientists without a basic understanding of the translocation process of mitochondrial based apoptosis inducing factors to the cytosol for activation of the effector caspases.

Mitochondria research has not been given as much attention as it deserves during the last thirty years. In the past, the Mitchell hypothesis was the major driving force behind research on mitochondria. Only recently through apoptosis research has the behavior of these critical organelles been appreciated. Research demonstrating their ability the move, change shape, and respond to cellular physiological changes illustrate how these "organisms within an organism" operate. Inverse metabolic engineering strategies that focus on the development of cell lines with desirable mitochondrial physiology should play a definite role in future biochemical engineering research.

NOMENCLATURE

A	Matrix of biochemical reaction network stoichiometry
a_i	Extent of reaction reversibility
b_j	Fractional enrichment of labeled input substrate
C_i	Metabolite or nutrient concentration (mmole/L)
D	Dilution rate (hr^{-1})
E	Matrix of redundant equations
H_i	Henry's law coefficient for species i (Pa/mole L)
h	Consistency index
K	Kernal matrix for **N**
k_d	Death rate (hr^{-1})
k_La	Mass transfer coefficient
m	Number of metabolites in a reaction network
N	Steady state internal metabolite matrix
N_T, N_V	Total and viable cell density (cells/ml)
n	Number of reactions in a reaction network
P	Pentose phosphate pathway non-oxidative reaction flux
P_i	Partial pressure of species i
Δp	Proton motive force (mV)
q_c	Metabolite or nutrient uptake rate (mmole/cell/hr)
r	Vector of metabolite production and consumption rates
v_i	Reaction velocity or metabolic flux for reaction i (mmole/cell hr)
v	Vector of reaction fluxes
V_R	Reactor volume (L)
x_i	Concentration of metabolite i (mmole/cell)
y_i	Isotope fractional enrichment of metabolite i
z_i	Gas phase mole fraction of species i

Greek Letters

$\alpha_{i,j}$, $\beta_{i,j}$	Stoichiometric coefficient for metabolite j and reaction i
ε	Defined in equation 4.15
φ	Defined in equation 4.16
$\Delta\Psi_m$	Mitochondrial membrane potential (mV)
Ψ	Variance-covariance matrix for the measurement vector, **r**
μ	Growth rate (hr^{-1})

Abbreviations

CER	Carbon dioxide evolution rate
Ery4P	Erythrose 4-phosphate
Gra3P	Glyceraldehyde 3-phosphate
Hex6P	Hexose pool consisting of glucose 6-phosphate and fructose 6-phosphate
MMP	Mitochondrial membrane potential
MTT	3-(4,5-dimethylthiazol-2-yl)-2,5-diphenyl tetrazolium bromide
OUR	Oxygen uptake rate
Pen5P	Pentose pool consisting of ribulose 5-phosphate, ribose 5-phosphate, and xylulose 5-phosphate
Sed7P	Sedoheptulose 7-phosphate.
Rh123	Rhodamine 123
RQ	Respiratory quotient

REFERENCES

Adams, J. M., and Cory, S. (1998). The Bcl-2 protein family: arbiters of cell survival. Science *281*, 1322-1326.

Alnemri, E. S. (1999). Hidden powers of the mitochondria. Nature Cell Biology *1*, E40-E42.

Antonsson, B., Conti, F., Ciavatta, A. M., Montessuit, S., Lewis, S., Martinou, I., Bernasconi, L., Bernard, A., Mermod, J.-J., Mazzei, G., Maundrell, K., Gambale, F., Sadoul, R., and Martinou, J.-C. (1997). Inhibition of Bax channel-forming activity by Bcl-2. Science *277*, 370-372.

Appenzeller, T. (1999). Test tube evolution catches time in a bottle. Science *284*, 2108-2110.

Ashkenazi, A., and Dixit, V. M. (1998). Death receptors: signaling and modulation. Science *281*, 1305-1308.

Avgerinos, G. C., Drapeau, D., Socolow, J. S., Mao, J.-I., Hsiao, K., and Broeze, R. J. (1990). Spin filter perfusion system for high density cell culture: production of recombinant urinary type plasimogen activator in CHO cells. Bio/Technol. *8*, 54-58.

Bailey, J. E. (1999). Lessons from metabolic engineering for functional genomics and drug discovery. Nat. Biotechnol. *17*, 616-618.

Bailey, J. E., and Ollis, D. F. (1986). Biochemical Engineering Fundamentals, 2nd edition Edition (New York: McGraw-Hill, Inc.).

Bailey, J. E., Sburlati, A., Hatzimanikatis, V., Lee, K., Renner, W. A., and Tsai, P. S. (1996). Inverse metabolic engineering: A strategy for directed genetic engineering of useful phenotypes. Biotechnol. Bioeng. *52*, 109-121.

Balcarcel, R. R. (1999). Effects of rapamycin and insulin on the cell cycle and apoptosis of hybridoma cell cucltures. In Chemical Engineering (Cambridge, MA: Massachusetts Institute of Technology).

Barnes, D., and Sato, G. (1980). Methods for growth of cultured cells in serum-free medium. Anal. Biochem. *102*, 255-270.

Batt, B. C., Davis, R. H., and Kompala, D. S. (1990). Inclined sedimentation for selective retention of viable hybridomas in a continuous suspension bioreactor. Biotechnol. Prog. *6*, 458-464.

Batt, B. C., and Kompala, D. S. (1989). A structured kinetic modeling framework for the dynamics of hybridoma growth and monoclonal antibody production in continuous suspension cultures. Biotechnol. Bioeng. *34*, 515-531.

Bedner, E., Li, X., Gorczyca, W., Melamed, M., and Darzynkiewicz, Z. (1999). Analysis of apoptosis by laser scanning cytometry. Cytometry *35*, 181-195.

Behal, R. H., Buxton, D. B., Robertson, J. G., and Olson, M. S. (1993). Regulation of the pyruvate dehydrogenase multienzyme complex. Annu. Rev. Nutr. *13*, 497-520.

Benel, L., Ronot, X., Mounolou, J. C., Gaudemer, F., and Adolphe, M. (1989). Compared flow cytometric analysis of mitochondria using 10-n-nonyl acridine orange and rhodamine 123. Bas. Appl. Histochem. *33*, 71-80.

Bereiter-Hahn, J., and Vöth, M. (1994). Dynamics of mitochondria in living cells: shape changes, dislocations, fusion, and fission of mitochondria. Microsc. Res. Tech. *27*, 198-219.

Berthon, H. A., Bubb, W. A., and Kuchel, P. W. (1993). 13-C NMR isotopomer and computer-simulation studies of the non-oxidative pentose phosphate pathway of human erythrocytes. Biochem. J. *296*, 379-387.

Bibila, T. A., Ranucci, C. S., Glazomitsky, K., Buckland, B. C., and Aunins, J. G. (1994). Monoclonal antibody process development using medium concentrates. Biotechnol. Prog. *10*, 87-96.

Bonarius, H. P. J., de Gooijer, C. D., Tramper, J., and Schmid, G. (1995). Determination of the respiration quotient in mammalian cell culture in bicarbonate buffered media. Biotechnol. Bioeng. *45*, 524-535.

Bonarius, H. P. J., Hatzimanikatis, V., Meesters, K. P. H., de Gooijer, C. D., Schmid, G., and Tramper, J. (1996). Metabolic flux analysis of hybridoma cells in different culture media using mass balances. Biotechnol. Bioeng. *50*, 299-318.

Bonarius, H. P. J., Houtman, J. H. M., de Gooijer, C. D., Tramper, J., and Schmid, G. (1998a). Activity of glutamate dehydrogenase is increased in ammonia-stressed hybridoma cells. Biotechnol. Bioeng. *57*, 447-453.

Bonarius, H. P. J., Timmerarends, B., de Gooijer, C. D., and Tramper, J. (1998b). Metabolite-balancing techniques vs. ^{13}C tracer experiments to determine metabolic fluxes in hybridoma cells. Biotechnol. Bioeng. *58*, 258-262.

Borys, M. C., Linzer, D. I. H., and Papoutsakis, E. T. (1993). Culture pH affects expression rates and glycosylation of recombinant mouse placental lactogen proteins by Chinese hamster ovary (CHO) cells. Bio/Technology *11*, 720-724.

Bossy-Wetzel, E., and Green, D. R. (1999). Caspases induce cytochrome *c* release from mitochondria by activating cytosolic factors. J. Biol. Chem. *274*, 17484-17490.

Bossy-Wetzel, E., Newmeyer, D. D., and Green, D. R. (1998). Mitochondrial cytochrome *c* release in apoptosis occurs upstream of DEVD-specific caspase activation and independently of mitochondrial transmembrane depolarization. EMBO. J. *17*, 37-49.

Brand, M. D., Chien, L. F., Ainscow, E. K., Rolfe, D. F., and Porter, R. K. (1994). The causes and functions of mitochondrial proton leak. Biochim. Biophys. Acta *1187*, 132-139.

Bronowski, J. (1976). The ascent of man (New York: Little Brown & Co.).

Buja, L. M., Eigenbrodt, M. L., and Eigenbrodt, E. H. (1993). Apoptosis and necrosis. Basic types and mechanisms of cell death. Arch. Pathol. Lab. Med. *117*, 1208-1214.

Butler, M., and Jenkins, H. (1989). Nutritional aspects of the growth of animal cells in culture. J. Biotechnol. *12*, 97-110.

Chang, Y.-H. D. (1994). Augmentation of mass transfer through electrical means and nutrient enrichment for suspension and entrapment cell cultures. In Chemical Engineering (Cambridge, MA: Massachusetts Institute of Technology).

Chen, L. B. (1988). Mitochondrial membrane potential in living cells. Ann. Rev. Cell Biol. *4*, 155-181.

Cheng, E. H.-Y., Kirsch, D. G., Clem, R. J., Ravi, R., Kastan, M. B., Bedi, A., Ueno, K., and Hardwick, J. M. (1997). Conversion of Bcl-2 to a Bax-like death effector by caspases. Science *278*, 1966-1968.

Christensen, B., and Nielsen, J. (1999). Isotopomer analysis using GC-MS. Metab. Eng. *1*, E8-E16.

Chung, J. D., Sinskey, A. J., and Stephanopoulos, G. (1998). Growth factor and bcl-2 mediated survival during abortive proliferation of hybridoma cell line. Biotechnol. Bioeng. *57*, 164-171.

Chung, J. D., and Stephanopoulos, G. (1996). On physiological multiplicity and population heterogeneity of biological systems. Chem. Eng. Sci. *51*, 1509-1521.

Chung, J. D., Zabel, C., Sinskey, A. J., and Stephanopoulos, G. (1997). Extension of Sp2/0 hybridoma cell viability through interleukin-6 supplementation. Biotechnol. Bioeng. *55*, 439-446.

Cohen, G. M. (1997). Caspases: the executioners of apoptosis. Biochem. J. *326*, 1-16.

Cossarizza, A., Ceccarelli, D., and Masini, A. (1996). Functional heterogeneity of an isolated mitochondrial population revealed by cytofluorometric analysis at the single organelle level. Exp. Cell Res. *222*, 84-94.

Crow, J. F. (1983). Genetic notes. An introduction to genetics (New York, NY: Macmillan Publishing Co.).

Delgado, J., and Liao, J. C. (1992b). Determination of flux control coefficients from transient metabolite concentrations. Biochem. J. *282*, 919-927.

Delgado, J., and Liao, J. C. (1992a). Metabolic control analysis using transient metabolite concentrations. Biochem. J. *285*, 965-972.

Deveraux, Q. L., Roy, N., Stennicke, H. R., Arsdale, T. V., Zhou, Q., Srinivasula, S. M., Alnemri, E. S., Salvesen, G. S., and Reed, J. C. (1998). IAPs block apoptotic events induced by caspase-8 and cytochrome *c* by direct inhibition of distinct caspases. EMBO J. *17*, 2215-2223.

Devos, R., Cheroutre, H., Taya, Y., Degrave, W., Van Heuverswyn, H., and Fiers, W. (1982). Molecular cloning of human immune interferon cDNA and its expression in eukaryotic cells. Nucleic Acids Res. *10*, 2487-2501.

Diaz, G., Setzu, M. D., Zucca, A., Isola, R., Diana, A., Murru, R., Sogos, V., and Gremo, F. (1999). Subcellular heterogeneity of mitochondrial membrane potential: relationship with organelle distribution and intercellular contacts in normal, hypoxic and apoptotic cells. J. Cell Sci. *112*, 1077-1084.

Dykhuizen, D. E., and Hartl, D. L. (1983). Selection in chemostats. Microbiol. Rev. *47*, 150-168.

Earnshaw, W. C. (1999). A cellular poison cupboard. Nature *397*, 387-389.

Eigenbrodt, E., Fister, P., and Reinacher, M. (1985). New perspectives on carbohydrate metabolism in tumor cells. In Regulation of carbohydrate metabolism, R. Beitner, ed. (Boca Raton, FL: CRC Press, Inc.), pp. 141-179.

Emaus, R. K., Grunwald, R., and Lemasters, J. J. (1986). Rhodamine 123 as a probe of transmembrane potential in isolated rat-liver mitochondria: spectral and metabolic properties. Biochim. Biophys. Acta *850*, 436-448.

Enari, M., Sakahira, H., Yokoyama, H., Okawa, K., Iwamatsu, A., and Nagata, S. (1998). A caspase-activated DNase that degrades DNA during apoptosis, and its inhibitor ICAD. Nature *391*, 43-50.

Evan, G., and Littlewood, T. (1998). A matter of life and cell death. Science *281*, 1317-1322.

Ferlini, C., Biselli, R., Nisini, R., and Fattorossi, A. (1995). Rhodamine 123: a useful probe for monitoring T cell activation. Cytometry *21*, 284-293.

Finucane, D. M., Bossy-Wetzel, E., Waterhouse, N. J., Cotter, T. G., and Green, D. R. (1999). Bax-induced caspase activation and apoptosis via cytochrome *c* release from mitochondria is inhibitable by Bcl-xL. J. Biol. Chem. *274*, 2225-2233.

Flanigan, I., Collins, J. G., Arora, K. K., Macleod, J. K., and Williams, J. F. (1993). Exchange reactions catalyzed by group-transferring enzymes oppose the quantitation and the unravelling of the identity of the pentose pathway. Eur. J. Biochem. *213*, 477-485.

Follstad, B. D., and Stephanopoulos, G. (1998). Effect of reversible reactions on isotope label redistribution. Analysis of the pentose phosphate pathway. Eur. J. Biochem. *252*, 360-371.

Frame, K. K., and Hu, W.-S. (1991a). Kinetic study of hybridoma cell growth in continuous culture. I. A model for non-producing cells. Biotechnol. Bioeng. *37*, 55-64.

Frame, K. K., and Hu, W.-S. (1991b). Kinetic study of hybridoma cell growth in continuous culture: II. Behavior of producers and comparison to nonproducers. Biotechnol. Bioeng. *38*, 1020-1028.

Frame, K. K., and Hu, W.-S. (1990). The loss of antibody productivity in continuous culture of hybridoma cells. Biotechnol. Bioeng. *35*, 469-476.

Fraser, A., and Evan, G. (1996). A license to kill. Cell *85*, 781-784.

Fulda, S., Scaffidi, C., Susin, S. A., Krammer, P. H., Kroemer, G., Peter, M. E., and Debatin, K.-M. (1998). Activation of mitochondria and release of mitochondrial apoptogenic factors by betulinic acid. J. Biol. Chem. *273*, 33942-33948.

Garland, J. M., and Halestrap, A. (1997). Energy metabolism during apoptosis. J. Biol. Chem. *272*, 4680-4688.

Glacken, M. W., Adema, E., and Sinskey, A. J. (1988). Mathematical descriptions of hybridoma culture kinetics: I. Initial metabolic rates. Biotechnol. Bioeng. *32*, 491-506.

Glacken, M. W., Adema, E., and Sinskey, A. J. (1989a). Mathematical descriptions of hybridoma culture kinetics: II. The relationship between thiol chemistry and the degradation of serum activity. Biotechnol. Bioeng. *33*, 440-450.

Glacken, M. W., Adema, E., and Sinskey, A. J. (1989b). Mathematical descriptions of hybridoma culture kinetics: III. Simulation of fed-batch reactors. J. Biotechnol. *10*, 39-66.

Glacken, M. W., Fleischaker, R. J., and Sinskey, A. J. (1986). Reduction of waste product excretion via nutrient control: Possible strategies for maximizing product and cell yields on serum in cultures of mammalian cells. Biotechnol. Bioeng. *28*, 1376-1389.

Glassy, M. C., Tharakan, J. P., and Chau, P. C. (1988). Serum-free media in hybridoma culture and monoclonal antibody production. Biotechnol. Bioeng. *32*, 1015-1028.

Goochee, C. F., Gramer, M. J., Anderson, D. C., Bahr, J. B., and Rasmussen, J. R. (1991). The oligosaccharides of glycoproteins: bioprocess factors affecting oligosaccharide structure and their effect on glycoprotein properties. Bio/technology *9*, 1347-1355.

Goossens, V., Grooten, J., and Fiers, W. (1996). The oxidative metabolism of glutamine. A modulator of reactive oxygen intermediate-mediated cytotoxicity of tumor necrosis factor in L929 fibrosarcoma cells. J. Biol. Chem. *271*, 192-196.

Goswami, J., Sinskey, A. J., Steller, H., Stephanopoulos, G. N., and Wang, D. I. C. (1999). Apoptosis in batch cultures of Chinese hamster ovary cells. Biotechnol. Bioeng. *62*, 632-640.

Green, D. R., and Reed, J. C. (1998). Mitochondria and apoptosis. Science *281*, 1309-1312.

Hale, A. J., Smith, C. A., Sutherland, L. C., Stoneman, V. E. A., Longthorne, V. L., Culhane, A. C., and Williams, G. T. (1996). Apoptosis: molecular regulation of cell death. Eur. J. Biochem. *236*, 1-26.

Hansen, H. A., and Emborg, C. (1994). Influence of ammonium on growth, metabolism, and productivity of a continuous suspension chinese hamster ovary culture. Biotechnol. Prog. *10*, 121-124.

Hassell, T., Gleave, S., and Butler, M. (1991). Growth inhibition in animal cell culture. Appl. Biochem. Biotechnol. *30*, 29-41.

Hayter, P. M., Curling, E. M. A., Baines, A. J., Jenkins, N., Salmon, I., Strange, P. G., Tong, J. M., and Bull, A. T. (1992a). Glucose-limited chemostat culture of Chinese hamster ovary cells producing recombinant human interferon-γ. Biotechnol. Bioeng. *39*, 327-335.

Hayter, P. M., Curling, E. M. A., Gould, M. L., Baines, A. J., Jenkins, N., Salmon, I., Strange, P. G., and Bull, A. T. (1993). The effect of the dilution rate on CHO cell physiology and recombinant interferon-γ production in glucose-limited chemostat culture. Biotechnol. Bioeng. *42*, 1077-1085.

Hayter, P. M., Kirkby, N. F., and Spier, R. E. (1992b). Relationship between hybridoma growth and monoclonal antibody production. Enzyme Micro. Technol. *14*, 454-461.

Heinrich, R., and Rapoport, T. A. (1974). A linear steady-state treatment of enzymatic chains. General properties, control, and effector strength. Eur. J. Biochem. *42*, 89-95.

Heiskanen, K. M., Bhat, M. B., Wang, H.-W., Ma, J., and Nieminen, A.-L. (1999). Mitochondrial depolarization accompanies cytochrome *c* release during apoptosis in PC6 cells. J. Biol. Chem. *274*, 5654-5658.

Hiller, G. W., Clark, D. S., and Blanch, H. W. (1994). Transient responses of hybridoma cells in continuous culture to step changes in amino acid and vitamin concentrations. Biotechnol. Bioeng. *44*, 303-321.

Hockenbery, D. M. (1995). *bcl-2*, a novel regulator of cell death. BioEssays *17*, 631-638.

Horvitz, H. R., and Herskowitz, I. (1992). Mechanisms of asymmetric cell division: two Bs or not two Bs, that is the question. Cell *68*, 237-255.

Hostetler, K., Cooperstein, S. J., Landau, B. R., and Lazarow, A. (1966). Pathways of glucose metabolism in the isolated islet of the goosefish in vitro. Am. J. Physiol. *211*, 1057-1062.

Hu, W.-S., and Peshwa, M. V. (1991). Animal cell bioreactors - recent advances and challenges to scale-up. Can. J. Chem. Eng. *69*, 409-420.

James, T. W., and Bohman, R. (1981). Proliferation of mitochondria during the cell cycle of the human cell line (HL-60). J. Cell Biol. *89*, 256-260.

Jan, D. C. H., Petch, D. A., Huzel, N., and Butler, M. (1997). The effect of dissolved oxygen on the metabolic profile of a murine hybridoma grown in serum-free medium in continuous culture. Biotechnol. Bioeng. *54*, 153-164.

Jan, Y. N., and Jan, L. Y. (1998). Asymmetric cell division. Nature *392*, 775-778.

Jo, E., Park, H., Park, J., and Kim, K. (1990). Balanced nutrient fortification enables high-density hybridoma cell culture in batch culture. Biotechnol. Bioeng. *36*, 717-722.

Jöbses, I., Martens, D., and Tramper, J. (1991). Lethal events during gas sparging in animal cell culture. Biotechnol. Bioeng. *37*, 484-490.

Joshi, A., and Palsson, B. O. (1989a). Metabolic dynamics in the human red cell. Part I - a comprehensive kinetic model. J. Theor. Biol. *141*, 515-528.

Joshi, A., and Palsson, B. O. (1989b). Metabolic dynamics in the human red cell. Part II - interactions with the environment. J. Theor. Biol. *141*, 529-545.

Joshi, A., and Palsson, B. O. (1990a). Metabolic dynamics in the human red cell. Part III - metabolic reaction rates. J. Theor. Biol. *142*, 41-68.

Joshi, A., and Palsson, B. O. (1990b). Metabolic dynamics in the human red cell. Part IV - data prediction and some model computations. J. Theor. Biol. *142*, 69-85.

Juan, G., Cavazzoni, M., Sáez, G. T., and O'Connor, J.-E. (1994). A fast kinetic method for assessing mitochondrial membrane potential in isolated hepatocytes with rhodamine 123 and flow cytometry. Cytometry *15*, 335-342.

Juin, P., Tremblais, K., LeCabellec, M. T., Grégoire, M., Meflah, K., and Vallette, F. M. (1998). Potentiation of apoptosis by mitochondria in a cell-free system. Biochem. Biophys. Res. Comm. *253*, 185-191.

Kacser, H., and Burns, J. A. (1973). The control of flux, D. D. Davies, ed. (Cambridge: Cambridge University Press).

Kamo, N., Muratsugu, M., Hongoh, R., and Kobatake, Y. (1979). Membrane potential of mitochondria measured with an electrode sensitive to tetraphenyl phosphonium and relationship between proton electrochemical potential and phosphorylation potential in steady state. J. Membrane Biol. *49*, 105-121.

Katz, J., and Rognstad, R. (1967). The labeling of pentose phosphate from glucose-14C and estimation of the rates of transaldolase, transketolase, and the contribution of the pentose cycle, and ribose phosphate synthesis. Biochemistry *6*, 2227-2247.

Katz, J., and Wood, H. G. (1963). The use of $C^{14}O_2$ yields from glucose-1- and -6-C^{14} for the evaluation of the pathways of glucose metabolism. J. Biol. Chem. *238*, 517-523.

Katz, J., and Wood, H. G. (1960). The use of glucose-C-14 for the evolution of the pathways of glucose metabolism. J. Biol. Chem. *235*, 2165-2177.

Kaufman, R. J. (1989). Genetic engineering of factor VIII. Nature *342*, 207-208.

Kaufman, R. J., Wasley, L. C., and Dorner, A. J. (1988). Synthesis, processing, and secretion of recombinant human factor VIII expressed in mammalian cells. J. Biol. Chem. *263*, 6352-6362.

Kim, C. N., Wang, X., Huang, Y., Ibrado, A. M., Liu, L., Fang, G., and Bhalla, K. (1997). Overexpression of Bcl-x_L inhibits Ara-C-induced mitochondrial loss of cytochrome *c* and other perturbations that activate the molecular cascade of apoptosis. Cancer Res. *57*, 3115-3120.

Kingsley-Hickman, P. B., Ross, B. D., and Krick, T. (1990). Hexose monophosphate shunt measurement in cultured cells with [1- 13C]glucose: correction for endogenous carbon sources using [6-13C] glucose. Anal. Biochem. *185*, 235-237.

Kirsch, D. G., Doseff, A., Chau, B. N., Lim, D. S., de Souza-Pinto, N. C., Hansford, R., Kastan, M. B., Lazebnik, Y. A., and Hardwick, J. M. (1999). Caspase-3-dependent cleavage of Bcl-2 promotes release of cytochrome *c*. J. Biol. Chem. *274*, 21155-21161.

Klapa, M. I., Park, S. M., Sinskey, A. J., and Stephanopoulos, G. (1999). Metabolite and isotopomer balancing in the analysis of metabolic cycles: I. Theory. Biotechnol. Bioeng. *62*, 375-391.

Kluck, R. M., Bossy-Wetzel, E., Green, D. R., and Newmeyer, D. D. (1997). The release of cytochrome *c* from mitochondria: a primary site for Bcl-2 regulation of apoptosis. Science *275*, 1132-1136.

Knorr, B. (1999). Growth and apoptosis of serum-free CRL-1606 hybridoma cells immobilized in cellulose-sulfate/polyDADMAC hollow spheres. In Fachbereich Biotechnologie (Berlin: Technische Universität Berlin).

Köhler, G., Howe, S. C., and Milstein, C. (1976). Fusion between immunoglobulin-secreting and nonsecreting myeloma cell lines. Eur. J. Immunol. *6*, 292-5.

Kompala, D. S., Ramkrishna, D., Jansen, N. B., and Tsao, G. T. (1986). Investigation of bacterial growth on mixed substrates: experimental evaluation of cybernetic models. Biotechnol. Bioeng. *28*, 1044-1055.

Kothakota, S., Azuma, T., Reinhard, C., Klippel, A., Tang, J., Chu, K., McGarry, T. J., Kirschner, M. W., Koths, K., Kwiatkowski, D. J., and Williams, L. T. (1997). Caspase-3-generated fragment of gelsolin: effector of morphological change in apoptosis. Science *278*, 294-298.

Kowaltowski, A. J., Netto, L. E. S., and Vercesi, A. E. (1998). The thiol-specific antioxidant enzyme prevents mitochondrial permeability transition. J. Biol. Chem. *273*, 12766-12769.

Krippner, A., Matsuno-Yagi, A., Gottlieb, R. A., and Babior, B. M. (1996). Loss of function of cytochrome *c* in Jurkat cells undergoing fas- mediated apoptosis. J. Biol. Chem. *271*, 21629-21636.

Kroemer, G., Petit, P., Zamzami, N., Vayssière, J.-L., and Mignotte, B. (1995). The biochemistry of programmed cell death. FASEB J. *9*, 1277-1287.

Landau, B. R., and Katz, J. (1964). A quantitative estimation of the pathways of glucose metabolism in rat adipose tissue *in vitro*. J. Biol. Chem. *239*, 697-704.

Landau, B. R., and Wood, H. G. (1983). The pentose cycle in animal tissues: evidence for the classical and against the 'L-type' pathway. Trends Biol. Sci. *8*, 292-296.

Lanks, K. W., and Li, P.-W. (1988). End products of glucose and glutamine metabolism by cultured cell lines. J. Cell. Physiol. *135*, 151-155.

Larrabee, M. G. (1989). The pentose cycle (hexose monophosphate shunt). Rigorous evaluation of limits to the flux from glucose using $^{14}CO_2$ data, with applications to peripheral ganglia of chicken embryos. J. Biol. Chem. *264*, 15875-15879.

Lauffenburger, D. A., and Linderman, J. J. (1993). Receptors. Models for binding, trafficking, and signaling (New York, NY: Oxford University Press).

Lee, Y.-K., Yap, P.-K., and Teoh, A.-P. (1995). Correlation between steady-state cell concentration and cell death of hybridoma cultures in chemostat. Biotechnol. Bioeng. *45*, 18-26.

Li, P., Nijhawan, D., Budihardjo, I., Srinivasula, S. M., Ahmad, M., Alnemri, E. S., and Wang, X. (1997). Cytochrome c and dATP-dependent formation of Apaf-1/caspase-9 complex initiates an apoptotic protease cascade. Cell *91*, 479-489.

Liao, J. C., and Delgado, J. (1993). Advances in metabolic control analysis. Biotechnol. Prog. *9*, 221-233.

Linardos, T. I., Kalogerakis, N., Behie, L. A., and Lamontagne, L. R. (1991). The effect of specific growth rate and death rate on monoclonal antibody production in hybridoma chemostat cultures. Can. J. Chem. Eng. *69*, 429-438.

Linsinger, G., Wilhelm, S., Wagner, H., and Häcker, G. (1999). Uncouplers of oxidative phosphorylation can enhance a Fas death signal. Mol. Cell. Biol. *19*, 3299-3311.

Liu, X., Zou, H., Slaughter, C., and Wang, X. (1997). DFF, a heterodimeric protein that functions downstream of caspase-3 to trigger DNA fragmentation during apoptosis. Cell *89*, 175-184.

Ljunggren, J., and Häggström, L. (1994). Catabolic control of hybridoma cells by glucose and glutamine limited fed-batch cultures. Biotechnol. Bioeng. *44*, 808-818.

Lodish, H., Baltimore, D., Berk, A., Zipursky, S. L., Matsudaira, P., and Darnell, J. (1995). Molecular cell biology, 3rd Edition (New York, NY: W. H. Freeman and Company).

Maddox, J. (1992). Is molecular biology yet a science. Nature *355*, 201.

Mancini, M., Nicholson, D. W., Roy, S., Thornberry, N. A., Peterson, E. P., Casciola-Rosen, L. A., and Rosen, A. (1998). The caspase-3 precursor has a cytosolic and mitochondrial distribution: implications for apoptotic signaling. J. Cell Biol. *140*, 1485-1495.

Mancuso, A., Sharfstein, S. T., Fernandez, E. J., Clark, D. S., and Blanch, H. W. (1998). Effect of extracellular glutamine concentration on primary and secondary metabolism of a murine hybridoma: An in vivo ^{13}C nuclear magnetic resonance study. Biotechnol. Bioeng. *57*, 172-186.

Mancuso, A., Sharfstein, S. T., Tucker, S. N., Clark, D. S., and Blanch, H. W. (1994). Pathways in a murine hybridoma with carbon-13 nuclear magnetic resonance spectroscopy. Biotechnol. Bioeng. *44*, 563-585.

Margulis, L. (1996). Archaeal-eubacterial mergers in the origin of Eukarya: phylogenetic classification of life. Proc. Natl. Acad. Sci. U S A *93*, 1071-1076.

Margulis, L. (1998). Symbiotic planet. A new look at evolution (New York, NY: Basic Books).

Martens, D. E., de Gooijer, C. D., van der Velden-de Groot, C. A. M., Beuvery, E. C., and Tramper, J. (1993). Effect of dilution rate on growth, productivity, cell cycle and size, and shear sensitivity of a hybridoma cell in a continuous culture. Biotechnol. Bioeng. *41*, 429-439.

Martinou, J. C. (1999). Apoptosis. Key to the mitochondrial gate. Nature *399*, 411-412.

Marx, A., deGraaf, A. A., Weichert, W., Eggeling, L., and Sahm, H. (1996). Determination of the fluxes in the central carbon metabolism of *Corynebacterium glutamicum* by nuclear magnetic resonance spectroscopy combined with metabolite balancing. Biotechnol. Bioeng. *49*, 111-129.

McAdams, H. H., and Arkin, A. (1999). It's a noisy business! Genetic regulation at the nanomolar scale. Trends Genet. *15*, 65-69.

McAdams, H. H., and Arkin, A. (1998). Simulation of prokaryotic genetic circuits. Annu. Rev. Biophys. Biomol. Struct. *27*, 199-224.

McConnell, S. J., Stewart, L. C., Talin, A., and Yaffe, M. P. (1990). Temperature-sensitive yeast mutants defective in mitochondrial inheritance. J. Cell Biol. *111*, 967-976.

Meier, S. J., Hatton, T. A., and Wang, D. I. C. (1999). Cell death from bursting bubbles: role of cell attachment to rising bubbles in sparged reactors. Biotechnol. Bioeng. *62*, 468-478.

Meijer, J. J., and van Dijken, J. P. (1995). Effects of glucose supply on myeloma growth and metabolism in chemostat culture. J. Cell. Physiol. *162*, 191-198.

Mercille, S., and Massie, B. (1994). Induction of apoptosis in nutrient-deprived cultures of hybridoma and myeloma cells. Biotechnol. Bioeng. *44*, 1140-1154.

Mignotte, B., and Vayssière, J.-L. (1998). Mitochondria and apoptosis. Eur. J. Biochem. *252*, 1-15.

Miller, W. M., Blanch, H. W., and Wilke, C. R. (1988). A kinetic analysis of hybridoma growth and metabolism in batch and continuous suspension culture: Effect of nutrient concentration, dilution rate, and pH. Biotechnol. Bioeng. *32*, 947-965.

Miller, W. M., Wilke, C. R., and Blanch, H. W. (1989a). Transient responses of hybridoma cells to nutrient additions in continuous culture: I. Glucose pulse and step changes. Biotechnol. Bioeng. *33*, 477-486.

Miller, W. M., Wilke, C. R., and Blanch, H. W. (1989b). Transient responses of hybridoma cells to nutrient additions in continuous culture: II. Glutamine pulse and step changes. Biotechnol. Bioeng. *33*, 487-499.

Mitchell, P. (1979). Keilin's respiratory chain concept and its chemiosmotic consequences. Science *206*, 1148-1159.

Möllborn, F. (1996). Application of stoichiometric modeling in software design and animal cell cultivation. In Chemical Engineering (Cambridge, MA: Massachusetts Institute of Technology).

Mosmann, T. (1983). Rapid colorimetric assay for cellular growth and survival: application to proliferation and cytotoxicity assays. J. Immunol. Methods *65*, 55-63.

Mosser, D. D., and Massie, B. (1994). Genetically engineering mammalian cell lines for increased viability and productivity. Biotech. Adv. *12*, 253-277.

Muzio, M., Stockwell, B. R., Stennicke, H. R., Salvesen, G. S., and Dixit, V. M. (1998). An induced proximity model for caspase-8 activation. J. Biol. Chem. *273*, 2926-2930.

Nyberg, G. B., Balcarcel, R. R., Follstad, B. D., Stephanopoulos, G., and Wang, D. I. C. (1999b). Metabolic Effects on recombinant interferon-gamma glycosylation in continuous culture of chinese hamster ovary cells. Biotechnol. Bioeng.

Nyberg, G. B., Balcarcel, R. R., Follstad, B. D., Stephanopoulos, G., and Wang, D. I. C. (1999a). Metabolism of peptide amino acids by chinese hamster ovary cells grown in a complex medium. Biotechnol. Bioeng. *62*, 324-335.

Ozturk, S. S., and Palsson, B. O. ('991). Effect of medium osmolarity on hybridoma growth, metabolism, and antibody production. 1991 *37*, 989-993.

Pan, G., O'Rourke, K., and Dixit, V. M. (1998). Caspase-9, Bcl-X_L, and Apaf-1 form a ternary complex. J. Biol. Chem. *273*, 5841-5845.

Park, S. M. (1996). Investigation of Carbon Fluxes in Central Metabolic Pathways of *Corynebacterium glutamicum*. In Chemical Engineering (Cambridge, MA: Massachusetts Institute of Technology).

Park, S. M., Klapa, M. I., Sinskey, A. J., and Stephanopoulos, G. (1999). Metabolite and isotopomer balancing in the analysis of metabolic cycles: II. Applications. Biotechnol. Bioeng. *62*, 392-401.

Park, S. M., Shaw, C. A., Sinskey, A. J., and Stephanopoulos, G. (1997). Elucidation of anaplerotic pathways in *Corynebacterium glutamicum* via ^{13}C NMR spectroscopy and GC-MS. Appl. Microbiol. & Biotech. *47*, 430-440.

Pastorino, J. G., Simbula, G., Yamamoto, K., Glascott, J., P. A., Rothman, R. J., and Farber, J. L. (1996). The cytotoxicity of tumor necrosis factor depends on induction of the mitochondrial permeability transition. J. Biol. Chem. *271*, 29792-29798.

Petit, P. X., O'Connon, J. E., Grunwald, D., and Brown, S. C. (1990). Analysis of the membrane potential of rat- and mouse-liver mitochondria by flow cytometry and possible applications. Eur. J. Biochem. *194*, 389-397.

Petit, P. X., Susin, S.-A., Zamzami, N., Mignotte, B., and Kroemer, G. (1996). Mitochondria and programmed cell death: back to the future. FEBS Lett. *396*, 7-13.

Petit, P. X., Zamzami, N., Vayssière, J.-L., Mignotte, B., Kroemer, G., and Castedo, M. (1997). Implication of mitochondria in apoptosis. Mol. Cell. Biochem. *174*, 185-188.

Pipeleers, D. G. (1992). Heterogeneity in pancreatic beta-cell population. Diabetes *41*, 777-81.

Portais, J.-C., Schuster, R., Merle, M., and Canioni, P. (1993). Metabolic flux determination in C6 glioma cells using carbon-13 distribution upon [1-^{13}C]glucose incubation. Eur. J. Biochem. *217*, 457-468.

Pörtner, R., and Schäfer, T. (1996). Modelling hybridoma cell growth and metabolism - comparison of selected models and data. J. Biotechnol. *49*, 119-135.

Prescott, L. M., Harley, J. P., and Klein, D. A. (1993). Microbiology, 2nd Edition (Oxford: Wm. C. Brown Publishers).

Rappaport, L., Oliviero, P., and Samuel, J. L. (1998). Cytoskeleton and mitochondrial morphology and function. Mol. Cell. Biochem. *184*, 101-105.

Reed, J. C. (1997). Cytochrome c: can't live with it - can't live without it. Cell *91*, 559-562.

Renner, W. A., Lee, K. H., Hatzimanikatis, V., Bailey, J. E., and Eppenberger, H. M. (1995). Recombinant cyclin E expression activates proliferation and obviates surface attachment of chinese hamster ovary (CHO) cells in protein-free medium. Biotechnol. Bioeng. *47*, 476-482.

Rognstad, R. (1995). Models of the liver pentose cycle. J. Theor. Biol. *173*, 195-206.

Rossé, T., Olivier, R., Monney, L., Rager, M., Conus, S., Fellay, I., Jansen, B., and Borner, C. (1998). Bcl-2 prolongs cell survival after Bax-induced release of cytochrome *c*. Nature *391*, 496-499.

Sahara, S., Aoto, M., Eguchi, Y., Imamoto, N., Yoneda, Y., and Tsujimoto, Y. (1999). Acinus is a caspase-3-activated protein required for apoptotic chromatin condensation [In Process Citation]. Nature *401*, 168-73.

Salvesen, G. S., and Dixit, V. M. (1997). Caspases: intracellular signaling by proteolysis. Cell *91*, 443-446.

Salvioli, S., Ardizzoni, A., Franceschi, C., and Cossarizza, A. (1997). JC-1, but not $DiOC_6(3)$ or rhodamine 123, is a reliable fluorescent probe to asses $\Delta\Psi$ changes in intact cells: implications for studies on mitochondrial functionality during apoptosis. FEBS Lett. *411*, 77-82.

Scahill, S. J., Devos, R., Van der Heyden, J., and Fiers, W. (1983). Expression and characterization of the product of a human immune interferon cDNA gene in Chinese hamster ovary cells. Proc. Natl. Acad. Sci. U S A *80*, 4654-4658.

Schoen, R. C., Bentley, K. L., and Klebe, R. J. (1982). Monoclonal antibody against human fibronectin which inhibits cell attachment. Hybridoma *1*, 99-108.

Schumpe, A., Quicker, G., and Deckwer, W. D. (1982). Gas solubilities in microbial culture media. Adv. Biochem. Eng. *24*, 1-38.

Sharfstein, S. T., Tucker, S. N., Mancuso, A., Blanch, H. W., and Clark, D. S. (1994). Quantitative in vivo nuclear magnetic resonance studies of hybridoma metabolism. Biotechnol. Bioeng. *43*, 1059-1074.

Simpson, N. H., Singh, R. P., Emery, A. N., and Al-Rubeai, M. (1999). Bcl-2 over-expression reduces growth rate and prolongs G_1 phase in continuous chemostat cultures of hybridoma cells. Biotechnol. Bioeng. *64*, 174-186.

Simpson, N. H., Singh, R. P., Perani, A., Goldenzon, C., and Al-Rubeai, M. (1998). In hybridoma cultures, deprivation of any single amino acid leads to apoptotic death, which is suppressed by the expression of the *bcl-2* gene. Biotechnol. Bioeng. *59*, 90-98.

Simpson, T. W., Follstad, B. D., and Stephanopoulos, G. (1999). Analysis of the pathway structure of metabolic networks. J. Biotechnol. *71*, 207-223.

Slater, T. F., Sawyer, B., and Sträuli, U. (1963). Studies on succinate-tetrazolium reductase systems. III. Points of coupling of four different tetrazolium salts. Biochim. Biophys. Acta *77*, 383-393.

Smirnova, E., Shurland, D.-L., Ryazantsev, S. N., and van der Bliek, A. M. (1998). A human dynamin-related protein controls the distribution of mitochondria. J. Cell Biol. *143*, 351-358.

Spudich, J. L., and Koshland, J., D. E. (1976). Non-genetic individuality: chance in the single cell. Nature *262*, 467-471.

Steller, H. (1995). Mechanisms and genes of cellular suicide. Science *267*, 1445-1449.

Stennicke, H. R., Jürgensmeier, J. M., Shin, H., Deveraux, Q., Wolf, B. B., Yang, X., Zhou, Q., Ellerby, H. M., Ellerby, L. M., Bredesen, D., Green, D. R., Reed, J. C., Froelich, C. J., and Salvesen, G. S. (1998). Pro-caspase-3 is a major physiologic target of caspase-8. J. Biol. Chem. *273*, 27084-27090.

Stephanopoulos, G., and Simpson, T. W. (1997). Flux amplification in complex metabolic networks. Chem. Eng. Sci. *52*, 2607-2627.

Stephanopoulos, G., and Vallino, J. J. (1991). Network rigidity and metabolic engineering in metabolite overproduction. Science *252*, 1675-1681.

Stephanopoulos, G. N., Aristidou, A. A., and Nielsen, J. (1998). Metabolic engineering: priciples and methodologies (San Diego: Academic Press).

Stryer, L. (1988). Biochemistry, 3rd Edition (New York: W.H. Freeman & Co.).

Susin, S. A., Lorenzo, H. K., Zamzami, N., Marzo, I., Brenner, C., Larochette, N., Prévost, M.-C., Alzari, P. M., and Kroemer, G. (1999b). Mitochondrial release of caspase-2 and -9 during the apoptotic process. J. Exp. Med. *189*, 381-393.

Susin, S. A., Lorenzo, H. K., Zamzami, N., Marzo, I., Snow, B. E., Brothers, G. M., Mangion, J., Jacotot, E., Costantini, P., Loeffler, M., Larochette, N., Goodlett, D. R., Aebersold, R., Siderovski, D. P., Penninger, J. M., and Kroemer, G. (1999a). Molecular characterization of mitochondrial apoptosis-inducing factor. Nature *397*, 441-446.

Susin, S. A., Zamzami, N., and Kroemer, G. (1998). Mitochondria as regulators of apoptosis: doubt no more. Biochim. Biophys. Acta *1366*, 151-165.

Szyperski, T. (1995). Biosynthetically directed fractional 13C-labeling of proteinogenic amino acids. An efficient analytical tool to investigate intermediary metabolism. Eur. J. Biochem. *232*, 433-448.

Tartaglia, L. A., Ayres, T. M., Wong, G. H. W., and Goeddel, D. V. (1993). A novel domain within the 55 kd TNF receptor signals cell death. Cell *74*, 845-853.

Thornberry, N. A., and Lazebnik, Y. (1998). Caspases: enemies within. Science *281*, 1312-1316.

Tomita, M., Hashimoto, K., Takahashi, K., Shimizu, T. S., Matsuzaki, Y., Miyoshi, F., Saito, K., Tanida, S., Yugi, K., Venter, J. C., and Hutchison, C. A., 3rd (1999). E-CELL: software environment for whole-cell simulation. Bioinformatics *15*, 72-84.

Tsuchiya, H. M., Fredrickson, A. G., and Aris, R. (1966). Dynamics of microbial cell populations. Adv. Chem. Eng. *6*, 125-206.

Vallino, J. J. (1991). Identification of branch-point restrictions in microbial metabolism through metabolic flux analysis and local network perturbations. In Chemical Engineering (Cambridge: Massachusetts Institute of Technology).

Vallino, J. J., and Stephanopoulos, G. (1994b). Carbon flux distributions at the glucose 6-phosphate branch point in *Corynebacterium glutamicum* during lysine overproduction. Biotechnol. Prog. *10*, 327-334.

Vallino, J. J., and Stephanopoulos, G. (1994a). Carbon flux distributions at the pyruvate branch point in *Corynebacterium glutamicum* during lysine overproduction. Biotechnol. Prog. *10*, 320-326.

Vallino, J. J., and Stephanopoulos, G. (1993). Metabolic flux distributions in *Corynebacterium glutamicum* during growth and lysine overproduction. Biotechnol. Bioeng. *41*, 633-646.

van der Heijden, R. T. J. M., Heijnen, J. J., Hellinga, C., Romein, B., and Luyben, K. C. A. M. (1994a). Linear constraint relations in biochemical reaction systems: I. Classification of the calculability and the balanceability of conversion rates. Biotechnol. Bioeng. *43*, 3-10.

van der Heijden, R. T. J. M., Heijnen, J. J., Hellinga, C., Romein, B., and Luyben, K. C. A. M. (1994b). Linear constraint relations in biochemical reaction systems: II. Diagnosis and estimation of gross errors. Biotechnol. Bioeng. *43*, 11-20.

Vander Heiden, M. G., Chandel, N. S., Williamson, E. K., Schumacker, P. T., and Thompson, C. B. (1997). Bcl-x_L regulates the membrane potential and volume homeostasis of mitochondria. Cell *91*, 627-637.

Varma, A., and Palsson, B. O. (1994). Metabolic flux balancing: basic concepts, scientific and practical use. Bio/Technology *12*, 994-998.

Vaux, D. L., Cory, S., and Adams, J. M. (1988). *Bcl-2* gene promotes haemopoietic cell survival and cooperates with *c-myc* to immortalize pre-B cells. Nature *335*, 440-442.

Vriezen, N., and van Dijken, J. P. (1998). Fluxes and enzyme activities in central metabolism of myeloma cells grown in chemostat culture. Biotechnol. Bioeng. *59*, 28-39.

Wallach, D. (1997). Cell death induction by TNF: a matter of self control. TIBS *22*, 107-109.

Wang, N. S., and Stephanopoulos, G. (1983). Application of macroscopic balances to the identification of gross measurement errors. Biotechnol. Bioeng. *25*, 2177-2208.

Wertz, I. E., and Hanley, M. R. (1996). Diverse molecular provocation of programmed cell death. TIBS *21*, 359-364.

Wiechert, W., and de Graaf, A. A. (1997a). Bidirectional reaction steps in metabolic networks: I. Modeling and simulation of carbon isotope labeling experiments. Biotechnol. Bioeng. *55*, 101-117.

Wiechert, W., and de Graaf, A. A. (1996). In vivo stationary flux analysis by ^{13}C labeling experiments. Adv. Biochem. Eng. *54*, 109-154.

Wiechert, W., Siefke, C., de Graaf, A. A., and Marx, A. (1997b). Bidirectional reaction steps in metabolic networks: II. Flux estimation and statistical analysis. Biotechnol. Bioeng. *55*, 118-135.

Williams, G. T. (1991). Programmed cell death: apoptosis and oncogenesis. Cell *65*, 1097-1098.

Williams, G. T., and Smith, C. A. (1993). Molecular regulation of apoptosis: genetic controls on cell death. Cell *74*, 777-779.

Williams, J. F. (1980). A critical examination of the evidence for the reactions of the pentose phosphate pathway. Trends Biol. Sci. *5*, 315-320.

Williams, J. F., and Blackmore, P. F. (1983). Non-oxidative synthesis of pentose 5-phosphate from hexose 6-phosphate and triose phosphate by the L-type pentose pathway. Int. J. Biochem. *15*, 797-816.

Williams, J. F., Blackmore, P. F., and Clark, M. G. (1978). New reaction sequences for the non-oxidative pentose phosphate pathway. Biochem. J. *176*, 257-282.

Willis, J. A., Williams, W. F., and Schleich, T. (1986). Dynamic assessment of hexose monophosphate shunt activity in the intact rabbit lens by proton NMR spectroscopy. Biochem Biophys Res Commun *138*, 1068-73.

Wittmann, C., and Heinzle, E. (1999). Mass spectrometry for metabolic flux analysis. Biotechnol. Bioeng. *62*, 739-750.

Wolter, K. G., Hsu, Y.-T., Smith, C. L., Nechushtan, A., Xi, X.-G., and Youle, R. J. (1997). Movement of Bax from the cytosol to mitochondria during apoptosis. J. Cell Biol. *139*, 1281-1292.

Wolvetang, E. J., Johnson, K. L., Krauer, K., Ralph, S. T., and Linnane, A. W. (1994). Mitochondrial respiratory chain inhibitors induce apoptosis. FEBS Lett. *339*, 40-44.

Wood, T. (1985). The pentose phosphate pathway (New York, NY: Academic Press).

Xie, L. (1997). Stoichiometric medium design and nutritional control in fed-batch cultivation of animal cells. In Chemical Engineering (Cambridge, MA: Massachusetts Institute of Technology).

Xie, L., and Wang, D. I. C. (1994c). Applications of improved stoichiometric model in medium design and fed-batch cultivation of animal cells in bioreactor. Cytotechnology *15*, 17-29.

Xie, L., and Wang, D. I. C. (1994b). Fed-batch cultivation of animal cells using different medium design consepts and feeding strategies. Biotechnol. Bioeng. *43*, 1175-1189.

Xie, L., and Wang, D. I. C. (1994a). Stoichiometric analysis of animal cell growth and its application in medium design. Biotechnol. Bioeng. *43*, 1164-1174.

Xiu, Z.-L., Zeng, A.-P., and Deckwer, W.-D. (1998). Multiplicity and stability analysis of microorganisms in continuous culture: effects of metabolic overflow and growth inhibition. Biotechnol. Bioeng. *57*, 251-261.

Yang, B.-C., Chang, H.-M., Wang, Y.-S., Chen, R.-F., and Lin, S.-J. (1996). Transient induction of apoptosis in serum-starved glioma cells by insulin and IGF-1. Biochim. Biophys. Acta *1314*, 83-92.

Yang, J., Liu, X., Bhalla, K., Kim, C. N., Ibrado, A. M., Cai, J., Peng, T.-I., Jones, D. P., and Wang, X. (1997). Prevention of apoptosis by Bcl-2: release of cytochrome *c* from mitochondria blocked. Science *275*, 1129-1132.

Zamzami, N., Susin, S. A., Marchetti, P., Hirsch, T., Gómez-Monterry, I., Castedo, M., and Kroemer, G. (1996). Mitochondrial control of nuclear apoptosis. J. Exp. Med. *183*, 1533-1544.

Zeng, A.-P., Deckwer, W.-D., and Hu, W.-S. (1998). Determinants and rate laws of growth and death of hybridoma cells in continuous culture. Biotechnol. Bioeng. *57*, 642-654.

Zhou, W., Rehm, J., and Hu, W.-S. (1995). High viable cell concentration fed-batch cultures of hybridoma cells through on-line nutrient feeding. Biotechnol. Bioeng. *46*, 579-587.

Zou, H., Henzel, W. J., Liu, X., Lutschg, A., and Wang, X. (1997). Apaf-1, a human protein homologous to C. elegans CED-4, participates in cytochrome c-dependent activation of caspase-3. Cell *90*, 405-413.

Zupke, C., Sinskey, A. J., and Stephanopoulos, G. (1995b). Intracellular flux analysis applied to the effect of dissolved oxygen on hybridomas. Appl. Microbiol. Biotechnol. *44*, 27-36.

Zupke, C., and Stephanopoulos, G. (1995a). Intracellular flux analysis in hybridomas using mass balances and in vitro ^{13}C NMR. Biotechnol. Bioeng. *45*, 292-303.

Zupke, C. A. (1993). Metabolic flux analysis in mammalian cell culture. In Chemical Engineering (Cambridge, MA: Massachusetts Institute of Technology).

THESIS PROCESSING SLIP

FIXED FIELD: ill. _____ name _____

index _____ biblio _____

▶ COPIES: (Archives) Aero Dewey Eng Hum

Lindgren Music Rotch (Science)

TITLE VARIES: ▶ ☐ _____

NAME VARIES: ▶ ☐ / David _____

IMPRINT: (COPYRIGHT) _____

▶ COLLATION: 206 P

▶ ADD: DEGREE: _____ ▶ DEPT.: _____

SUPERVISORS: _____

NOTES:

cat'r: date:

page: F/8

▶ DEPT: Chem. Eng.

▶ YEAR: 2000 ▶ DEGREE: Ph.D.

▶ NAME: FOLLSTAD